DESIGN OF SELF-CONSOLIDATING PRECAST CONCRETE USING POWDERED LIMESTONE

A Dissertation
Presented to
The Academic Faculty

by

Natalia H. Cardelino

In Partial Fulfillment
of the Requirements for the Degree
Doctor of Philosophy in the
School of Civil and Environmental Engineering

Georgia Institute of Technology
August 2018

DESIGN OF SELF-CONSOLIDATING PRECAST CONCRETE USING POWDERED LIMESTONE

Approved by:

Dr. Kimberly Kurtis, Co-advisor
School of Civil and Environmental Engineering
Georgia Institute of Technology

Dr. T. Russell Gentry
College of Design
Georgia Institute of Technology

Dr. Lawrence F. Kahn
School of Civil and Environmental Engineering
Georgia Institute of Technology

Dr. Jason Brown
College of Design
Georgia Institute of Technology

Dr. Giovanni Loreto
College of Architecture and Construction Management
Kennesaw State University

Date Approved: July 23, 2018

ACKNOWLEDGEMENTS

I would like to first thank my advisors Dr. Kurtis and Dr. Gentry for their insightful guidance and advice throughout this process, for their confidence in me to carry out this research, and for supporting me all these years. I am especially grateful for my committee member and friend Dr. Loreto who was always available to guide me through the research process, both experimental and written, and whose knowledge of self-consolidating concrete was immensely valuable.

I could not accomplish much of the research without the support of the other PhD students in Dr. Kurtis' group: Mehdi Rashidi, Prasanth Alapati, La Sasha Walker, Scotty Smith, Bill Jin, Behnaz Zaribaf, Elizabeth Nadelman, and Lisa Burris who were always available to train me on the use of equipment, give me constructive advice, or to review presentations.

During the research process, I had several undergraduate assistants helping me. I would like to thank Jason Tam, Kelli Roberts, Emily Veal, Daniel Benkeser, and Jun Hyeok Lee for their hard work and dedication. I would also like to acknowledge Jeremy Mitchell, the manager of the Structure's Lab, for all his help. He taught me how to safely operate all the required equipment in the lab. I am grateful for two of his assistants, Nifemi Ajayi and Caleb Brown, who helped me mix concrete and fill cylinders for testing.

The cements used in this project were donated by LafargeHolcim. I would like to thank Wayne Wilson who was always available to supply me with additional cement. The

limestone powder used in this research were donated by Imerys. I would like to thank my contact there Anna Landreville for keeping my limestone powder supply stocked.

This research was funded through the PCI Daniel P. Jenny Fellowship. I thank Harry Gleich and Terry Snow (QC Manager) of Metromont along with Kevin Kirkley and Tyler Norten (Batch Plant Supervisor) of Tindall for giving me a tour of their facilities, providing technical guidance and helping me through the early portion of this project.

Finally, and most importantly, I would like to thank my family. I cannot thank my husband, Lui, and my two amazing children, Ella and Dominic, enough for their support and understanding, which kept me going throughout this process. I know there were times when my children felt mom-less, but it was always followed by times of constant attention from me. In addition, to my two wonderful parents who played multiple roles during this process. Not only were they babysitters when I needed them to be, having been through the PhD process before, they acted as my informal advisors. I could not have done this without them.

TABLE OF CONTENTS

ACKNOWLEDGEMENTS **iii**

LIST OF TABLES **viii**

LIST OF FIGURES **ix**

LIST OF SYMBOLS AND ABBREVIATIONS **xiv**

SUMMARY **xvii**

CHAPTER 1. Introduction **1**
1.1 Motivation **1**
1.2 Research objectives **7**
1.3 Research approach **8**

CHAPTER 2. Literature Review **11**
2.1 Historical use of limestone powder with cements **11**
2.2 Hydration of Portland cement with limestone powder **12**
2.3 Quantifying the effect of limestone median particle size distribution **14**
2.4 Properties of concrete produced with limestone powder **17**
2.4.1 Effects on Fresh Concrete Properties 17
2.4.2 Effects on Hardened Concrete Properties 18
2.5 Precast Concrete and Self-Consolidating Concrete (SCC) **19**
2.6 Drying Shrinkage **22**
2.6.1 ACI 209R-92 model 23
2.6.2 Bažant-Baweja B3 model 24
2.6.3 CEB MC90-99 model 25
2.6.4 GL2000 model 26
2.6.5 AASHTO-LRFD Model 27
2.7 Creep **28**
2.7.1 ACI 209R-92 model 30
2.7.2 Bažant-Baweja B3 model 31
2.7.3 CEB MC90-99 model 32
2.7.4 GL2000 model 33
2.7.5 AASHTO-LRFD Model 34
2.8 Multiscaling **35**

CHAPTER 3. Materials and Methods **39**
3.1 Introduction **39**
3.2 Material Characterization **40**
3.2.1 Chemical Composition of cement and limestone 40
3.2.2 Particle Size Distribution 45
3.2.3 Scanning Electron Microscope Images 49
3.3 Aggregates, Admixtures and Water **51**

CHAPTER 4. The Influence of Particle Size on Early Age Properties Of Limestone Blended Cements pastes and mortars **52**
4.1 Introduction **52**
4.2 Materials and Methods **53**
4.2.1 Isothermal Calorimetry 54
4.2.2 Vicat Time of Set 55
4.2.3 Mini slump spread diameter 56
4.2.4 Mortar Compressive Strength 57
4.3 Experimental Results **57**
4.3.1 Isothermal Calorimetry 58
4.3.2 Vicat Time of Set 71
4.3.3 Vicat time of Set and Median Limestone Particle Size 75
4.3.4 Workability - Mini slump 77
4.3.5 Mini slump and limestone median particle size 80
4.4 Mortar Compressive Strength **81**
4.5 Life Cycle Analysis **84**
4.6 Conclusions and Discussions **85**

CHAPTER 5. Workability and Surface Finish of Precast Concrete Made with Limestone Blended Cements **88**
5.1 Introduction **88**
5.2 Materials and Methods **90**
5.2.1 Slump flow, flow rate, S-groove and VSI 92
5.2.2 Surface Finish 94
5.3 Experimental Results **96**
5.3.1 Slump flow, flow rate, S-groove, and VSI 96
5.3.2 Influence of Concrete Mixer 98
5.3.3 Surface Finish 99
5.4 Conclusions and Discussion **102**

CHAPTER 6. Compressive strength, drying shrinkage, creep, and durability of Precast Concrete Made with Limestone Blended Cements **104**
6.1 Introduction **104**
6.2 Materials and Methods **107**
6.2.1 Compressive Strength 108
6.2.2 Volume Stability 109
6.2.3 Permeability 113
6.3 Experimental Results **116**
6.3.1 Compressive Strength 117
6.3.2 Drying Shrinkage 121
6.3.3 Drying shrinkage prediction models 129
6.3.4 Long-term creep 133
6.3.5 Creep prediction models 136
6.3.6 Surface Resistivity 138
6.3.7 Rapid Chloride Permeability Test (RCPT) 140
6.4 Comparison of SR and RCPT **142**
6.5 Correlation of Permeability Indices and Compressive Strength **143**

6.6 Conclusion and Discussion 147

CHAPTER 7. Predicting Long-term Creep of Precast Concrete from Nanoindentation Creep Studies 150
7.1 Introduction 150
7.2 Theoretical Background of Indentation Techniques 151
7.3 Materials and Methods 155
7.4 Experimental Results 157
7.4.1 Nanoindentation Creep 157
7.5 Comparison of creep compliance and specific creep 159
7.6 Upscaling from Paste to Concrete 161
7.7 Conclusions and Discussion 166

CHAPTER 8. Conclusions and Discussion 168
8.1 Conclusions 168
8.1.1 Effect of limestone median particle size 170
8.1.2 Effect of limestone percent replacement 172
8.1.3 Modelling drying shrinkage and creep of limestone blended cements 174
8.1.4 Upscaling of nanoindentation cement paste creep to concrete creep 175
8.2 Recommendations for Practice 175
8.3 Recommendations for Future Work 177

APPENDIX A: Blended D_{50} 179

APPENDIX B: Slump flow and vsi photos of mixes 184

APPENDIX C: Drying shrinkage data 185

APPENDIX D: Creep data 186

APPENDIX E: Creep prediction model comparison 188

APPENDIX F: Comparison of drying shrinkage studies 193

REFERENCES 194

LIST OF TABLES

Table 3-1	Cement	41
Table 3-2	Summary of Particle Size Distribution	48
Table 4-1	Particle Size Distribution of Limestone and Quartz	54
Table 4-2	Results from isothermal calorimetry showing the effect of 10% cement replacement of limestone powder of varying median particle size	59
Table 4-3	Comparison of heat paramters with increasing cement replacement	63
Table 5-1	Mix Proportions of SCC concrete mixes	91
Table 5-2	Visual Stability Index, VSI [65]	97
Table 6-1	Mix proportions of SCC concrete mixes	108
Table 6-2	Permeability classification according to AASHTO T358 surface permeability test	115
Table 6-3	Permeability classification of concretes tested according to ASTM C1202/AASHTO T277 Rapid Chloride Permeability method	116
Table 6-4	Compressive strength development (ksi) of concrete mixes with and without limestone powder and percentage difference from neat cement mixes	119
Table 7-1	Summary of results from nanoindentation	158
Table 7-2	Results of curve fit	162
Table 7-3	Upscaling results using Vu et al. and Mori-Tonka schemes	164
Table C-1	Drying shrinkage data for limewater cured specimens	185
Table C-2	Drying shrinkage data for air cured specimens	185
Table D-1	Total creep + shrinkage strains	186
Table D-2	Shrinkage strains and specific creep	186
Table D-3	Modulus of elasticity comparison	187

LIST OF FIGURES

Figure 1-1	Amount of anthropogenic carbon released	1
Figure 1-2	Impact of different cement reduction methods projected until 2050 [3]	2
Figure 1-3	Use and availability of cement alternatives [2]	3
Figure 1-4	Difference in energy production between the same concrete mix with limestone powder versus fly ash using Berkeley Green concrete	4
Figure 2-1	Timeline of limestone powder usage in cement	11
Figure 2-2	Total time-dependent strain of externally loaded concrete [58]	29
Figure 3-1	Raymond Mill for limestone powder production [65]	42
Figure 3-2	DTG comparison of Type I/II, III and IL cements showing a large peak between 600°C and 800°C where limestone breaks down	44
Figure 3-3	$CaCO_3$ content of cements and limestone powder	44
Figure 3-4	XRD analysis of the 3, 25, and 40 μm limestone powder	45
Figure 3-5	Particle size distribution of cements and limestone powder	47
Figure 3-6	Cumulative particle size distribution of cement and limestone powder	47
Figure 3-7	SEM images of 3μm (above), 25μm (middle), and 40μm (below) limestone	50
Figure 4-1	Heat evolution of Type I/II, Type III, and Type IL cements with 10% cement substitution of limestone powder of varying median particle size	60
Figure 4-2	Cumulative heat evlotion of Type I/II, Type II, and Type IL cements plus 10% cement replacement of limestone powder of varying median particle size	61
Figure 4-3	Heat evolution of Type I/II, Type III, and Type IL cements with varying percentages of cement substitution by a 25 μm limestone powder	64

Figure 4-4	Cumulative heat of Type I/II, Type III, and Type IL cements with varying percentages of cement substitution by a 25 μm limestone powder	65
Figure 4-5	Cumulative heat of hydration at 48 hours for Type I/II, III, and IL cements and varying percent substitutions of 25 μm limestone powder	67
Figure 4-6	Cumulative heat of hydration at 48 hours for a Types I/II, III and IL cements with varying percentage cement replacement of varying limestone powders	68
Figure 4-7	Heat evolution and cumulative heat comparison of limestone powder and quartz with similar particle size distributions	70
Figure 4-8	Vicat Time of Set with 10% limestone of varying median particle size	72
Figure 4-9	Vicat Time of Set with Increasing Cement Replacement	74
Figure 4-10	Time of Set with Type III cement replaced with varying percentages of 3, 25, and 40 μm limestone powders	76
Figure 4-11	Mini slump flow and D_f	77
Figure 4-12	Cement paste spread diameter with 10% limestone replacement	78
Figure 4-13	Cement paste spread diameter with varying percentage of limestone powder with 25 μm	79
Figure 4-14	Mini slump yield stress of Type III cement with varying % limestone replacement	80
Figure 4-15	Mortar Compressive Strength – Type I/II and limestone powder	82
Figure 4-16	Mortar Compressive Strength – Type III and limestone powder	82
Figure 4-17	Comparison of concrete mixes with and without 20% cement preplacement of fly ash or 25 μm limestone powder	85
Figure 5-1	S-groove test on SCC mix	93
Figure 5-2	Visual Stability Index, VSI [65]	94
Figure 5-3	Bug hole variations in two concrete specimens	95
Figure 5-4	Image of small (left) and large (right) bug holes on concrete samples	95

Figure 5-5	Concrete mixers used to compare workability	98
Figure 5-6	Slump flow comparison of concrete mix made in revolving mixer (left) and high shear mixer (right)	99
Figure 5-7	Surface finish comparison of concrete mix with no limestone (top) with 15% cement replacement (middle) and with 25% cement replacement (bottom)	100
Figure 5-8	Quantity of small and large bug holes for SCC mixes made from Type I/II cement (above) and Type III cement	101
Figure 6-1	Concrete cylinder in compression testing	109
Figure 6-2	Drying shrinkage measurement on concrete prisms	111
Figure 6-3	Cylinders loaded in creep frames	113
Figure 6-4	Measuring surface resistivity of a concrete cylinder	114
Figure 6-5	Epoxy coated specimen and specimen loaded in holder exposed to NaOH solution on one end and NaCl solution on other ready for voltage application	116
Figure 6-6	Compressive strength development of Type IL and Type III cement blended with various limestone powders	118
Figure 6-7	Compressive strength development of Type IL and Type I/II cement blended with various limestone powders	118
Figure 6-8	Drying shrinkage results for 7-day limewater cured concrete mixes made with Type IL and Type III cement blended with varying limestone powders (a) at 15% and (b) 25% cement replacement	123
Figure 6-9	Drying shrinkage results for 7-day limewater cured concrete mixes made with Type I/II cement blended with varying limestone powders at (a) 15% and (b) 25% cement replacement	124
Figure 6-10	Drying shrinkage results for air cured concrete mixes made with Type III cement blended with varying limestone powders (a) at 15% and (b) 25% cement replacement	125
Figure 6-11	Drying shrinkage results for air cured concrete mixes made with Type I/II cement blended with varying limestone powders (a) at 15% and (b) 25% cement replacement	126
Figure 6-12	Comparison between drying shrinkage of concrete mixes made with Type III and Type I/II limestone blended cements	128

Figure 6-13	Drying shrinkage comparison of T3L3(25) with (upper) and without limewater curing (lower) and five prediction models	130
Figure 6-14	Drying shrinkage comparison of concrete mixes with limewater curing (left) and without limewater curing (right) and the GL2000 drying shrinkage model	131
Figure 6-15	Total creep and shrinkage strains for concrete mixes with 15% limestone replacement (top) and 25% limestone replacement (bottom)	134
Figure 6-16	Specific creep of concrete mixes made with blended limestone cements	135
Figure 6-17	Comparing experimental total creep and shrinkage strains with five prediction models	137
Figure 6-18	Specific creep comparison of ACI 209 and AASHTO creep prediction models with experimental T3L25(25) data	137
Figure 6-19	Surface resistivity measurements of Type IL and Type III blended limestone cements with varying percentage cement substitution and limestone fineness	139
Figure 6-20	Surface resistivity measurements of Type I/II blended limestone cements with varying percentage cement substitution and limestone fineness	139
Figure 6-21	RCPT results for Type IL and Type III blended limestone cements	141
Figure 6-22	RCPT results for Type I limestone blended cements	141
Figure 6-23	Relationship between surface resistivity and rapid chloride permeability test for limestone blended cements	143
Figure 6-24	Correlation between RCPT results and compressive strength for all concrete mixes (Type III neat, Type I/II neat, Type IL, Type III limestone blends, and Type I/II limestone blends)	144
Figure 6-25	Correlation between Type III neat and Type III limestone blends with 15% cement replacement	146
Figure 6-26	Correlation between TypeI/II neat, Type I/II limstone blends, and Type III limestone blends with 25% cement replacement	146
Figure 7-1	Load displacment curve for indentation experiements [106]	152
Figure 7-2	Schematic representation of indenter [107]	153

Figure 7-3	Polished cement paste samples ready for loading into nanoindenter	156
Figure 7-4	Cement paste loaded into nanoindenter. Notice the reflection of the indenter tip on the polished surface of the cement paste.	156
Figure 7-5	Nanoindentation creep results of cement paste	159
Figure 7-6	Comparison of nanoindenation creep (above with) concrtete creep (below)	160
Figure 7-7	Example of curve fit data using equations 7-5 and 7-6 for mix T3L25(15) made with cement paste (above) and concrete (below)	162
Figure 7-8	Relationship between $C_{i,con}$ upscaled from the level of cement paste and $C_{u,con}$ obtained from a long-term concrete creep study	165
Figure A-1	Blended surface area of Type I/II cement and limestone	180
Figure A-2	Blended surface area of Type III cement and limestone	180
Figure A-3	Relationship between peak hydration and blended D_{50}	181
Figure A-4	Relationship between time of set and blended D_{50}	182
Figure A-5	Relationship between mini slump yield stress and blended D_{50}	183
Figure B-1	Unacceptable S-groove	184
Figure B-2	Insufficient slump flow	184
Figure B-3	Bleeding and segregation due to excessive HRWRA	184
Figure E-1	T1L total creep and shrinkage strains	188
Figure E-2	T3 total creep and shrinkage strains	189
Figure E-3	T2L3(15) total creep and shrinkage strains	190
Figure E-4	T3L3(25) total creep and shrinkage strains	191
Figure E-5	T3L25(15) total creep and shrinkage strains	192
Figure F-1	Shrinkage comparison between ASTM C157 and C512	193
Figure F-2	Shrinkage comparison between ASTM C157 and C512	193

LIST OF SYMBOLS AND ABBREVIATIONS

AASHTO	American Association of State Highway and Transportation
ACI	American Concrete Institute
ASTM	American Society for Testing and Materials
CEB	European Committee for Concrete (Comité Européen du Béton)
CSA	Canadian Standards Association
DEMEC	Detachable Mechanical Strain Gauge
DOT	Department of Transportation
DTG	Thermogravimetric derivative
EPA	Environmental Protection Agency
GHG	Greenhouse gas
HRWR(A)	High range water reducing (admixture)
ITZ	Interfacial transition zone
MSA	Maximum size aggregate
OPC	Ordinary Portland cement
PLC	Portland limestone cement
RCPT	Rapid chloride permeability test
RH	Relative humidity
SCC	Self-consolidating concrete
SCM	Supplementary cementitious material
SD	Standard deviation
SEM	Scanning electron microscope
SG	Specific gravity

SR	Surface resistivity
SSA	Specific surface area
TGA	Thermogravimetric analysis
VMA	Viscosity modifying agent
VSI	Visual Stability Index
XRD	X-ray diffraction

Cement Chemistry Abbreviations

A	Al_2O_3
AFm	Alumina-ferrite-monosulfate
C	CaO
C_2S	Belite, dicalcium silicate ($2CaO \cdot SiO_2$)
C_3A	Aluminate, tricalcium aluminate ($3CaO \cdot Al_2O_3$)
C_3S	Alite, tricalcium silicate ($3CaO \cdot SiO_2$)
C4AF	Ferrite, tetracalcium aluminoferrite ($4CaO \cdot Al_2O_3 \cdot Fe_2O_3$)
CH	Calcium hydroxide ($Ca(OH)_2$)
CSH	Calcium-silicate-hydrate

List of Symbols

d_{10}	10^{th} percentile particle diameter
$d_{3,2}$	Surface area weighted mean particle size
$d_{4,3}$	Volume weighted mean particle size

d_{50}	50^{th} percentile particle diameter
d_{90}	90^{th} percentile particle diameter
D_f	Mini slump final spread
E_c (E)	Concrete modulus of elasticity
f_c'	Design compressive strength of concrete
$J(t,t_0)$	Creep compliance
V	Volume
w/b	Water-to-binder ratio
w/c	Water-to-cement ratio
ε	Strain
ρ	Density
τ_0	Cement paste yield stress
φ	Creep coefficient

SUMMARY

With their adoption into ASTM C595 and AASHTO M240 in 2012, Type IL cements which contain 15% interground limestone, have the potential to improve the environmental impact and workability of concrete, while meeting the need for cost-effective alternative supplementary cementitious materials to replace the diminishing supply of fly ash. In the precast industry, where limestone powder is blended with Type III cement, additional benefits have been recognized, including reduced abrasion leading to increased equipment longevity, as well as production of concrete with increased cohesion and improved surface finish. Although there is extensive research on the fresh and hardened properties of concretes produced with Type IL cement, there is limited research on how the amount and fineness of limestone powder blended with varying cement types can be best utilized to tailor concrete mix designs.

This research compares self-consolidating concrete (SCC) mixes made with limestone powders of varying finenesses and varying limestone quantities of up to 25% cement replacement by mass. Limestone fillers from the same source were ground to finenesses ranging from 3 μm to 40 μm median particle size and blended with cements of the same base clinker but with varying fineness. These limestone blended cements were evaluated from early age hydration properties, to fresh concrete workability, and finally to long-term dimensional stability and durability.

Results show that early age hydration kinetics and workability are more affected by the median particle size of the limestone powder and that later-age compressive strength, dimensional stability and durability are more affected by percent cement replacement.

Existing drying shrinkage and creep models, which use compressive strength to predict volume stability, can be used with minor modifications to predict the long-term dimensional stability of concrete mixes made with limestone blended cements. Finally, minutes long nanoindentation creep studies conducted on limestone blended cement pastes were shown to correlate with long-term creep rates of concretes made with matching cement pastes, providing a reliable and more rapid means for creep assessment.

CHAPTER 1. INTRODUCTION

1.1 Motivation

Producing cement, the main constituent of concrete, is an energy-intensive process, which releases CO_2 into the atmosphere during the breakdown of $CaCO_3$ into CaO and CO_2 and through the burning of fossil fuels to reach necessary calcination temperatures. It is estimated that over 5% of the anthropogenic CO_2 in the atmosphere is attributed to cement production and is the fourth largest source of carbon in the atmosphere (Figure 1-1).

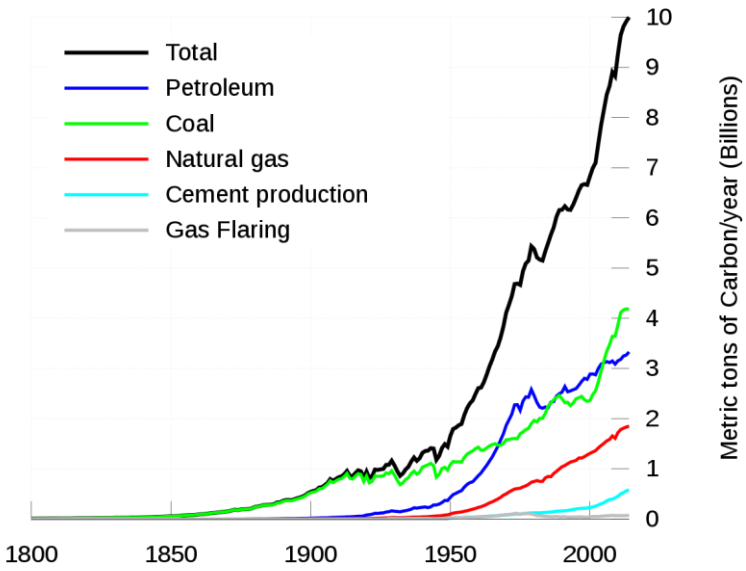

Figure 1-1: Amount of anthropogenic carbon released per industry from 1900-2009 [1]

With growing environmental concerns about CO_2 emissions related to cement production, finding industrially relevant alternative cement formulations are becoming more important in the construction industry. A 2016 report published by the United

Nations Environmental Program considered the question of how to reduce the carbon footprint of concrete [2]. The main conclusions drawn from this report for curbing global CO_2 emissions in concrete production was to either (1) increase the usage of reactive supplementary cementitious materials, such as slag and fly ash, by replacing a portion of Portland cement clinker with those or (2) reduce the use of Portland cement clinker in concrete mixes by use of a non-reactive filler, such as limestone powder. Other alternatives, such as non-Portland clinkers, were considered in that same report but were found to not be cost effective for global use. Similar conclusions were reported in the 2008 study by the World Wildlife Fund International which found that using cement more efficiently could reduce the CO_2 footprint of concrete by approximately one quarter by 2050 (Figure 1-2).

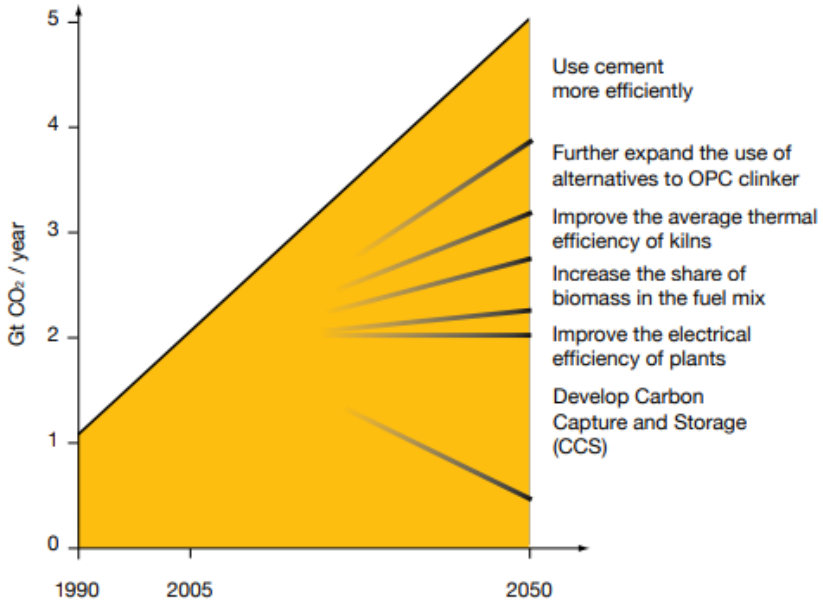

Figure 1-2: Impact of different cement reduction methods projected until 2050 [3]

The main drawbacks to using existing supplementary cementitious materials such as fly ash, slag and silica fume as opposed to using fillers to improve the efficiency of cement is in their availability (Figure 1-3).

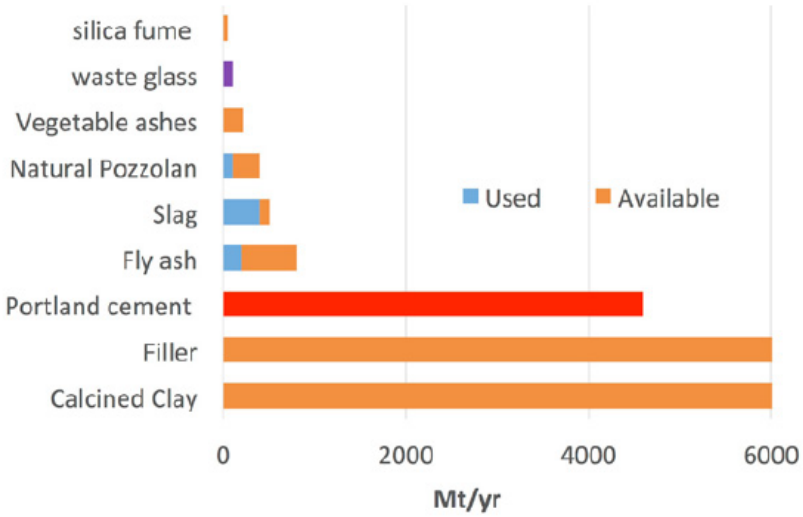

Figure 1-3: Use and availability of cement alternatives [2]

Fly ash, a by-product from burning coal to produce electricity, has been used as a partial substitute for Portland cement in concrete for nearly 80 years. It is estimated that fly ash is used in 50% of all ready-mixed concrete, typically at 20-40% replacement by mass. Not only is fly ash a more environmental friendly alternative to energy-intensive Portland cement, it has the added benefit of increasing workability and long-term durability of concrete at a reduced cost. However, the consequences of the recent 2011 EPA ruling placing higher restrictions on the greenhouse gases emitted by coal burning electricity producers coupled with cheaper natural gas being used to produce electricity, has been a significant reduction in the amount and quality of fly ash acceptable for concrete usage. Some precast concrete suppliers in Georgia, for example, are finding limited availability

of concrete-quality fly ash and are looking for alternatives. An alternative to fly ash being explored in the precast industry is ground limestone powder.

Although limestone powder has only minimal reactivity, it has other benefits, such as improved workability of concrete mixes. Additionally, due to the greater availability of limestone powder compared with fly ash and subsequent reduced transportation cost, an estimated 13% less energy is used in concrete mixes with the same percent cement substitution (Figure 1-4).

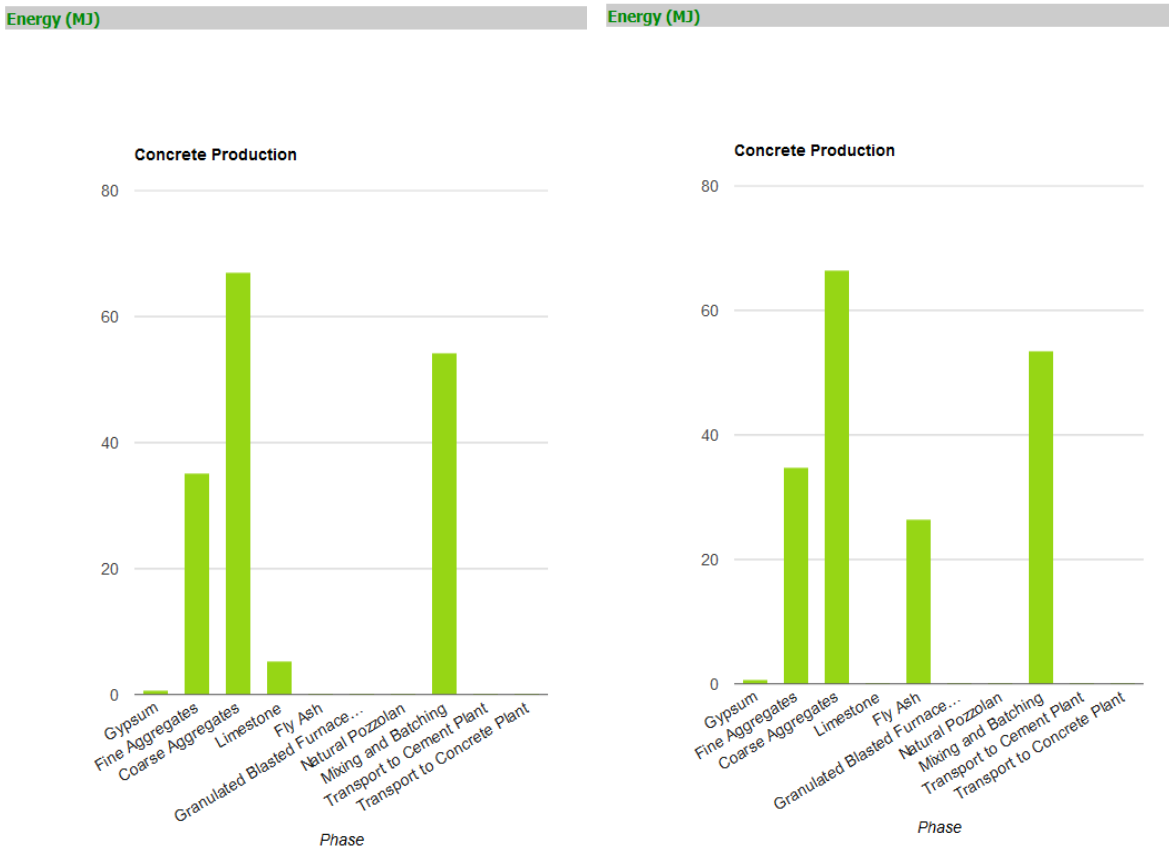

Figure 1-4: Difference in energy production between the same concrete mix with limestone powder versus fly ash using Berkeley Green concrete

Concrete made with limestone contents above 15% by mass are common outside the United States. In 2000, the European EN 197-1 allowed replacement of up to 35% by mass throughout Europe, while the Canadian CSA A3000 code was modified in 2008 to allow replacement of up to 15% by mass [4]. In the United States, ASTM C595 was revised in 2012 to allow the use of limestone in Type IL hydraulic cements at clinker replacements between 5 and 15% [4]. A study compiled by the Portland Cement Association (PCA) showed that concretes with limestone at around 15% replacement had comparable properties as Portland cement mixes and in some cases show improved properties [4]. Bonetti et al. noted that since some cement remains unhydrated in mixes with low water to cement (w/c) ratios, limestone powder can act as an inexpensive filler to replace the unhydrated cement particularly when combined with a more finely ground cement [5].

Fresh and hardened concrete properties of mixes made with limestone vary depending on whether limestone is added as filler (as a replacement for fine aggregate), interground with clinker to produce a Portland Limestone Cement (PLC) or blended with Portland cement and introduced together during the mixing process. Interground limestone blends produce cements with a wider particle size distribution [6]. Limestone that is ground separately and then blended with Portland cement uses less energy, can further contribute to the sustainability of concrete, and allows for increased material tailorability [4]. This tailorability is particularly advantageous in precast concrete production, as the workability, time to set, rate of strength development, and quality of surface finish can be adjusted, even seasonally, with changes in limestone fineness and rate of addition.

One benefit noted from using limestone blended cements is that, when ground more finely than ordinary Portland cement, the increase in paste fineness contributes to increased

cohesion of concrete mixes. This enhanced cohesion may be of particular interest to concrete suppliers using self-consolidating concrete (SCC) or flowing concretes where concrete flows under its own weight to fill formworks and voids. Self-consolidating concrete improves finishes of concrete members, reduces labor costs due to less patching and finishing work, reduces labor cost due to the elimination of vibration, and extends the longevity of formwork due to the lack of vibration [7]. Concrete mixes using limestone powder show improved workability leading to better surface finish, improved slump without additional water, reduced bug holes in vertical surfaces and less segregation and bleeding [8]. This greater finish aesthetic and reduced need for patching speeds up the post processing time at precast concrete plants. Precast plants have also noticed less segregation and more uniform aggregate distribution when using mixes with limestone powder [9]. Precast plants have found that the introduction of limestone reduced the demand for sand and that the soft powder is less abrasive than other additives, leading to increased equipment longevity [9].

Although extensive research exists on interground limestone cements, limited research currently exists regarding the use and long-term performance of limestone powder used in self-consolidating concrete. Existing research shows inconclusive results as to the impacts on physical and mechanical properties of concrete. Oftentimes, the actual influence of the limestone filler cannot be isolated since comparisons were made to mixes containing fly ash with different percent substitution rates, varying superplasticizer dosages, and mixes at varying water to cement (w/c) or water to cementitious material (w/cm) ratios [10] [11] [12]. Few studies investigate the impact of the particle size

distribution of both the cement and the limestone powder and how this influences early age and late age concrete properties.

In this research, the effects of the limestone powder on cement hydration, rheology, and mechanical properties are explored, with a focus on producing SCC mixtures suitable for precast concrete. Three cements made from the same base clinker and four limestone powders from the same quarry ground at varying median particle sizes were evaluated. The focus was the influence of a) cement type, either ASTM C150 Type I/II or Type III from the same manufacturer, b) the median particle size of the limestone powder used as cement substitution with 3 μm, 15 μm, 25 μm, or 40 μm median particle size, and c) the percentage of cement replacement by mass of limestone powder. These results were compared with a Type IL cement produced by the same cement manufacturer as the OPC used, but with a limestone content of approximately 9%.

1.2 Research objectives

The primary objective of this research was to understand how both the particle size and percentage of limestone powder used to replace a portion of cement in self-consolidating concrete influence the fresh and hardened properties of concrete mixes. A multi-scale approach was used. That is, the research investigated the limestone-cement interactions at the cement paste level first to gain insights into developing concrete mixes with limestone used as partial cement replacement. Based upon paste compositions and observed behaviors, upscaling to concrete mixtures was then evaluated. The concrete mix designs were based on mixes used at local (Atlanta metropolitan area) precast suppliers but

were modified for specific laboratory considerations and to isolate the role that the limestone powder played on concrete properties. The specific goals were:

- To determine how limestone replacement quantity and median particle size affects early-age properties including hydration kinetics, time of set, and workability in cement pastes
- To determine how limestone replacement quantity and median particle size affects fresh concrete properties such as slump flow, viscosity, and surface finish
- To determine how limestone replacement quantity and median particle size affects hardened concrete properties such as strength evolution, volume stability and permeability
- To determine whether existing models can be used to predict the drying shrinkage and creep behavior of concrete made with limestone blended cements
- To investigate the validity of upscaling from paste to concrete in assessing rheology and creep in self-consolidating mixtures
- To provide recommendation for tailoring concrete mixtures to meet specific performance targets by varying the quantity and median particle size of cement and limestone powders

1.3 Research approach

The research was organized into two main sections. The first section studied the limestone influence at the cement paste level. The research investigated both the effect that median particle size of limestone powder has on hydrating cements of varying median particle size and the effect of replacing cement with varying percentages of limestone

powder. Measured quantities were heat of hydration determined through isothermal calorimetry, setting time determined by Vicat needle, and workability measured through mini slump tests.

The focus of the second section was on the fresh and hardened properties of fifteen concrete mixes produced with varying amounts of three limestone powders and three cements. During the cement paste study, the characteristics of the 15 and 25 μm limestone powder were found to be so similar, that concrete mixes were produced with only the 25 μm limestone powder. The cements therefore were blended with limestone powder that was ground finer, similar, and coarser to the base cement. The workability and stability of each concrete mix was evaluated through slump flow measurements and visual stability index. Compressive strength measurements were taken at 1, 3, 7, 28 and 90 days to evaluate how the hydration of each mix affects strength evolution. Dimensional stability was determined through month-long measurements of drying shrinkage and creep. To predict permeability and durability of the concrete mixes, both surface resistivity and rapid chloride penetration test were measured independently and then correlated.

Each section addresses both the influence of the cement-limestone percent substitution interaction and the cement-limestone fineness interaction. The pastes and concrete were prepared using three cements: Type I/II, III, and IL (from the same manufacturer) combined with four limestone powders of varying median particle size: 3 μm, 15 μm, 25 μm, and 40 μm (ground from the same limestone quarry). For all mixes, whether studying cement paste or concrete, the water-to-binder ratio and aggregate proportions were kept constant.

The various mixes produced with combinations of cement and limestone powders at various cement replacement substitutions and varying limestone median particle size are discussed in Chapter 4 and Chapter 5. Cement pastes, mortars and concrete mixes were classified by (1) the cement type used: T1 for Type I/II, T3 for Type III, and T1L for Type IL, (2) the size of the limestone powder: L3, L15, L25, and L40 for limestone powders with median particles sizes of 3, 15, 25, and 40 μm, respectively, and (3) the percent cement substitution denoted in parenthesis (X). Thus, T3L25(15) is a mix blending Type III cement with 25 μm limestone powder at a 15% cement replacement.

CHAPTER 2. LITERATURE REVIEW

2.1 Historical use of limestone powder with cements

Limestone powder has been used as a constituent of concrete since the 1960's when, during an energy crisis, Spain and Germany allowed the limestone powder to replace Portland cement by up to 10% by mass [4]. A decade later, France followed suit joining Spain to allow cement to be composed of up to 35% limestone by mass [4]. Other countries, such as New Zealand, began allowing limestone in their cements in the 1990's at a cement replacement of up to 15% by mass [4]. Today most countries in Europe allow limestone to replace cement by up to 35% by mass and worldwide over 39 countries allow some sort of cement replacement with values generally around 20 % by mass [4]. Canada and the United States only recently allowed limestone to replacement cement by up to 15% by mass (ASTM C595 and AASHTO M240) [4] [13]. A brief timeline is presented in Figure 2-1.

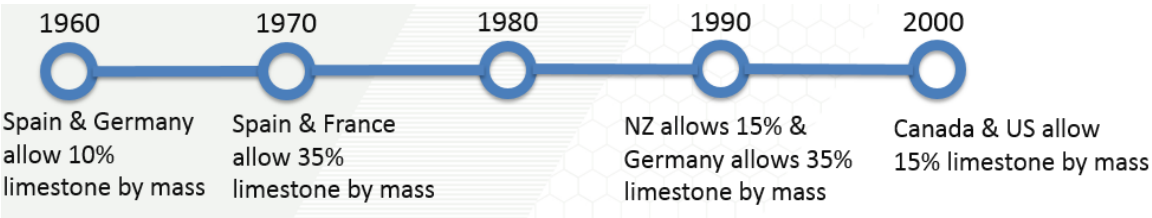

Figure 2-1: Timeline of limestone powder usage in cement

Limestone powder can be either interground with Portland cement referred to as PLC or blended with Portland cement during the mixing process. In Europe PLC is designated

as CEM X-L and CEM X-LL depending on the specific proportions and strengths. In Canada, it is referred to as GUL and in the United States it is called Type IL.

2.2 Hydration of Portland cement with limestone powder

Cement clinker is composed mainly of calcium, silica, alumina and iron oxides. The compounds' chemical composition are labeled in cement chemistry notation as C_3S, C_2S, C_3A and C_4AF where C = CaO, S = SiO_2, A = Al_2O_3, and F = Fe_2O_3 [14]. Gypsum, $C\bar{S}H_2$, is also added to cement to control the rate of hydration of C_3A, where $\bar{S}$ = SO_3. When water is added to cement, calcium sulfate and high temperature compounds of calcium disassociate into the pore solution [14]. During the first few minutes, C_3A reacts with sulfates to form ettringite or $C_6A\bar{S}_3H_{32}$. Within the first few hours of hydration, calcium hydroxide (CH) and then calcium silicate hydrates (CSH) form from the hydration of C_3S and C_2S. CSH occupies around 50-60% of the hydrated cement solids and is considered the most important in determining concrete properties [14]. CH occupies 20-25% of the solid volume of hydration cement and contributes less to concrete properties. After a few days, ettringite can further react with any remaining C_3A to form monosulfate, $C_4A\bar{S}H_{12}$. The remaining solid volume is occupied by calcium sulfoaluminate hydrates and unhydrated cement [14].

The addition of limestone powder to concrete affects cement hydration in four ways:

1) Dilution – Due to the replacement of cement with a much less reactive filler, the properties associated with the hydration of cement diminish, leading to an increase in the effective water to cement ratio (w/c). However, at w/c below 0.356, cement does not fully hydrate due to insufficient available space and at w/c ratios above 0.42, the

cement cannot fully hydrate if there is no additional source of water [15]. Recognizing that not all cement hydrates between these two ranges of w/c, limestone powder becomes a viable option as an inexpensive filler if it replaces the unhydrated cement [15].

2) Particle packing density – Particles of varying sizes pack better than particles of the same or similar sizes. Cements blended with limestone powder ground finer than the base cement have decreased interparticle spacing compared with coarser limestone. Due to increased surface area, this can lead to accelerated hydration. But, it may also lead to higher capillary stresses and increased autogenous shrinkage [16]. Cements blended with limestone particles ground coarser than the base cement have increased interparticle spacing and have been found to decrease autogenous shrinkage and early age cracking [16].
3) Nucleation sites – Due to its increased surface area, finer ground limestone provides nucleation sites for CSH precipitation [4] [17]. This increased surface area also leads to an acceleration of C_3S hydration, faster set times and reduced overall porosity [15, 18] [19]. Although other fillers can act as nucleation sites, Oye found that limestone was much more effective than quartz due to its ability to participate in ion exchange [20].
4) Chemical interactions – Although limestone powder was once considered to be inert, there is conflicting research regarding its potential to react with certain cement compounds. Studies show that instead of reacting with ettringite to form monosulfate, excess C_3A may react with limestone ($CaCO_3$) to make a more stable monocarbonate and tricalcium aluminum carbonate hydrates [10, 21, 22]. This stabilized ettringite

leads to an increase in the volume of hydrates, which should lower porosity [22, 23]. On the other hand, Ye used thermal analysis and BSE imaging analysis of the hydration of self-consolidating cement pastes during various ages and concluded that limestone did not chemically react with the cement [11]. This difference in conclusions could be due to the type of limestone used in each study. Bentz found that calcitic limestone, such as what is used in this research, provided favorable surfaces for nucleation of CSH to occur and for carbonate ions to react with C_3A, whereas aragonite polymorph limestone did not react with the aluminate phases unless it was calcined [24].

In summary, many competing factors influence the hydration of cement with limestone powders. The particle size distribution of both the limestone and cement becomes important to understand hydration and the physical and mechanical properties of the concrete produced. Finer ground limestone enhances hydration by creating more nucleation sites and improving packing density [25]. Neto and Campiteli found that there is a balance between viscosity and yield stress when using limestone powders at substitution rates of up to 15% [26]. Although finely ground limestone powders improve cohesion, they can have a negative effect on workability, while coarser ground limestone powders improve workability. How these four competing factors influence concrete properties is not clearly understood.

2.3 Quantifying the effect of limestone median particle size distribution

Quantifying the influence that the limestone powder has on the cement blends would be an important contribution to predicting the effect on various properties and to better tailor concrete mixes. When investigating blends of various cements, Bentz used

law of mixtures to determine the influence of hydration kinetics, chemical and autogenous shrinkage, setting time and compressive strength using Equation 2-1 below [27]:

$$P_{blend} = P_{comp\,1}\, x\, f_{comp\,1} + P_{comp\,2}\, x\, f_{comp2} \qquad 2\text{-}1$$

where the blended property is the sum of the property component multiplied by the mass fraction of each component. Bentz used this for cements, which have equal hydrating possibilities. It is unclear if this method would work for limestone and cement blends where the limestone is inert and less reactive.

Kumar et al. quantified the effect of the particle size distribution and proposed an area multiplier, AM, which can be estimated based on the percent cement replacement, r, and the specific surface area of the cement, SSA_C, and limestone filler, SSA_F, using the following equation [28] [29]:

$$AM = \frac{100 + \frac{(r.SSA_F) + ((100 - r)\ \mathrm{x}\ SSA_C)}{(100 - r)\ \mathrm{x}\ SSA_C}}{100} \qquad 2\text{-}2$$

The quantity AM becomes a scaling factor for use in determining concrete properties. AM is equal to unity when the specific surface area of the limestone filler is closest to the specific surface area of the cement. When the limestone powder is ground finer than the cement and has a larger specific surface area or is used in greater cement replacement quantities, AM will be greater than unity. AM becomes large when a large quantity of fine particles is present, without accounting for the dilution effect. Knop showed that the AM multiplier may work well for blends with fine limestone powder but

does not work well for blends made with coarser limestone particles, where the dilution is more pronounced and not accounted for with the AM factor [30].

Knop proposed determining a blended surface area of the cement-limestone mix by the rule of mixtures, similar to Bentz. He proposes using a blended surface area ratio that is the ratio between the cumulative sum of each percent powder, *f*, multiplied by its specific surface area (either $SA_{limestone}$ or SA_{cement}) as a function of the surface area of the cement, SA_{cement} [30]:

$$Surface\ Area\ Ratio\ = \frac{fSA_{limestone} + (1-f)SA_{cement}}{SA_{cement}} \qquad 2\text{-}3$$

In order to determine rheological properties of blended limestone cement mortars, Yahia used a packing density formula based on a model proposed by Caquot, adapted by de Larrard and reported by Hu et al. [31, 32]

$$\beta = 1 - 0.45\left(\frac{D_{10}}{D_{90}}\right)^{0.19} \qquad 2\text{-}4$$

where only the influence from the D_{10} and D_{90} particles are quantified. The D_{10} and D_{90} represents that 10% and 90%, respectively, of particles are smaller than these values.

Nadelman in her dissertation determined that the hydration kinetics such as time to peak, magnitude of peak, and degree of hydration of the Type IL cements she was investigating were most influenced by specific surface area, D_{10}, $D_{3,2}$, $D_{4,3}$ and D_{90} [33].

The $D_{3,2}$ and $D_{4,3}$ are the surface-weighted and volume-weighted median particle size. It is clear from all these studies that the particle size distribution has a major influence on hydration kinetics and being able to determine blends of these can help better predict the behavior of limestone blended cements. Comparisons of parameters and cement hydration properties are presented in Appendix A.

2.4 Properties of concrete produced with limestone powder

Intergrinding limestone with cement or blending ground limestone powder with commercially manufactured cements affects concrete rheology, volume of voids, and water demand. Schmidt found using 15% to 20% limestone resulted in optimal packing density of concrete mixes, when mixed with optimal cement particle size [34].

2.4.1 Effects on Fresh Concrete Properties

Research shows conflicting results regarding the increased workability of concrete with increasing use of limestone replacement and is highly dependent on the fineness of the limestone. Vuk et al., Nehdi and Tsivilis et al. found that using a finely ground limestone as a partial cement replacement improved rheological properties, while El-Didamony found that workability decreased as limestone powder percent replacement increased [35] [36] [37] [38]. Although there is disagreement regarding the effect limestone powder has on workability, most researchers agree that finely ground limestone powders with increased surface area reduced bleeding [35] [36] [37] [38].

Research also shows conflicting results for how limestone affects set time [6]. El-Didamony found that at low levels of cement replacement with limestone, set time

increased, while at higher limestone addition rates, the set times decreased. Decreased set times can be attributed to more efficient particle packing and carboaluminate reactions occurring in limestone blended cements [35] [39]. On the other hand, Ezziane found that set times were increased due to the dilution effect in mortars made with limestone replacements of up to 30% [40].

Cement hydration is an exothermic process. The heat generated by the hydration of cements can also be affected by the replacement of limestone with cement. Since limestone powder can provide nucleation sites for hydrating cement, increases in rate and heat of hydration have been observed [17]. When limestone acts to dilute cement, less heat is generated during cement hydration. This decreased heat can be of interest in mass concrete projects. Mass concrete is defined to be any concrete element with size larger than three feet [41]. With such large structures, the surface of the element exposed to air or curing water tends to cool more rapidly during hydration than the center, which remains insulated by the surrounding concrete. This differential in temperature gradient across the section of concrete can lead to thermal damage and cracking [14].

2.4.2 Effects on Hardened Concrete Properties

When limestone powder replaces a portion of the cement, due to dilution effects, concrete strength decreases. However, similar strength concretes can be achieved with interground limestone blends, when it is ground finer than the base cement due to increased nucleation sites and increased particle packing [4]. Most studies aimed at comparing compressive strengths of ordinary Portland cements (OPC) with Portland limestone cements (PLC) are comparing two cements of vastly different particle size distributions

since generally the PLC had been ground finer to achieve similar compressive strengths to that of the OPC [5]. It is unclear how compressive strength would be affected by blending limestone powders of varying median particle size with OPC. Although it would be expected that if finely ground limestone powders are blended with OPC, the increased hydration rate due to enhanced nucleation should lead to higher early strengths [17].

Alunno-Rosetti and Curcio found that due to reduced volume of "cement gel", concretes produced with 20% cement replacement by mass had significantly higher creep rates when loaded at 28 days than corresponding OPC concretes, but had similar shrinkage strains [42]. However, Dhir found similar creep rates and slightly reduced shrinkage for concretes made with blended cements of up to 45% limestone [43]. Bucher also found slightly reduced shrinkage values with limestone blended cements of up to 10% cement replacements rather than OPC concrete [44]. Most shrinkage and creep research looked at specimens cured for 28 days before measuring shrinkage and creep, whereas precast plants typically stress concrete members at far earlier ages.

It is worth noting that most studies conducted are on cements where the limestone has been interground with the clinker and less research pertains to concrete where the limestone is added as a concrete constituent. Adding limestone to concrete mixes is more common in precast plants and mainly used to improve workability to achieve flowing concrete similar to self-consolidating concrete mixes [8, 9].

2.5 Precast Concrete and Self-Consolidating Concrete (SCC)

Self-consolidating concrete (SCC) was first developed in Japan in the late 1980's and is slowly finding more commercial usage [45]. SCC must be fluid enough to fill forms

without external energy, must remain homogenous throughout placement, and be flowable through dense reinforcement [46]. A good SCC mix is described by its ability to fill voids in the formwork of any shape, pass around reinforcement and be stable enough to experience no segregation or bleeding [47]. Precast plants use flowing concretes similar to self-consolidating concrete mixes to increase production, reduce or eliminate the need to vibrate formwork and to achieve concretes with improved surface finish, leading to reduced post-production time [45].

To reduce bleeding, SCC mixes must either have a high fine particle content or use a viscosity modifying agent (VMA) [48]. Replacing a portion of the cement with an inexpensive filler, such as limestone powder, would be cost effective since according to workers at a metro Atlanta precast plant, cement costs around $100/ton, while white limestone powder costs roughly half as much, around $50/ton, and impure limestone powder costs even less [8]. As a comparison, Type IL cement is only a few dollars per ton less than Type I cement. Additionally, the soft limestone powder is less abrasive to mixing equipment and precast plants are finding that they need to replace augers less frequently with limestone powder [9]. Not only is limestone powder cost effective, it provides architectural benefits as well. Due to its white color, limestone powder additions do not interfere with the color of architectural precast panels as other additives might. Precast suppliers have also noticed that limestone powder mixes have less agglomeration and segregation than other mixes, and show a uniform aggregate distribution [8].

Precast suppliers often use post-tensioned members where concrete beams and slabs are stressed in compression shortly after casting. The hardened concrete must reach a certain compressive strength before post-tensioning strands can be stressed. To speed up

assembly and clear concrete beds for the next batch of members to be cast, precast suppliers rely on members reaching a high early strength. Any change in the mix design using limestone powders must not negatively impact the high early strength common in precast concrete mixes.

According to some studies, limestone cement blends can be beneficial to both cost and flowability by lowering the cement fraction, but may cause additional shrinkage and creep [12]. On the other hand, adding limestone powder to SCC may stabilize the mix due to the higher proportion of fines since smaller rounded particles flow better than larger angular particles. From discussion with precast suppliers, an optimal mix would contain around 20-25% limestone powder to optimize cost and workability, but still provide for high early strength to be able to demold and stress tendons of post-tensioned members [9]. The SCC mix developed used in this research are discussed further in Chapter 5.

High range water reducers (HRWR) are used to give self-consolidated mixes the workability they need without the addition of excess water, which would reduce compressive strength. HRWR have several characteristics that need to be considered when proportioning concrete mixes. They can act as a hydration accelerator, so caution should be used when comparing mixes with varying dosages of HRWR admixtures [49]. The effect of HRWR admixtures is time dependent, where initial workability takes a few minutes to take effect and is noticeably diminished within 30 to 60 minutes after mixing [50]. Therefore, workability of cement pastes and concrete mixes, which include HRWR, should be measured at set time intervals.

2.6 Drying Shrinkage

When concrete is kept below 100% relative humidity, free and adsorbed water evaporates from the hardened cement paste causing dimensional instability in the concrete [14]. First moisture is lost through evaporation of the large cavities found in the cement paste. With continued drying, adsorbed water and water in small capillaries is lost [14]. Finally, with severe drying, water bound in the interlayer of the cement paste CSH is removed. The loss of water results in a dimensional change to the concrete specimen. This change in dimensional stability ranges between 400 - 1000 microstrains and thus must be considered in structural design of concrete elements [14]. Restrained dimensional change could result in internal stress build up and cracking or failure of concrete specimens [14].

The dimensional instability of concrete members driven by the loss of moisture to the atmosphere is called drying shrinkage. Drying shrinkage is affected by the porosity of the concrete, the aggregate strength and content, the cement and water content, time of exposure to drying, the ambient relative humidity and the geometry of the concrete member [14]. The drying shrinkage versus time relationship tends to follow a hyperbolic curve tending to approach an ultimate value [51]. Over the past 30 years, several models have been proposed to assist structural designers in predicting drying shrinkage over time based on this hyperbolic behavior [51]. The models contain a measure of concrete mechanical properties either obtained by experimental results or predicted through mixture proportions. They all consider ambient relative humidity, duration of drying and specimen size. The models differ in what information is required to make predictions and what the basis of the model is. For example, in the model proposed by ACI 209R only cement content is used to assess mechanical properties, whereas the concrete mean compressive

strength at 28 days is used for the CEB MC90-99 model, and both compressive strength and water-cement ratio are used for the models proposed by Gardner-Lockman and Bažant-Baweja [51].

2.6.1 ACI 209R-92 model

The ACI model was first developed in 1971 by Branson and Christiason [52] and was later modified by ACI Committee 209. The model requires the age of concrete when drying starts t_c, the curing method (moist or steam curing), the ambient relative humidity, the volume to surface ratio of the concrete specimen *V/S*, and the cement type. Modifications to the ultimate shrinkage value can be made to account for the initial moist curing duration, concrete slump, the fine aggregate percentage, the cement content, and air content. The time dependent shrinkage function is expressed as a hyperbolic curve that tends to an asymptotic value called the ultimate shrinkage ε_{shu} and shown in equation 2-5 below.

$$\varepsilon_{sh}(t, t_c) = \frac{(t - t_c)^{\alpha}}{f + (t - t_c)^{\alpha}} \varepsilon_{shu} \qquad 2\text{-}5$$

In the above equation, f and α are constants accounting for curing regime and volume/surface ratio of the concrete, and $(t - t_c)$ represents the time from end of initial curing. The ultimate strain ε_{shu} can be modified by seven factors, γ_{sh},x, accounting for specific conditions such as moist curing duration, relative humidity, member geometry, the concrete slump, fine aggregate ratio, cement content, and air content with the general equation and factors listed below:

$$\varepsilon_{shu} = 780\,\gamma_{sh,tc}\,\gamma_{sh,RH}\,\gamma_{sh,vs}\,\gamma_{sh,s}\,\gamma_{sh,\Psi}\,\gamma_{sh,c}\,\gamma_{sh,\alpha} \times 10^{-6} \qquad 2\text{-}6$$

where $\gamma_{sh,tc}$ is the correction for moist curing, $\gamma_{sh,RH}$ is the correction for relative humidity, $\gamma_{sh,vs}$ is the correction for volume to surface ratio, $\gamma_{sh,s}$ represents the slump factor, $\gamma_{sh,\psi}$ adjusts for the aggregate ratio, $\gamma_{sh,c}$ is the cement content correction, and $\gamma_{sh,\alpha}$ is the air content adjustment.

2.6.2 Bažant-Baweja B3 model

The B3 model was proposed by Bažant and his co-workers at Northwestern University as a way to predict shrinkage and creep [53]. Similar to the ACI model, the model predicts the shrinkage strain based on a time dependent factor multiplied by the ultimate strain value $\varepsilon_{s\infty}$. It differs from the ACI method in that the effects of concrete composition such as slump and air content are not considered. The model requires the age of concrete when drying begins; the aggregate, water and cement contents; the cement type; the concrete compressive strength at 28 days; the curing condition; the relative humidity and shape of the specimen. The following equations, in in-lb units, show the calculations for drying shrinkage over time:

$$\varepsilon_{sh}(t, t_c) = -\varepsilon_{s\infty} \frac{E_{cm607}}{E_{cm(t_c+\tau_{sh})}} k_h S(t - t_c) \qquad 2\text{-}7$$

$$\varepsilon_{s\infty} = -\alpha_1 \alpha_2 [0.02565 w^{2.1} f_{cm28}^{-0.28} + 270] \times 10^{-6} \qquad 2\text{-}8$$

$$E_{cmt} = E_{cm28}(\frac{t}{4 + 0.85t})^{0.5} \quad 2\text{-}9$$

$$S(t - t_c) = tanh\sqrt{\frac{t - t_c}{\tau_{sh}}} \quad 2\text{-}10$$

$$\tau_{sh} = 190.8t_c^{-0.08}f_{cm28}^{-0.25}[2k_s(\frac{V}{S})]^2 \quad 2\text{-}11$$

where $E_{cm607}/E_{cm(tc+\tau sh)}$ is a factor accounting for time dependence of the ultimate shrinkage, k_h is the humidity dependence factor, $S(t - t_c)$ is the time curve and $(t - t_c)$ is the time from the end of initial curing. The parameters α_1 and α_2 account for the type of cement and curing condition. The main drawback of this model is that it does not take into account the effect of concrete composition and design strength on the model parameters [51].

2.6.3 CEB MC90-99 model

The CEB MC90 model was first proposed in 1990 by Muller and Hilsdorf and then modified in 1999 [54]. It differs from other models in that it does not require information regarding the curing condition or curing duration and that the correction term for relative humidity is extremely sensitive. The required parameters are age of concrete when drying starts, the concrete compressive strength at 28 days (f_{cm28}), the average relative humidity (h), the volume-surface ratio (V/S) and cement type. The total shrinkage strains $\varepsilon_{sh}(t,t_c)$, in in-lb units, at concrete age t of the concrete specimen are predicted as follows:

$$\varepsilon_{sh}(t, t_c) = \varepsilon_s(f_{cm28})\beta_{RH}(h)\beta_s(t - t_c) \quad 2\text{-}12$$

$$\varepsilon_s(f_{cm28}) = [160 + 10\beta_{SC}\left(9 - \frac{f_{cm28}}{1450}\right)] \times 10^{-6} \quad 2\text{-}13$$

$$\beta_{RH}(h) = -1.55[1 - (\frac{h}{h_0})^3] \quad 2\text{-}14$$

$$\beta_s(t, t_c) = [\frac{(t - t_c)/t_1}{350[(V/S)/(V/S)_0]^2 + (t - t_c)/t_1}]^{0.5} \quad 2\text{-}15$$

where $\beta_{RH}(h)$ is the coefficient for relative humidity between 40 and 99%, h is the relative humidity, $\beta s(t - t_c)$ is the time dependent coefficient of drying shrinkage, $(t - t_c)$ is the time since end of initial curing, f_{cm28} is the mean compressive cylinder strength of concrete at 28 days, β_{SC} is a factor to account for the cement type , h_0 is equal to 1, V/S is the volume-surface ratio and $(V/S)_0$ is equal to 2 in.

2.6.4 GL2000 model

The GL2000 model was first presented by Gardner and Lockman in 2001 and later modified in 2004 [55]. The approach is to have a model available to designers with information generally available at design, namely, the 28-day specified compressive strength (f_{cm28}), the strength at loading, element size expressed as volume-surface ratio (V/S) and relative humidity (h). The required parameters are age of concrete when drying starts ($t - t_c$), the mean compressive strength at both 28 days and time of loading, the relative humidity and the volume-surface ratio of the member. Predicted values can be improved

by measuring concrete strength development over time. The aggregate stiffness can be back calculated from the measured modulus of elasticity and the average measured cylinder strength. The time dependent drying shrinkage strains, $\varepsilon_{sh}(t,t_c)$, are defined by the following equations:

$$\varepsilon_{sh}(t,t_c) = 900k\left(\frac{4350}{f_{cm28}}\right)^{1/2} \times 10^{-6}\beta(h)\beta(t-t_c) \qquad 2\text{-}16$$

$$\beta(h) = (1 - 1.18h^4) \qquad 2\text{-}17$$

$$\beta(t-t_c) = \left[\frac{(t-t_c)}{(t-t_c) + 77(V/S)^2}\right]^{1/2} \qquad 2\text{-}18$$

where $\beta(h)$ corrects for relative humidity, h is the relative humidity, $\beta(t - t_c)$ accounts for the time effect of drying and k is a shrinkage constant based on cement type.

2.6.5 AASHTO-LRFD Model

The AASHTO LRFD Bridge Design Specifications (Section 5.4.2.3.3) uses an equation based on an ultimate shrinkage value modified for volume-surface ratio, relative humidity, and strength of concrete at time of drying. The following equation is used to predict drying shrinkage in in-lb units:

$$\varepsilon_{sh}(t) = k_s k_{hs} k_f k_{td} 0.48x10^{-3} \qquad 2\text{-}19$$

$$k_s = \left[\frac{t}{\frac{26e^{0.36(V/S)} + t}{\frac{t}{45 + t}}}\right] x \left[\frac{1064 - 94(\frac{V}{S})}{923}\right] \quad 2\text{-}20$$

$$k_{hs} = 2.0 - 0.14H \quad 2\text{-}21$$

$$k_f = \frac{5}{1 + f'_{ci}} \quad 2\text{-}22$$

$$k_{td} = \frac{t}{61 - 4f'_{ci} + t} \quad 2\text{-}23$$

where *V/S* is the volume to surface area ratio, *H* is the relative humidity, *t* is the time since curing finished and drying began, and f_{ci}' is the concrete compressive strength at start of prestressing or loading and can be taken as $0.8f_c'$.

According to data evaluated by ACI Committee 209, the best shrinkage results were achieved using the Bažant-Baweja B3 and the Gardner-Lockman 2000, whereas the CEB MC90-99 tended to underestimate the shrinkage strains [56]. In Chapter 6 of this thesis, the experimental drying shrinkage results of the concrete mixes made with limestone blended cements are evaluated and compared with the five drying shrinkage models presented here.

2.7 Creep

Similar to drying shrinkage, creep is associated with the loss of water in cement paste voids and bound in the CSH interlayers [57]. Unlike drying shrinkage that occurs due to a

drop in ambient relative humidity, the driving force for creep is the application of a sustained load. Creep is affected by the cement porosity, microcracks in the interstitial zone (ITZ) between the aggregate and cement paste, aggregate strength and content, age of concrete at loading, relative humidity and member geometry [14].

The total strain experienced by concrete under sustained load is generally considered the summation of four phenomena – elastic strain, free shrinkage strain, basic creep, and drying creep (see Figure 2-2) [58]. Elastic strain is the reversible elastic deformation which occurs when load is applied to concrete in the elastic range, generally considered to be below 40% of the concrete strength at loading [14]. Free shrinkage strain is associated with the evaporation of free water in the cement pores. Even at a relative humidity of 100%, concrete under a sustained load will experience deformation, referred to as basic creep [57]. Drying creep is the additional strain that occurs when loaded concrete is exposed to low relative humidity [14]. Total creep is the sum of drying and basic creep.

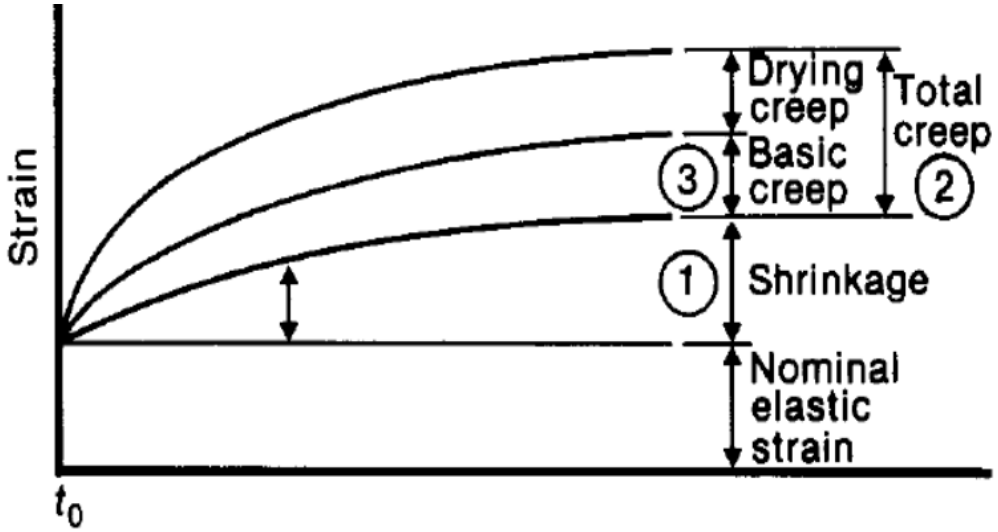

Figure 2-2: Total time-dependent strain of externally loaded concrete [58]

The models presented earlier for drying shrinkage have corresponding creep models. Most models normalize creep strain by presenting an approximation of creep compliance, $J(t,t_0)$, which represents the creep strain per unit uniaxial constant stress.

2.7.1 ACI 209R-92 model

Like its drying shrinkage equation counterpart, the ACI creep model assumes that creep behavior is hyperbolic and approaches an ultimate creep strain value, φ_u. Here the compliance function $J(t,t_0)$ that represents the total stress dependent strain by unit stress is calculated using the following equations in in-lb units:

$$J(t,t_0) = \frac{1+\varphi(t,t_0)}{E_{cmt0}} \quad \text{2-24}$$

$$E_{cmt0} = 33\gamma_c^{1.5}\sqrt{f_{cmt0}} \quad \text{2-25}$$

$$\varphi(t,t_0) = \frac{(t-t_0)^{\psi}}{d+(t-t_0)^{\psi}}\varphi_u \quad \text{2-26}$$

where $\varphi(t,t_0)$ is the creep coefficient at concrete age t due to applied load at age t_0; f_{cmt0} is the mean concrete compressive strength at the time of loading, d and ψ are constants for a given member geometry and φ_u is the ultimate strain. The ultimate strain can be modified based on curing regime, ambient relative humidity, volume-surface ratio, slump factor, fine aggregate content and air content.

2.7.2 Bažant-Baweja B3 model

The three-part B3 creep compliance equation, $J(t,t_0)$, has a component for instantaneous strain, q_1; a basic creep component, $C_0(t,t_0)$; and a drying creep factor, $C_d(t,t_0,t_c)$. The model differs from other models in that the drying creep component differentiates between age of concrete, t, the age drying began, t_c, and the age of concrete at onset of sustained loading, t_0. Creep compliance is defined by the following equations:

$$J(t,t_0) = q_1 + C_0(t,t_0) + C_d(t,t_0,t_c) \qquad 2\text{-}27$$

$$q_1 = \frac{0.6}{E_{cm28}} \qquad 2\text{-}28$$

$$C_0(t,t_0) = q_2 Q(t,t_0) + q_3 \ln[1 + (t-t_0)^n] + q_4 \ln(t/t_0) \qquad 2\text{-}29$$

$$C_d(t,t_0,t_c) = q_5[\exp(-8H(t)) - \exp(-8H(t_0))]^{1/2} \qquad 2\text{-}30$$

where $q_2Q(t,t_0)$ is a term for the aging viscoelastic compliance, q_3 is a nonaging viscoelastic parameter, q_4 is a parameter for the aging flow compliance, and q_5 is the drying creep compliance parameter. To calculate the q parameters knowledge of the concrete mean compressive strength f_{cm28}, the cement content c, the water-cement ratio w/c, and the aggregate-cement ration a/c is required. $H(t)$ and $H(t_0)$ are spatial averages of the pore relative humidity h as a function of the age of concrete and the age the concrete was loaded, respectively.

2.7.3 CEB MC90-99 model

The compliance function $J(t,t_0)$ for the CEB MC90-99 model is similar to the ACI model in that it has an initial strain component plus a time dependent creep coefficient component $\varphi_{28}(t,t_0)$, but differs in that the creep coefficient is normalized by the mean modulus of elasticity at 28 days rather than the modulus of elasticity at the time of load application. The compliance function and creep coefficient for the CEM MC90-99 model, in in-lb units, is defined by the following equations:

$$J(t,t_0) = \frac{1}{E_{cmt0}} + \frac{\varphi_{28}(t,t_0)}{E_{cm28}} \qquad 2\text{-}31$$

$$E_{cmt} = E_{cm28}\exp[\frac{s}{2}(1-\sqrt{\frac{28}{t}})] \qquad 2\text{-}32$$

$$E_{cm28} = 3{,}118{,}310\sqrt[3]{\frac{f_{cm28}}{1450}} \qquad 2\text{-}33$$

$$\varphi_{28}(t,t_0) = \varphi_{RH}(h)\beta(f_{cm28})\beta(t_0)\beta_c(t-t_0) \qquad 2\text{-}34$$

where $o_r(h)$is term accounting for ambient relative humidity and volume-surface ratio, $\beta(f_{cm28})$ accounts for the 28 day compressive strength, and both $\beta(t_0)$ and $\beta_c(t - t_0)$ describes the development of creep with time after loading. Additional factors can be included to modify the coefficients based on type of cement *s* and temperature conditions during curing or loading.

2.7.4 GL2000 model

The format of the compliance function $J(t,t_0)$ for the GL2000 model is similar to the CEM MC90-99 model in that it has an initial strain component normalized by the mean modulus of elasticity at time of load application plus a time dependent creep coefficient component $\varphi_{28}(t,t_0)$ normalized by the mean modulus of elasticity at 28 days. The equations, in in-lb units, used to calculate mean modulus of elasticity and creep coefficient differ from that of the CEM MC90-99 model and are defined by the following equations:

$$J(t,t_0) = \frac{1}{E_{cmt0}} + \frac{\varphi_{28}(t,t_0)}{E_{cm28}} \qquad 2\text{-}35$$

$$E_{cmt} = 500{,}000 + 52{,}000\sqrt{f_{cmt}} \qquad 2\text{-}36$$

$$\varphi_{28}(t,t_0) = 2\frac{(t-t_0)^{0.3}}{(t-t_0)^{0.3}+14} + \left(\frac{7}{t_0}\right)^{0.5}\left(\frac{(t-t_0)}{(t-t_0)+7}\right)^{0.5} + 2.5(1-1.086h^2)\left(\frac{(t-t_0)}{(t-t_0)+77(V/S)^2}\right)^{0.5} \qquad 2\text{-}37$$

where the creep coefficient contains two terms to describe basic creep as a function duration of loading $(t - t_0)$ and time of loading t_0, while the third term accounts for drying creep as a function of relative humidity h, duration of loading and volume-surface ratio V/S. Adjustments to the creep model can be made for the effect of drying before loading.

2.7.5 AASHTO-LRFD Model

The AASHTO-LRFD Bridge Design Specifications (Section 5.4.2.3.2) model for predicting creep coefficient is based an ultimate creep strain modified by the volume-surface ratio, relative humidity, and the compressive strength of concrete at the time of loading and is defined by the following equations:

$$\varphi(t, t_0) = 1.9 k_s k_{hc} k_f k_{td} t_i^{-0.118} \quad \text{2-38}$$

$$k_s = 1.45 - 0.13\left(\frac{V}{S}\right) \geq 1.0 \quad \text{2-39}$$

$$k_{hc} = 1.56 - 0.008H \quad \text{2-40}$$

$$k_f = \frac{5}{1 + f'_{ci}} \quad \text{2-41}$$

$$k_{td} = \frac{t}{61 - 4f'_{ci} + t} \quad \text{2-42}$$

where *V/S* is the volume to surface area ratio, *H* is the relative humidity, *t* is the time being considered since the load was applied, t_i is the time at which the load was applied, and f_{ci}' is the concrete compressive strength at start of prestressing or loading and can be taken as $0.8f_c'$.

A study conducted by the ACI Committee 209 found that the GL2000, CEB MC90-99 and Bažandt-Baweja B3 models best predicted the compliance function compared with

results from a databank. As previously mentioned, understanding the creep behavior of precast concrete mixes with limestone blended cements can assist designers make adjustments and account for dimensional instability of concrete. In Chapter 6, the five creep models presented here are compared with experimental data to determine whether one of the models can be used to predict long-term creep effects of concrete made with limestone blended cements.

2.8 Multiscaling

Since it is often impractical to perform long-term field and lab tests, upscaling experiments can be quite useful. Upscaling allows researchers to perform short-term experiments, usually on small-scale specimens, and correlate the results to larger scales. These tests require far less material than full-scale tests and usually take far less time to evaluate results. Two upscaling applications with limestone blended cements being explored are using mini slump tests on cement paste to determine the workability of concrete mixes and using nanoindentation measurement on cement paste to correlate with long-term concrete creep studies.

In the case of the mini slump test, the final spread of cement paste is measured as it leaves an acrylic cone. The yield stress τ_0 of the cement paste can be determined from the density ρ of the cement-limestone paste, the volume V of material in the mini slump cone and the final spread diameter of the cement paste, D_f [59].

$$\tau_o = \frac{7200\rho g V^2}{128\pi^2 D_f^5} \qquad 2\text{-}43$$

By understanding how the influence of limestone powder fineness and percent replacement affects workability, modification can be made to the HRWRA dosage of concrete mixes.

In the case of nanoindentation creep test, Zhang et al. was able to correlate minute-long creep studies performed at the microscale on cement paste with traditional year-long concrete creep studies [60]. During nanoindentation experiments, an indenter applies a load P_{max} to the cement paste. The load is help constant during a prescribed period during which time the penetration depth, $\Delta h(t)$, is measured. This change in depth over time is analogous to creep of concrete that deforms axially when a load is applied. Depending on the radius of the contact area between the material and the nanoindenter tip a_u, the contact creep function can then be determined during the hold period as:

$$L(t) - L(0) = L(t) - \frac{1}{M_o} = \frac{2a_u \Delta h(t)}{P_{max}} \qquad 2\text{-}44$$

Plotting this result with time yields a logarithmic curve analogous to the creep compliance curve of concrete. The contact creep modulus C_i, which is a measure of creep rate, can be determined from the steady-state slope of the measured contact creep data plotted on semi-log graph and curve fitted to the following equation:

$$L(t) - \frac{1}{M_o} = \frac{\ln(\frac{t}{\tau_i} + 1)}{C_i} \qquad 2\text{-}45$$

where τ_i represents the characteristic time when the creeping cement paste starts exhibiting logarithmic behavior [60].

Once C_i of the paste is determined, the contact creep modulus of the concrete can be upscaled to the level of concrete by knowing the percent aggregate f_{agg} in the concrete mix. Two schemes have been proposed for upscaling to the concrete level [60]. One method makes use of a Mori-Tonka scheme [61] and the other was presented by Vu et. al [62]. The two schemes are shown below:

$$C_{i,con} = C_i \frac{2 + 3f_{agg}}{2(1 - f_{agg})} \quad \text{2-46}$$

$$C_{i,con} = C_i \left(1 - \frac{f_{agg}}{f_{agg,m}}\right)^{-1.43} \quad \text{2-47}$$

$C_{i,con}$ can then be compared with the uniaxial creep modulus C_u determined from long-term creep studies performed on concrete cylinders according to ASTM C512 [63]. The uniaxial creep modulus is also determined by fitting the specific creep data with the following equation:

$$J_u(t) - \frac{1}{E_o} = \frac{\ln\left(\frac{t}{\tau_u} + 1\right)}{C_u} \quad \text{2-48}$$

where τ_u represents the characteristic time when the creeping concrete specimen starts exhibiting logarithmic behavior [60].

As can be noted from the Equation 2-48 above, the uniaxial creep modulus C_u is just the inverse of the creep rate F(K) determined from ASTM C512 [63]. The benefits of

obtaining creep results of various concrete mixes in minutes rather than years could have a positive impact in the concrete industry and in the development of concrete mixes.

CHAPTER 3. MATERIALS AND METHODS

3.1 Introduction

As discussed in Chapter 2, limestone affects the hydration of cement in several ways. Due to the replacement of reactive cement with inert or slightly reactive limestone, a dilution effect is anticipated. Secondly, depending on the particle size of the limestone powder, additional nucleation sites for cement hydration products may be introduced [17]. Thirdly, depending on the median particle size of the limestone powder, it may produce an anhydrous, more efficient particle packing, and hence lower porosity. Finally, there is some evidence to suggest that cements with limestone powder convert ettringite to a more stable calcium monocarboaluminate rather than calcium monosulfate hydration. One hypothesis is that limestone powder with particle size distribution that matches closer to the particle size distribution of the cement grains will dilute the matrix and produce less efficient particle packing, while limestone powders with a particle size distribution with a greater variation from that of the base cement will improve the matrix packing density. Limestone powders ground finer than the base cement should increase nucleation, accelerate hydration and lead to increased early compressive strengths [17]. Coarser ground limestone powders might improve workability but could also lower packing density by aiding in dispersion of cement grains, and through dilution, potentially promoting enhancements in cement hydration [16] [30].

In this chapter, the materials used for the research are characterized by both their chemical and physical compositions. The chemical composition and Blaine fineness of the three cements studied are presented, a thermogravimetric analysis was used to determine

the calcium carbonate ($CaCO_3$) content of the cements and limestone powder, the crystallinity of the limestone powders was determined through X-ray diffraction and laser diffraction was used to determine and compare the particle size distribution of the cements and limestone powders.

3.2 Material Characterization

Three cements manufactured from the same clinker base provided by LafargeHolcim (Holly Hill, SC) and four limestone powders provided by Imerys Carbonates (Marble Hill, GA) were used throughout this research. The three cements are a Type I/II and Type III conforming to ASTM C150, and a Type IL conforming to ASTM C595 and have specific gravities of 3.10, 3.10, and 3.05, respectively [64] [13]. The four limestone powders are classified by the supplier according to their median particle size of 3, 15, 25, and 40 μm and have specific gravities of 2.7. In addition to presenting the chemical compositions of the materials, laser diffraction was used to determine the physical particle size distribution of the materials.

3.2.1 Chemical Composition of cement and limestone

The Type I/II and Type III cements have similar compositions as seen in Table 3-1, with the main difference being in their Blaine fineness. The Type IL cement was produced by the manufacturer by intergrinding cement and limestone powder. As can be seen, based on Blaine fineness, the Type IL cement is more similar to the Type III cement than the Type I/II, even though it is marketed as a Type I replacement.

Table 3-1: Cement composition as provided by cement manufacturer

Component	Type I	Type III	Type IL
SiO_2 (%)	19.8	20.0	19.1
Al_2O_3 (%)	4.6	4.6	4.6
Fe_2O_3 (%)	3.4	3.3	3.5
CaO (%)	64.0	63.6	62.4
MgO (%)	1.3	1.3	1.2
SO_3 (%)	3.3	3.2	3.5
LOI	2.5	2.3	5.5
CO_2 (%)	1.3	1.0	-
C_3S (%)	62	59	53
C_2S (%)	12	14	18
C_3A (%)	7	7	2
C_4AF (%)	10	10	12
Blaine Fineness (m^2/kg)	395	509	551

3.2.1.1 Limestone Powder Production

The limestone powders used are a ground white calcitic marble manufactured from the same quarry source, Marble Hill in Georgia, and were ground by the producer to varying particle size distributions. The powders are classified according to their median particle size, D_{50}, and are from finest to coarsest: 3 µm, 15 µm, 25 µm, and 40 µm. Producing the limestone powder consists of hauling ore from the mine to a jaw crusher [65]. Ore from the jaw crusher passes over a screen and is sorted according to size [65]. Material greater than 2 inches goes through a secondary crusher while material less than 2 inches goes to a Raymond roller mill [65]. Air is blown into the bottom of the Raymond mill, which lifts the smaller particles up to a separator [65]. The rotational speed of the separator determines the particle size of the material that leaves the Raymond mill [65].

Increasing the speed of the air classifier decreases the particle size of the material leaving the mill [65].

The limestone powder with median particle size of 3 µm spends more time in the Raymond mill and requires more power from the air classifier than the limestone powder with median particle size of 40 µm. A 60-inch Raymond mill can produce about 5 tons of a limestone with median particle size of 25 µm per hour consuming around 30 kW-hr per ton. Similarly, the mill can produce about 3.5 tons of a limestone with median particle size of 15 µm per hour while consuming 45 kW-hr per ton. Figure 3-1 below shows an image of the Raymond mill.

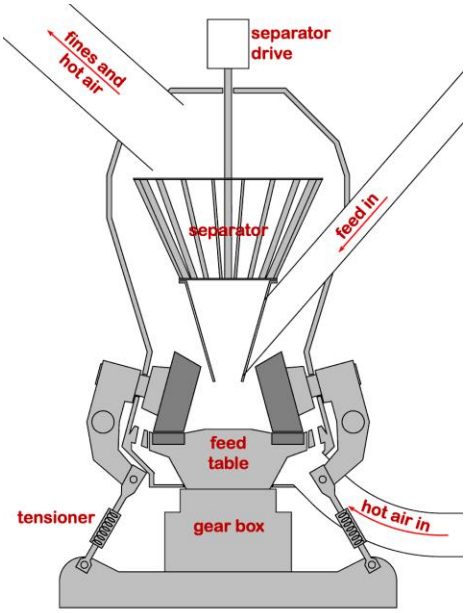

Figure 3-1: Raymond Mill for limestone powder production [65]

3.2.1.2 Thermogravimetric Analysis (TGA) and X-ray Diffraction (XRD)

A thermogravimetric analysis (TGA) was conducted to determine and verify the amount of $CaCO_3$ present in the cement and limestone powders. During TGA, a small amount of material, 20mg, was placed into a container and the mass of the material was measured while subjected to a heating regime. Cements and limestone powders were heated from ambient temperature to 900°C at a rate of 10°C/min with a 30-minute hold time at 105°C to evaporate free moisture. Limestone, $CaCO_3$, breaks down to CO_2 and CaO at temperatures approximately between 600°C and 800°C, so that the amount of limestone in a material can be calculated from Equation 3-1 below, where the molecular weights of $CaCO_3$ and CO_2 are taken as 100.09 g/mol and 44.01 g/mol, respectively [66].

$$\%CaCO_3 = \frac{m_{600} - m_{800}}{m_{105}} \, x \, \frac{MW_{CaCO_3}}{MW_{CO_2}} \qquad 3\text{-}1$$

Figure 3-2 shows the different curves generated for the Type I/II, III and IL cements and the large peak generated by the additional limestone in the Type IL at temperatures between 600°C and 800°C.

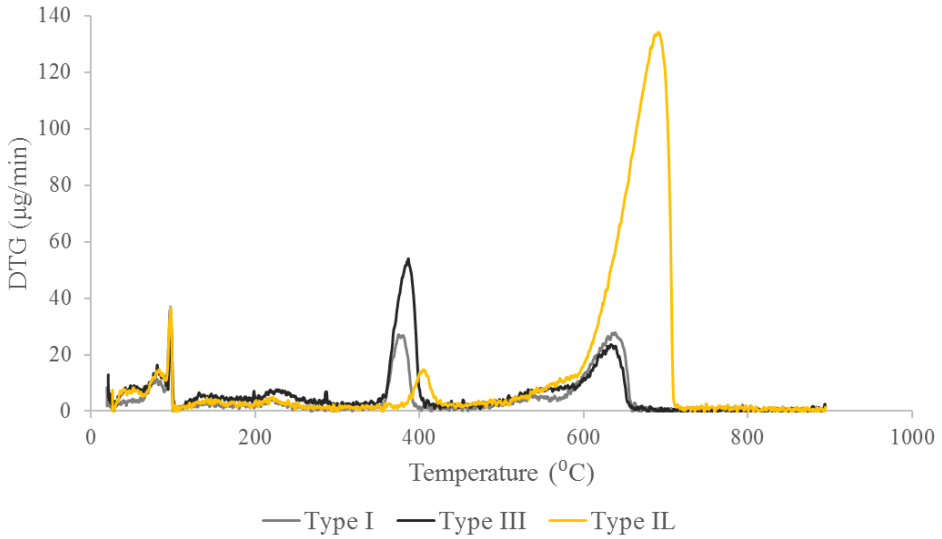

Figure 3-2: DTG comparison of Type I/II, III and IL cements showing a large peak between 600°C and 800°C where limestone breaks down

The results from the TGA shown in Figure 3-3 suggest that the three limestone powders having median particle size of 3, 25, and 40 µm all have limestone contents above 92%. Cement Type I/II and III have limestone contents of a little over 1% and the Type IL cement with interground limestone has a limestone content of around 9%.

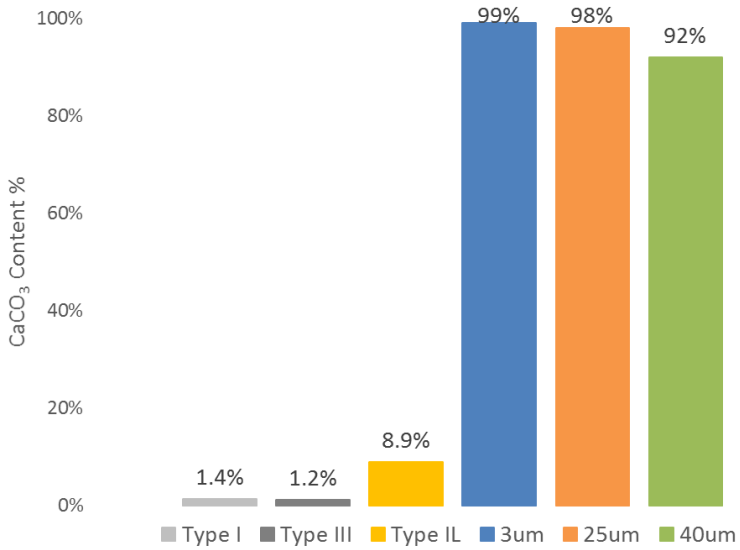

Figure 3-3: $CaCO_3$ content of cements and limestone powder

An X-ray diffraction (XRD) analysis of the 3, 25 and 40 μm limestone powder was used to verify that the limestone powder was in fact calcitic. As seen in Figure 3-4, the highest intensity peak occurs at a 2θ angle of 29.4º corresponding to the location of calcite. The largest intensity was achieved by the 40 μm limestone followed by the 25 and 3 μm limestone, signifying that there is more crystallinity for the coarser limestone due to the lower degree of grinding. The 25 μm limestone powder showed a small amount of impure dolomite at 30.9º.

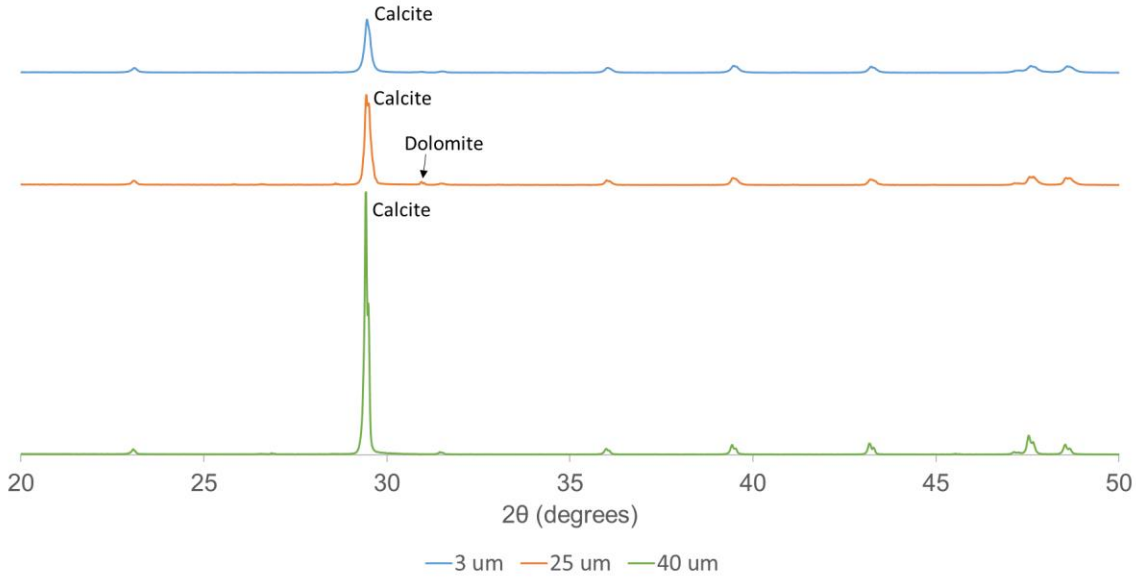

Figure 3-4: XRD analysis of the 3, 25, and 40 μm limestone powder

3.2.2 Particle Size Distribution

Since the size of the cement particle relative to the limestone powder can affect the physical properties of the concrete due to optimized particle packing and additional nucleation sites, it is important to understand the particle size distribution of the three cements and four limestone powders used throughout this thesis.

The particle size distribution of the cements and limestone powders was determined by laser particle diffraction (A Malvern Mastersizer 300), with a range of 10 nm to 35 mm. A laser passes through a dispersed particle sample and the angular variation in intensity of the scattered light is measured. During the analysis, the material was dispersed in ethanol until reaching an obscurity level of 10%-15%. The material was mixed at a rate of 1500 rpm and sonicated for 30 seconds, before taking measurements, to avoid agglomeration. Using Mie Theory of light scattering, the particle size distribution was determined by averaging five measurements of each sample collected over a 60 second interval. The cement refractive index and absorption index were taken as 1.68 and 0.01, respectively. Based on Michael & Courard [67], the limestone refractive index and absorption were taken as 1.57 and 0.1, respectively.

The particle size distribution and cumulative volume distributions are shown in Figure 3-5 and Figure 3-6. The graphs show a narrow particle distribution range among the three cements, with more similar characteristics between the Type III and Type IL. More variation and spread are seen between the four limestone powders, especially between the limestone powders having a median particle size of 3μm and 40μm. Visually, the figures confirm that the particle size distribution of the three cements are bound between the finer 3 μm limestone powder and the coarsest 40 μm limestone powder, and that the cements are most similar to the 15 and 25 μm limestone powders.

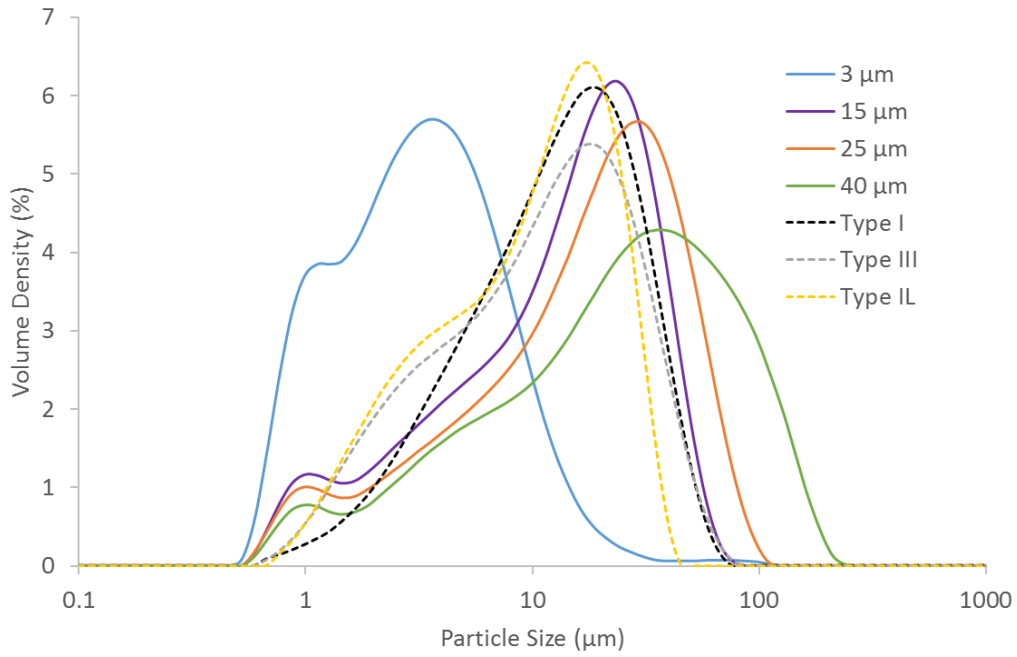

Figure 3-5: Particle size distribution of cements and limestone powder by laser diffraction

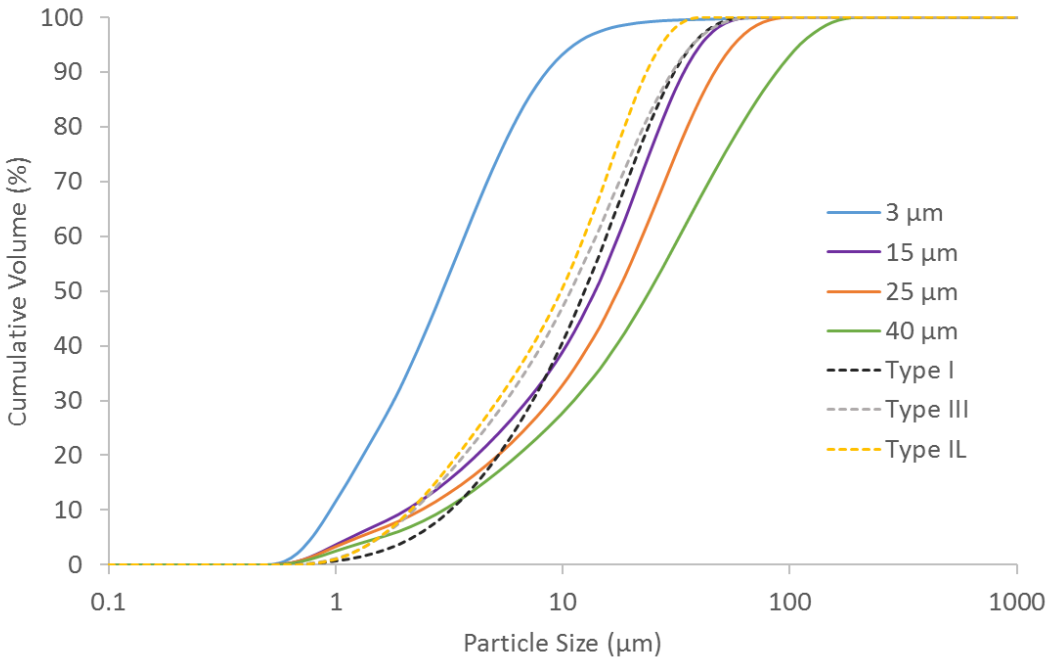

Figure 3-6: Cumulative particle size distribution of cement and limestone powder by laser diffraction

The results from the particle size analysis are summarized in Table 3-2 below. The table shows the specific surface area (SSA) of each material, which represents the total surface area per unit mass. A finer ground material will have a greater SSA than a coarser ground material. The $D_{3,2}$ and $D_{4,3}$ is the surface-weighted and volume-weighted median particle size. The $D_{4,3}$ is also referred to as the volume based median diameter and is influenced by larger particles. The D_i is the cumulative distribution of particle sizes by volume. For example, the D_{10} represents that 10% of particles are smaller than this value.

Table 3-2: Summary of Particle Size Distribution

		SSA m^2/kg	$D_{3,2}$ µm	$D_{4,3}$ µm	D_{10} µm	D_{50} µm	D_{90} µm
Limestone	3 µm	917.7	2.41	4.89	1.07	3.35	9.62
	15 µm	363.2	6.10	18.4	2.31	15.7	38.8
	25 µm	316.9	6.99	24.4	2.69	19.8	53.0
	40 µm	259.2	8.54	40.6	3.38	27.3	99.5
Cement	Type I/II	246.9	8.10	17.2	3.63	14.1	35.2
	Type III	316.8	6.31	15.8	2.50	12.3	34.5
	Type IL	335.8	5.96	12.9	2.42	11.1	26.5

Table 3-2 shows that the 15 µm and 25 µm are very similar to each other, while the 3 µm and 40 µm limestone powders show larger differences, especially the SSA and D_{50}. This will become important in later chapters when determining concrete mixes where it was deemed that the 15 and 25 µm limestone powders were so similar that making concrete mixes with both would be unnecessary.

As can also be deduced from the table, the specific surface area and median particle size D_{50} do not always correlate. For example, the specific surface area of the Type I/II cement is most similar to that of the 40 µm limestone powder but has a D_{50} value closer in value to that of the 15 µm limestone powder. In fact, the Type I/II cement shows the

narrowest band of values in that the specific surface area is the smallest of all the various solids measured, but its median particle size, D_{50}, is in the middle range of the solids measured. It has less spread than the other cements, which demonstrates the benefit of grinding cements to achieve a more diverse particle size distribution. The 25 and 40 μm limestone powders appear to be mislabelled in that the median particle size, D_{50}, closer to 20 and 27 μm, respectively. Nonetheless, the nomenclature provided by the manufacturer will be used throughout this thesis.

The specific surface area of the Type III is most similar to the 25 μm limestone powders. It is hypothesised that concrete mixes with limestone powders with similar particle size distributions as the base cement will lead to greater dilution effects, whereas limestone powders with particle distributions more dissimilar to the cement base will show greater filler and nucleation effects. The specific surface area and the other particle size distribution parameters of the Type IL cement which has been interground with limestone more closely resembles the Type III cement rather than the Type I/II.

3.2.3 Scanning Electron Microscope Images

A scanning electron microspore (SEM) was used to produce high-resolution images of the 3, 25, and 40 μm limestone powders. The images shown in Figure 3-7 show that the limestone particles are flat, and non-spherical.

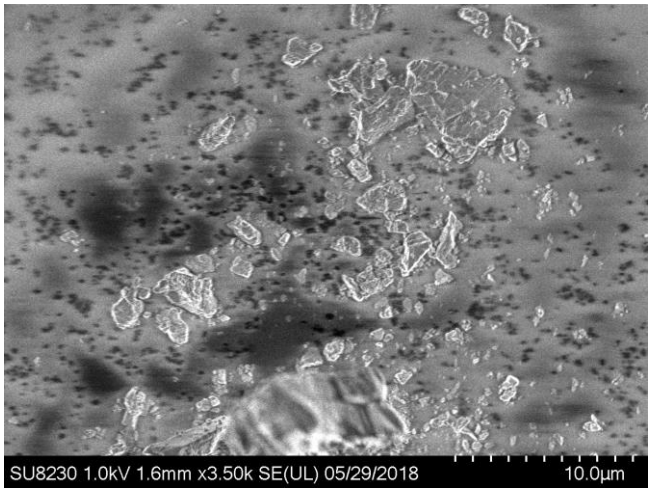

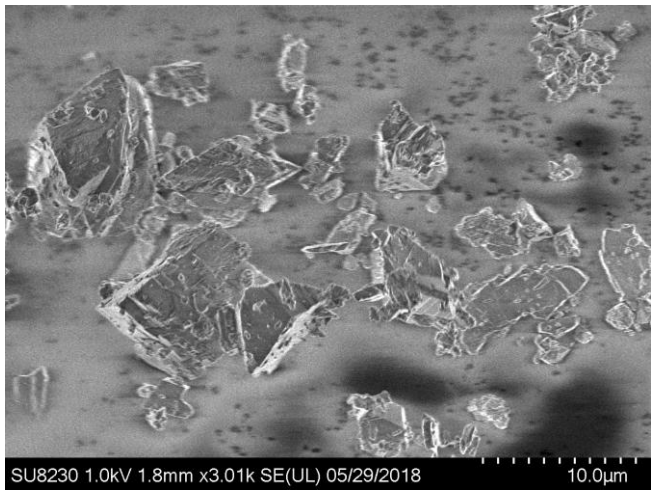

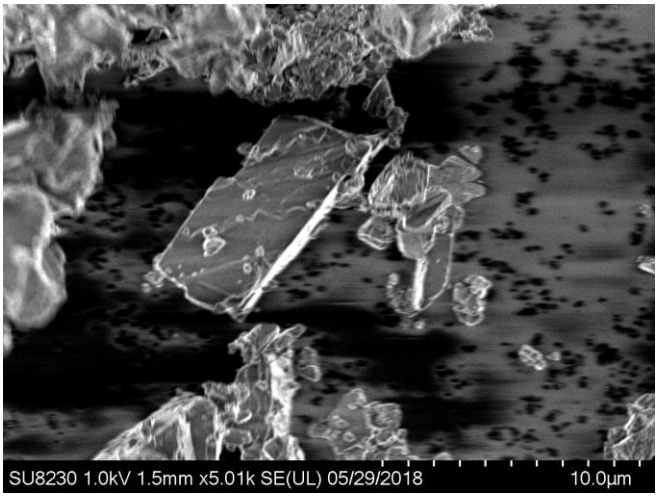

Figure 3-7: SEM images of 3µm (above), 25µm (middle), and 40µm (below) limestone

3.3 Aggregates, Admixtures and Water

In addition to cement and limestone powder, self-consolidating concrete mixes discussed in Chapter 5 are made with coarse aggregate, fine aggregate and a high range water reducing admixture. The coarse aggregate is a granitic gneiss from Lithonia, GA meeting the requirements for AASHTO #67 stone with a maximum aggregate size of 3/4 inch (19 mm), a specific gravity of 2.61 and an absorption capacity of 0.58%. The aggregate was proportioned at 1724 lb/ft^3 (1023 kg/m^3). The fine aggregate was a natural, alluvial sand from Vulcan Materials in Lithia Springs, GA with a specific gravity of 2.63, a fineness modulus of 2.4, and an absorption capacity of 0.4%. The sand was proportioned at 1200 lb/ft3 (712 kg/m3). For producing flowing concrete mixes, a high range water reducing admixture (HRWRA) was used. The polycarboxylate HRWRA was a Master Glenium 3400 produced by BASF Master Builders, which met the classification of ASTM C494 Type A and F. The dosage rate for the HRWRA ranged between 31 - 60 oz/lb^3 depending on the cement type. All studies on cement paste were mixed with deionized water while all studies with concrete mixtures used potable water.

The various mixes produced with combinations of cement and limestone powders at various cement replacement substitutions and varying limestone median particle size are discussed in Chapter 4 and Chapter 5. Cement pastes, mortars and concrete mixes are classified by (1) the cement type used: T1 for Type I/II, T3 for Type III, and T1L for Type IL, (2) the size of the limestone powder: L3, L15, L25, and L40 for limestone powders with median particles sizes of 3, 15, 25, and 40 μm, respectively, and (3) the percent cement substitution denoted in parenthesis (X). Thus, T3L25(15) is a mix blending Type III cement with 25 μm limestone powder at a 15% cement replacement.

CHAPTER 4. THE INFLUENCE OF PARTICLE SIZE ON EARLY AGE PROPERTIES OF LIMESTONE BLENDED CEMENTS PASTES AND MORTARS

4.1 Introduction

As discussed in Chapter 3, heat of hydration, time of set and workability is affected by the relative particle size distribution between the base cement and the limestone powder being used as partial cement replacement by mass. Understanding these influences can be used to better tailor concrete mixtures used for precast applications and to adjust water reducing admixtures based on workability. Although there is ample research regarding the blending of cements with fine limestone powders, there is limited information regarding the blending of limestone powders with coarser particle size which may help workability and lower heat of hydration [68]. Cements and limestone powders having finer particle size distributions react more quickly than coarser ground powders due to their increased surface area, smaller interparticle spacing and increased number of sites for CSH nucleation [33]. This accelerated hydration can lead to a decreased initial and final set time. Increased fineness leads to increased paste cohesion and stability but may in turn reduce workability. On the other hand, when coarser ground limestone is blended with cement, the increased particle dispersion may improve workability. How different cements interact with limestone powders of varying median particle sizes and at varying percent cement substitution rates by mass to affect heat of hydration, time of set, workability and mortar compressive strength is the main focus of this chapter. Although compressive

strength from mortar tests are not always consistent with concrete specimens, general trends can be inferred from mortar results and are thus presented here.

Being able to predict hydration and workability trends based on both the size of the limestone particle cement substitutions and the limestone content would assist concrete suppliers in tailoring concrete mixes. Guidelines such as the ACI 211.7R provide very general trends for how limestone affects concrete properties, but specific guidelines based on limestone median particle size are not available [69]. How these constituents influence pastes made with Type III cement is of particular interest to the precast industry, which almost exclusively uses high early strength cement. Although this chapter studies three cement types and four limestone powders of varying median particle size, the main focus will be on quantifying hydration trends using Type III cement to be able to provide guidelines for the use of limestone blended cements to the precast industry.

4.2 Materials and Methods

Cement pastes were produced by blending cement and limestone powders of varying median particle size. Three cements supplied by LafargeHolcim - Type I/II and III cements conforming to ASTM C150 and a Type IL conforming to ASTM C595 - were used. The three cements were produced from the same base clinker and have the same basic chemistry (Table 3-1). The Type III is ground finer than the Type I/II while the Type IL was produced by intergrinding Type I/II cement with limestone powder at a 9% cement replacement by mass. Four limestone powders having median particle sizes of 3, 15, 25, and 40 μm supplied by Imerys Carbonates were used. As discussed in Chapter 3, the median particle size of the limestone powders brackets the median particle size of the cements. The 3 μm

limestone powder was ground finer than the three cements and the 40 μm limestone powder was ground coarser than the three cements (Table 3-2). An additional study was conducted to compare the hydration of the limestone powder with median particle size of 3μm with an inert quartz having similar particle size distribution as the limestone powder (Table 4-1).

Table 4-1: Particle Size Distribution of Limestone and Quartz

	SSA m^2/kg	$D_{3,2}$ μm	$D_{4,3}$ μm	D_{10} μm	D_{50} μm	D_{90} μm
Limestone 3 μm	917.7	2.41	4.89	1.07	3.35	9.62
Quartz 15	905.0	2.50	5.72	1.06	3.69	13.5

Cement pastes were produced with varying cement replacement by mass (0-30%) of each of the 3, 15, 25, and 40 μm limestone powders. A high range water reducing admixture (HRWRA), Master Glenium 3400 by BASF, was used for the mini slump cement paste mixes at a dosage rate of 0.75 g per 200 g of binder (cement plus limestone). Sand used for compressive strength testing of mortar cubes was a natural, alluvial sand from Vulcan Materials in Lithia Springs, GA.

4.2.1 Isothermal Calorimetry

To understand the hydration kinetics of hydrating blended limestone cements, isothermal calorimetry was used to measure the heat produced by the hydrating cement pastes and to determine the cumulative heat (the integral of the hydration curve) over 48 hours, per ASTM C1679 [70]. Cement and limestone powder blends were mixed with deionized water keeping a constant water-to-binder (w/b) ratio of 0.38. The pastes were first mixed for 30 seconds by hand, followed by 1 minute on low speed of a 5-speed hand

mixer and 1 minute at medium speed. Approximately 7 ± 0.5 grams of cement paste were placed into ampules and loaded into a TAM Air Thermometric Calorimeter. Two ampules of each sample were measured to compare for consistency. Measurements were taken every minute for a period of 72 hours at a constant temperature of 25ºC.

4.2.2 Vicat Time of Set

The procedures outlined in ASTM C191 were followed to determine the time that cement pastes reached initial set, indicated by a needle penetrating the paste 25 mm, and the time at which the paste reached final set, indicated by a needle making no penetration into the cement paste [71]. The experiments were performed on three cements, Type I/II, Type III and Type IL, with varying cement replacements of limestone powders previously discussed. The ASTM standard calls for using a water-to-binder ratio that produces a paste with normal consistency defined by ASTM C187 as a 10 mm diameter needle penetrating the cement paste no deeper than 10 ± 1 mm [72]. Normal consistency of each of the three cements was determined and used for each cement class experiment. Therefore, the three base cements Type I/II, Type III and Type IL have slightly different water to cement ratios of 0.249, 0.272, and 0.271, respectively, but all cement-limestone blends with the same cement type have the same water-to-binder ratio. In studies using blended cements where the normal consistency was determined of each limestone-cement blend, it was not clear whether the inconsistent set times were due to variations in particle size or due to the varying w/b ratios [30].

Cement pastes were made by mixing 650 g of cement or cement plus limestone powder with deionized water. The mixing of cement pastes followed the procedures

outlined in ASTM C305 [73]. Using a 2-speed electrically driven mechanical mixer, cement or blended cements were added to water in a mixing bowl, the paste was allowed to rest 30 seconds, followed by mixing at low speed for 30 seconds, a 15 second rest period, and finally a 60 second mix at medium speed. Per ASTM C191, cement pastes were formed into a ball, tossed six times between hands spaced approximately 150 mm apart and then placed into a conical ring and rested on a glass plate [71]. After cutting off excessive paste, the conical specimens were stored in a moist cabinet at 73.5 ± 3.5 ^{0}F until ready for measurement taking. After an initial rest period of 30 minutes, measurements were taken at 15-minute intervals for Type I/II cement pastes and every 10 minutes for the Type III and Type IL cement pastes. Three specimens were made from each batch and the results were averaged.

4.2.3 Mini slump spread diameter

As an indicator of workability, mini slump experiments using an acrylic cone measuring 2.25 in (57 mm) tall and having top and bottom diameters of 0.75 in (19 mm) and 1.5 in (38.5 mm), respectively were performed. Cement pastes were prepared using limestone of varying median particle size and with varying percentages of cement replacement by mass keeping a constant water-to-binder ratio of 0.38, matching the cement paste mixes used for isothermal calorimetry. The pastes were prepared using the same mixing procedure used for the isothermal calorimetry study, differing in that a HRWRA was added to the deionized water before mixing. Care was taken in lifting the slump cone since any lateral movement or change in the rate of the lifting can affect final spread, Df. Since HRWRA was used, the measurements were taken at a set time (10 minutes after

mixing) to avoid time dependency issues. The reported spread diameters are the average of three measurements.

4.2.4 Mortar Compressive Strength

Following the procedures of ASTM C109, mortar cubes of limestone blended cements were cast into 2 in. x 2 in. x 2in. (50 mm x 50 mm x 50 mm) cubic molds [74]. The mortars had a constant water-to-binder ratio of 0.44 and were made with 0, 10 and 20% cement replacement by limestone powders each of median particle size of 3, 25, and 40 μm. The mortars were cast in two layers and tamped 32 times in 4 rounds using a flat rubber tamper. The molds were placed in a moist cabinet at 73.5 ± 3.5 ^{0}F conforming to ASTM C511 to cure for 24 hours [75]. Three molds of each cement blend were cast. After curing, the mortar cubes were demolded and stored in limewater at 73.5 ± 3.5 ^{0}F until time of testing. Mortar compressive strength was determined at 7 and 28 days.

4.3 Experimental Results

Isothermal calorimetry, Vicat time of set, mini slump test and mortar compressive strength were used as indicators of the early age properties of cement pastes and mortars made with limestone blended cements. The blended cements had varying percent cement replacement of limestone powder with median particle sizes of 3, 15, 25, or 40 μm. By measuring the heat released during hydration, isothermal calorimetry provides an indicator of quickly or slowly the cement reaction is occurring. The Vicat time of set provides an indication as to how quickly the cement will set. Workability of cement paste was measured using a mini-slump cone.

4.3.1 Isothermal Calorimetry

4.3.1.1 Effect of limestone median particle size

Figure 4-1 and Figure 4-2 shows the heat release and cumulative heat during the first 48 hours of hydration of Type I/II, Type III and Type IL cements where 10% of the cements have been replaced by limestone powders of varying median particle size (3 μm, 15 μm, 25 μm, and 40 μm). During the first few hours of hydration, ions from the cement begin to dissolve into solution and signifies the initial cement hydration. This dissolution is followed by the formation of ettringite. The acceleration portion of the curve between 1 to 6 hours happens during the initiation of silicate hydration reaching a peak. The peak is followed by the depletion of sulphate from the cement. A final much smaller peak is seen around 30 hours where the cement begins to react with the aluminate phases.

The three neat cements have similar hydration profiles. Due to its higher specific surface area, the peak of T3 occurs earlier than the other cements indicating a slightly faster reaction than the other two cements. Tabulated hydration results are shown in Table 4-2. Even though T1L has a higher specific surface area than T1, the peak hydration is slightly less perhaps due to the interground limestone, but the time to peak is faster. This shows the conflicting dynamics between accelerated hydration due to a finer ground cement and the dilution effect of the added limestone powder.

Table 4-2: Results from isothermal calorimetry showing the effect of 10% cement replacement of limestone powder of varying median particle size

	Time to Peak	Peak Hydration	Cumulative Heat (*J/g binder*)				
Mix	***hr***	***mW/g binder***	**@ 8hr**	**@ 12 hr**	**@16 hr**	**@24 hr**	**@48 hr**
T1	7.23	5.53	80.5	145.2	183.2	218.3	279.1
T1L3(10)	6.26	5.12	89.3	148.0	182.5	214.8	261.5
T1L15(10)	7.11	4.87	73.9	131.9	167.8	200.6	248.5
T1L25(10)	7.18	4.81	71.1	128.5	163.9	196.2	243.1
T1L40(10)	7.53	4.73	69.7	127.0	162.4	195.7	237.7
T3	5.77	5.67	105.0	162.7	190.5	217.9	268.3
T3L3(10)	4.66	5.66	112.1	161.4	185.6	210.9	255.1
T3L15(10)	5.29	5.36	103.5	155.2	180.7	206.3	251.7
T3L25(10)	5.33	5.27	100.6	152.1	177.6	202.6	249.2
T3L40(10)	5.86	5.17	92.7	147.5	175.4	202.0	247.8
T1L	6.56	5.43	85.7	145.9	181.4	214.8	264.4
T1L-L3(10)	5.72	5.25	91.1	146.1	177.5	209.1	252.9
T1L-L15(10)	6.41	4.97	79.6	135.3	169.5	202.7	247.1
T1L-L25(10)	6.46	4.92	78.4	134.0	168.5	201.7	245.2
T1L-L40(10)	6.63	4.92	75.9	131.9	166.8	200.5	244.8

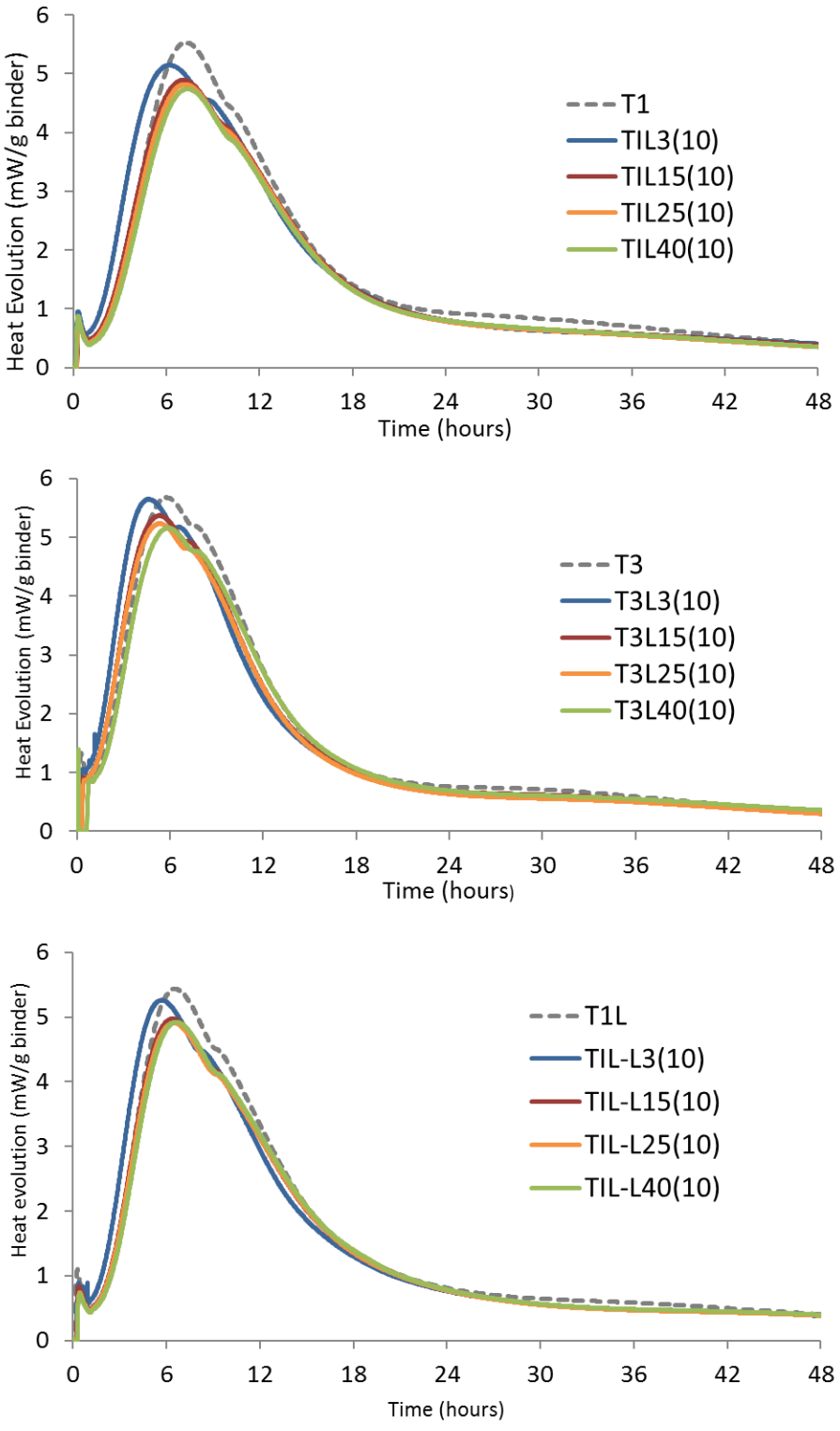

Figure 4-1: Heat evolution of Type I/II, Type III, and Type IL cements with 10% cement substitution of limestone powder of varying median particle size

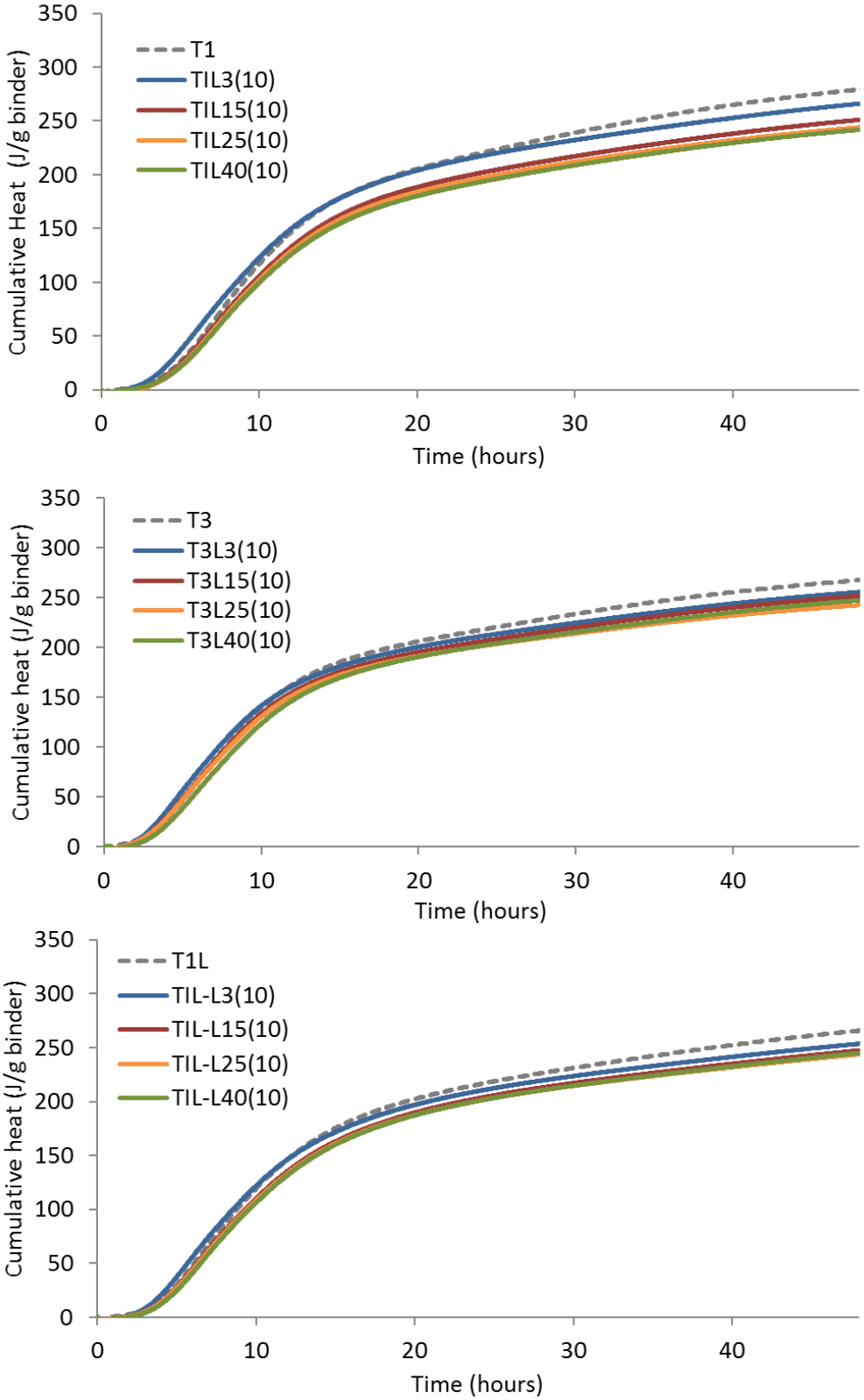

Figure 4-2: Cumulative heat evlotion of Type I/II, Type II, and Type IL cements plus 10% cement replacement of limestone powder of varying median particle size

In comparing the three graphs, there is a leftward shift in the curves during the cement hydration occurring with the finest limestone powder having median particle size of 3 μm. This shift indicates an acceleration in the rate of hydration due to increased specific surface area of the finer particles providing additional nucleation sites for cement hydration. From Table 4-2, it can be seen that the acceleration occurs in the first 12 hours of hydration where cumulative heat is higher for the 3 μm limestone powder compared with the neat cement, but then reduces at later ages. The peak hydration of T3L3(10) shows almost no dilution effect, whereas the peak hydration with the T1L3(10) and T1L-L3(10) is reduced.

Compared with the neat cements, replacing 10% cement with either the 15, 25 and 40 μm limestones reduce the peak hydration and cumulative heat. Cement blends with 15 and 25 μm limestones show an accelerated time to peak indicating some nucleation effects, whereas blends with 40 μm limestone show a longer time to peak when compared with the neat cements. Recall from Table 3-2, the specific surface area of 15 μm limestone is somewhat larger than the three cements and therefore some nucleation is expected. The 25 μm limestone, however, has a similar specific surface area as the Type III cement, so the acceleration to peak hydration is more surprising. The cumulative heat of all cements with limestone powders with median particle sizes of 15, 25, and 40 μm show a clear dilution effect. The cumulative heat data shows a constant trend that regardless of cement type, at 48 hours, the limestone with the largest median particle size (40 μm) reduces heat of hydration more than the smallest median particle size.

4.3.1.2 Effect of percent cement substitution by limestone powder

Additional studies were conducted to study the effect on hydration of replacing greater quantities of cement with limestone powders. Figure 4-3 and Figure 4-4 show the heat evolution and cumulative heat, respectively, of cements with varying percentages (5 to 25%) of a 25 μm limestone powder. It is clear from these graphs that as the amount of limestone powder increases leaving less cement available to hydrate, a more pronounced dilution effect occurs on the total and cumulative heat released during hydration. The results for 10 and 20% cement replacement of 3, 25, and 40 μm limestone powders are tabulated below in Table 4-3.

Table 4-3: Comparison of heat paramters with increasing cement replacement

	Time to Peak	**Peak Hydration**	**Cumulative Heat (*J/g binder*)**		
Mix	***hr***	***mW/g binder***	**@ 8hr**	**@ 12 hr**	**@48 hr**
T1	7.23	5.53	80.5	145.2	279.1
T1L3(10)	6.26	5.12	89.3	148.0	261.5
T1L3(20)	5.95	4.61	79.8	139.5	250.0
T1L25(10)	7.18	4.81	71.1	128.5	243.1
T1L25(20)	6.75	4.35	66.7	118.2	229.3
T1L40(10)	7.53	4.73	69.7	127.0	237.7
T1L40(20)	7.42	4.23	62.0	114.1	219.4
T3	5.77	5.67	105.0	162.7	268.3
T3L3(10)	4.66	5.66	112.1	161.4	255.1
T3L3(20)	4.83	5.41	104.4	154.0	241.8
T3L25(10)	5.33	5.27	100.6	152.1	249.2
T3L25(20)	5.53	4.75	88.8	138.4	228.1
T3L40(10)	5.86	5.17	92.7	147.5	247.8
T3L40(20)	6.33	4.45	76.7	128.1	222.8
T1L	6.56	5.43	85.7	145.9	264.4
T1L-L3(10)	5.72	5.25	91.1	146.1	252.9
T1L-L3(20)	5.68	4.54	83.7	136.8	233.4
T1L-L25(10)	6.46	4.92	78.7	134.0	245.2
T1L-L25(20)	6.25	4.70	79.6	133.5	239.0
T1L-L40(10)	6.63	4.92	75.9	131.9	244.8
T1L-L40(20)	7.15	3.96	64.5	113.9	218.5

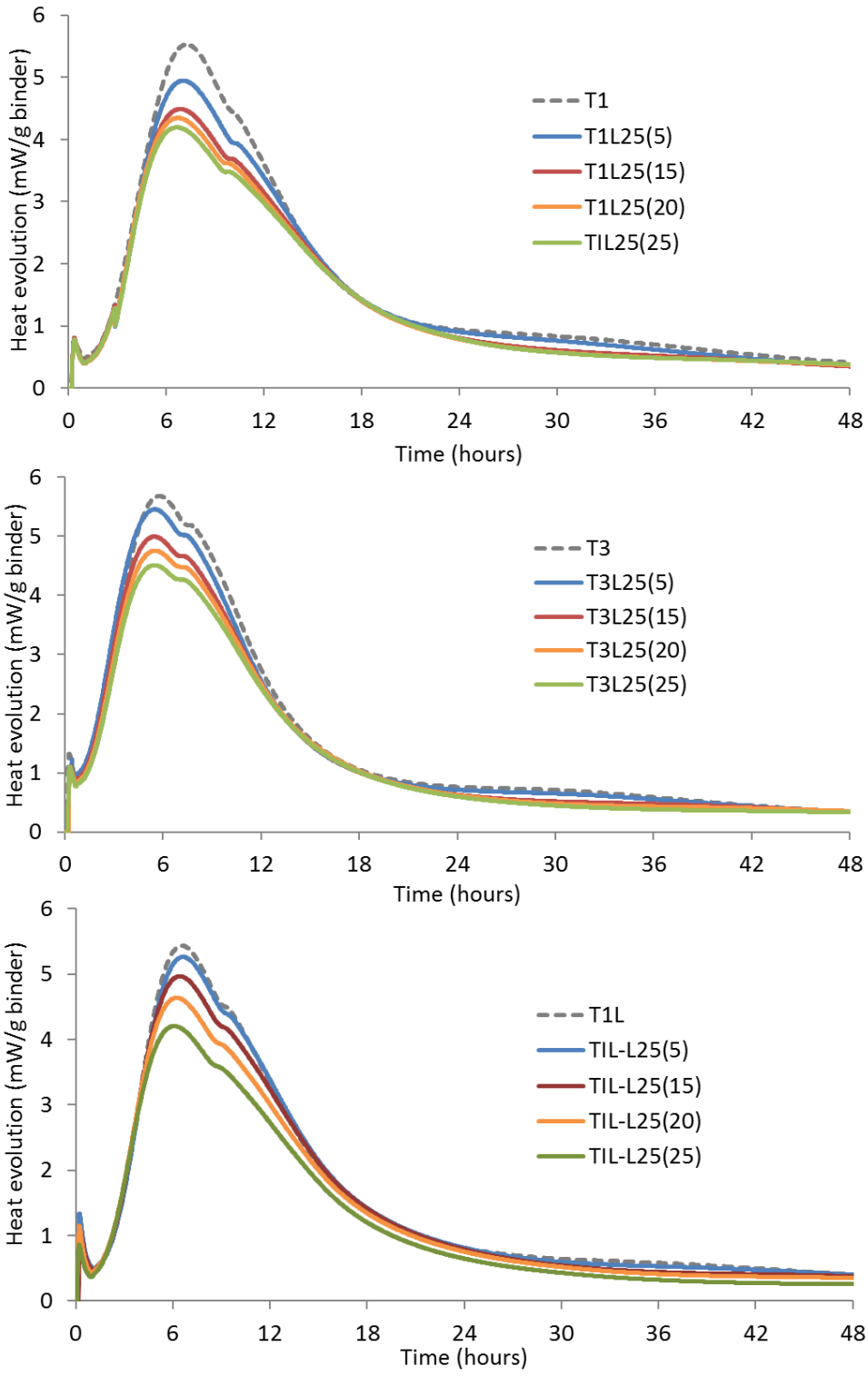

Figure 4-3: Heat evolution of Type I/II, Type III, and Type IL cements with varying percentages of cement substitution by a 25 µm limestone powder

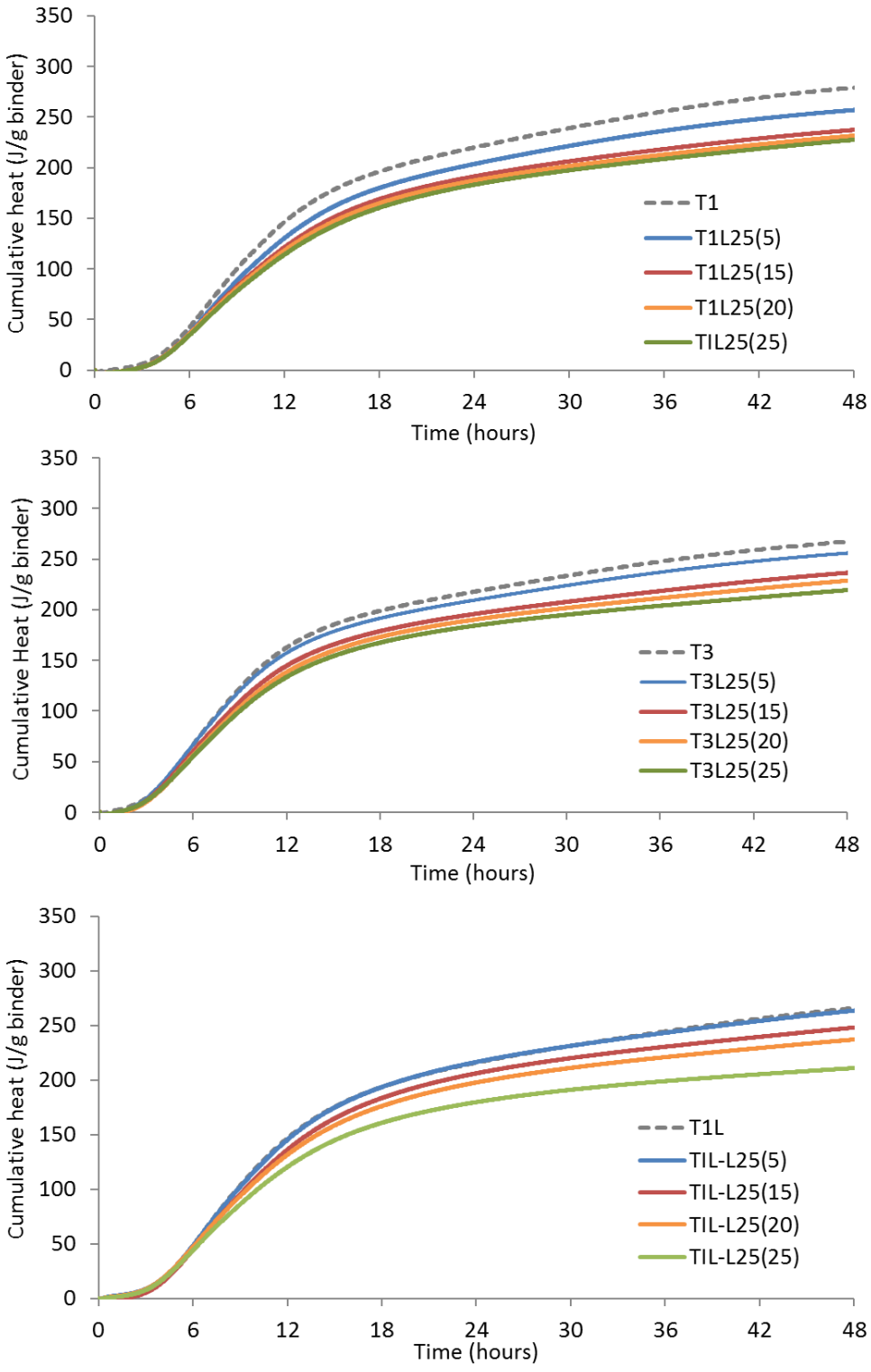

Figure 4-4: Cumulative heat of Type I/II, Type III, and Type IL cements with varying percentages of cement substitution by a 25 µm limestone powder

Table 4-3 shows that for the Type I/II and Type IL cement blends, the time to peak accelerates as the cement replacement increases from 10 to 20%. Whereas for the Type III cement blends, the time to peak is slower as the cement replacement increases from 10 to 20%. Due to dilution, the peak hydration of all cement blends decrease as the amount of limestone increases from 10 to 20%. For all three cements, the 40 μm at 20% cement replacement produces the lowest cumulative heat of hydration at all ages. This heat reduction could be useful for hot weather concrete placements or when casting large concrete sections were heat control is essential.

When comparing the cumulative heat of hydration at 48 hours for the three cements with the effect of the limestone median particle size and the percent substitution, it appears that the median particle size effects the cumulative heat of hydration of the three cements in similar ways. Figure 4-5 shows a plot of how varying percentages of the 25 μm limestone powder affects the cumulative heat of each of the hydrating cements. The graph shows that regardless of cement type, the decrease in cumulative heat at 48 hours as the percent substitution increases follows a similar trend. This trend was also observed with the 3 and 40 μm limestone powders. In other words, it appears that replacing up to 25% of cement with limestone powder of a particular median particle size will affect the cumulative heat of hydration of cements similarly, regardless of cement type.

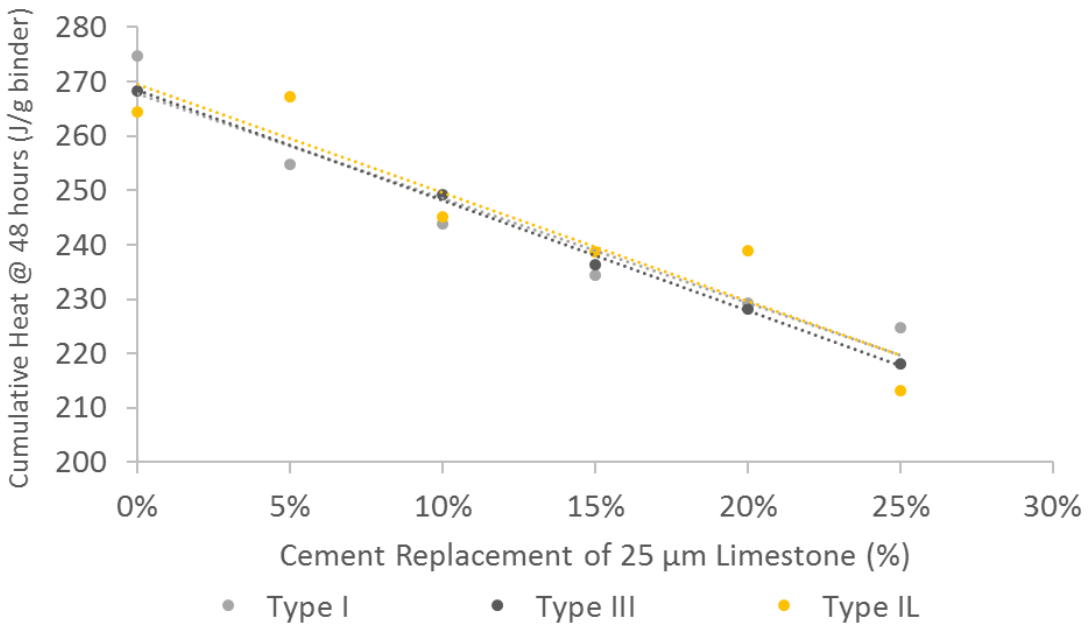

Figure 4-5: Cumulative heat of hydration at 48 hours for Type I/II, III, and IL cements and varying percent substitutions of 25 µm limestone powder

Figure 4-6 shows how the cumulative heat at 48 hours of various limestone powders affect the hydration of the Types I/II, III and IL cements. The graphs show that, regardless of cement type, the finer limestone powder (3 µm) has less of an effect on cumulative heat than the coarser powder (40 µm), visually shown by the shallower and steeper sloped graphs, respectively. The effects of each limestone size have a similar effect, regardless of cement type, indicated by the similar slopes associated with each median particle size. Since the trend is linear, predictions can be made as to the effect of cement substitutions. For instance, for each 10% cement substitution of the 3, 25, and 40 µm limestone powder, cumulative heat at 48 hours is reduced approximately 5%, 7%, and 9%, respectively, regardless of cement type. This information would allow designers concerned about heat gain in concrete mixes the ability to predict the cumulative heat of various mixes depending on percent cement replacement and limestone median particle size.

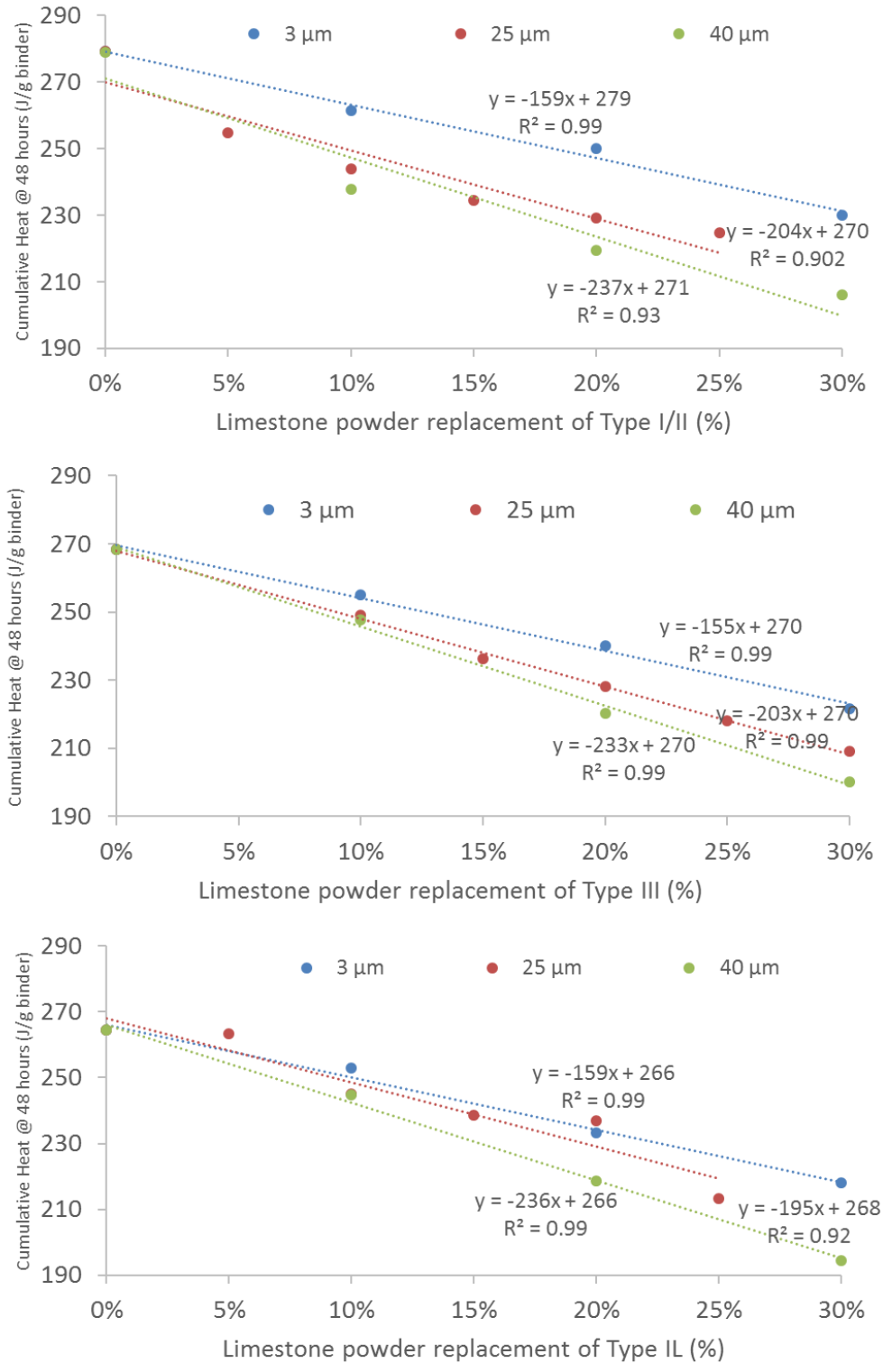

Figure 4-6: Cumulative heat of hydration at 48 hours for a Types I/II, III and IL cements with varying percentage cement replacement of varying limestone powders

4.3.1.3 Comparison of Limestone and Quartz Hydration

To distinguish between the physical and chemical effects of hydration with limestone powder, a comparison was made with a truly inert filler, quartz. The heat of hydration and cumulative heat gain over 48 hours was compared between the 3 μm limestone and a quartz having almost identical particle size distribution. The full laser particle analysis is shown in Table 4-1, but the SSA is 917.7 and 905 kg/m^2, and the D_{50} is 3.35 and 3.61 for the limestone powder and quartz, respectively. The isothermal calorimetry comparison between the hydration of limestone powder with median particle size of 3 μm and an inert quartz powder at cement substitution rates of 10 and 20% by mass shows that even fillers with similar particle size distributions can have slightly different reaction rates (Figure 4-7). In the case of the limestone powder, the hydration curve shifts to the left showing greater nucleation effects and very little dilution effect at either the 10 or 20% cement replacement by mass. Whereas, the quartz hydration shows less nucleation effects and more dilution compared with the limestone powder. This result seems to favor the hypothesis that concrete mixes made with cement substitutions of a 3 μm calcitic limestone powder may have favorable results for precast applications in terms of early strength gain [17]. The cumulative heat gain of the limestone and quartz with similar particle size distribution and percent substitution is more similar than the heat gain evolution, showing that although the limestone powder hydration is accelerated initially, it eventually slows down and the quartz hydration catches up.

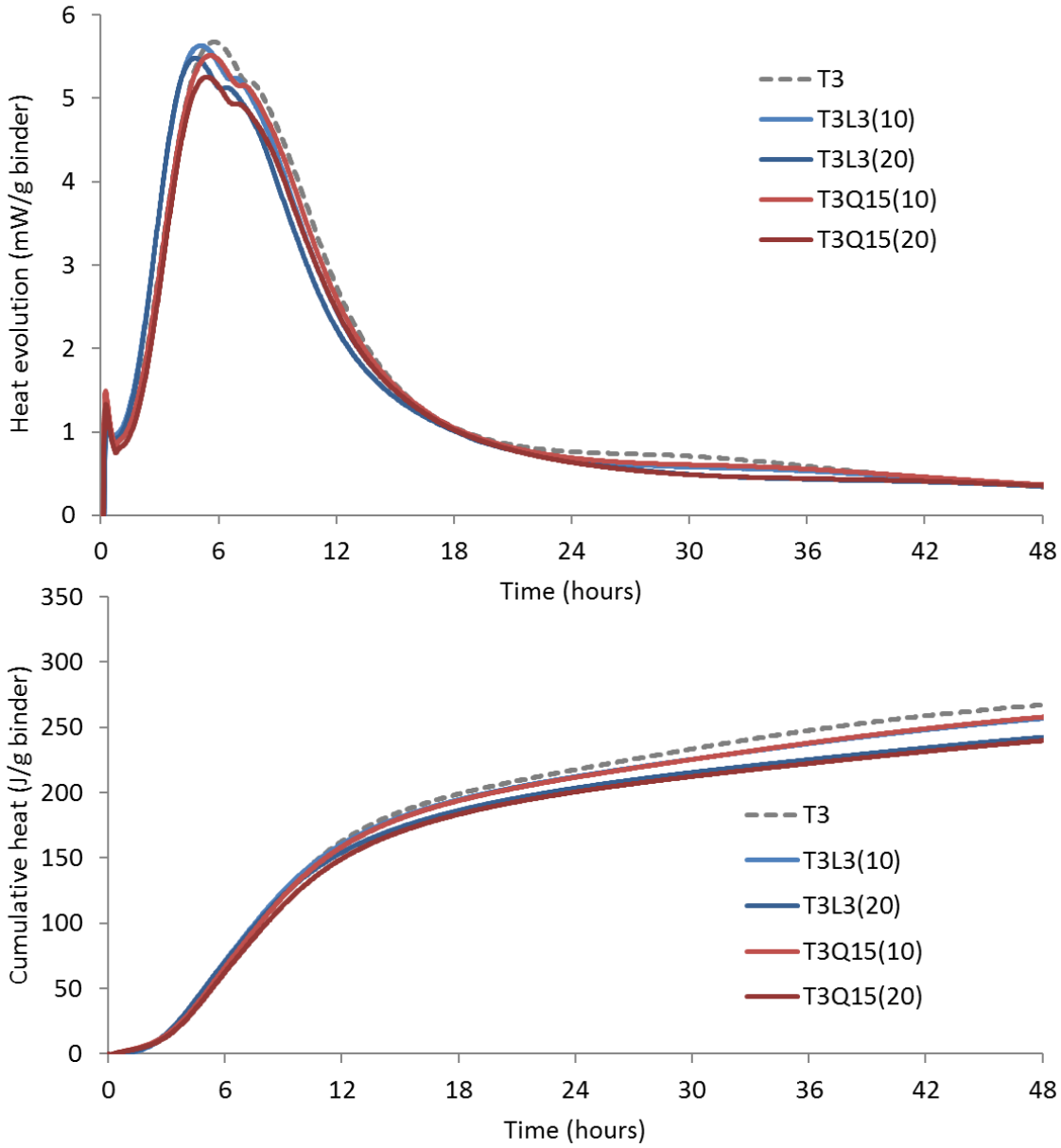

Figure 4-7: Heat evolution and cumulative heat comparison of limestone powder and quartz with similar particle size distributions

4.3.2 Vicat Time of Set

4.3.2.1 Effect of limestone median particle size

Vicat time of set was measured for Type I/II, Type III and Type IL cements with 10% cement substitutions of a 3, 15, 25, and 40 μm limestone powders. Figure 4-8 shows how the four varying fineness limestone powders affect the time of set for each of the three cements differently, depending on the relative fineness between the cement and limestone, and the balance between nucleation, dilution and particle packing. In some cases, set time is accelerated while in other instances it is delayed. For all three cements, the finest 3 μm limestone powder accelerated time of set and the 40 μm powder had the longest set time.

For the coarser ground Type I/II cement, the cement substitution of 10% of any of the limestone powder accelerates both initial and final set, regardless of median particle size. This result correlates with the calorimetry study were the time to peak hydration was accelerated for all the limestone powders except the 40 μm. For the finely ground Type III cement, only the finest 3μm limestone powder accelerates initial and final set, while the courser ground powders delay set times. This result is slightly unexpected since the calorimetry study showed the same trend of speeding up the time to peak hydration similar to the Type I/II cement. Although the Type IL cement is a finely ground cement with a large specific surface area and was mixed at similar water-to-binder ratios as the Type III cement, due to the conflicting effects of dilution and nucleation, the initial and final set times are much longer than either the Type I/II and III cement set times. The cement substitution of 3, 15, and 25 μm decreased initial and final time of set, while the 40 μm prolonged it.

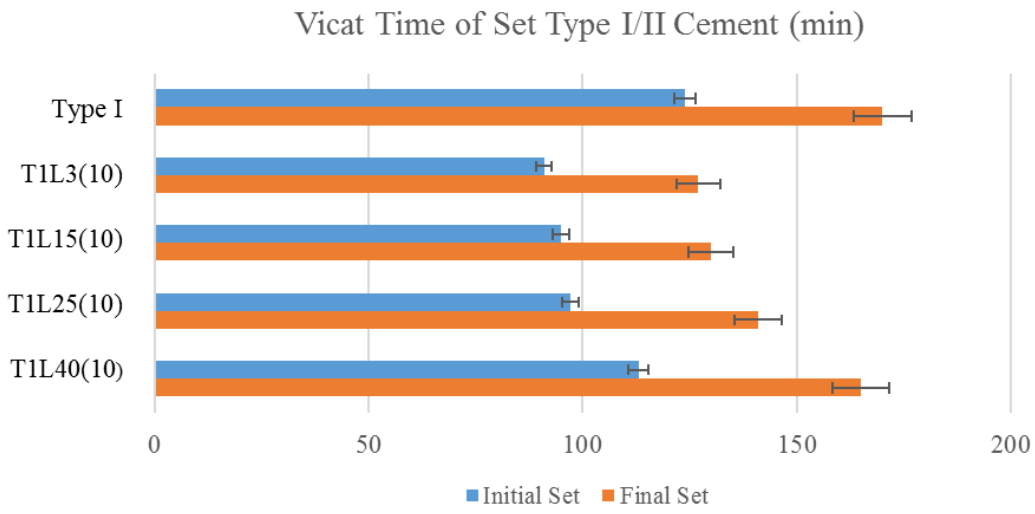

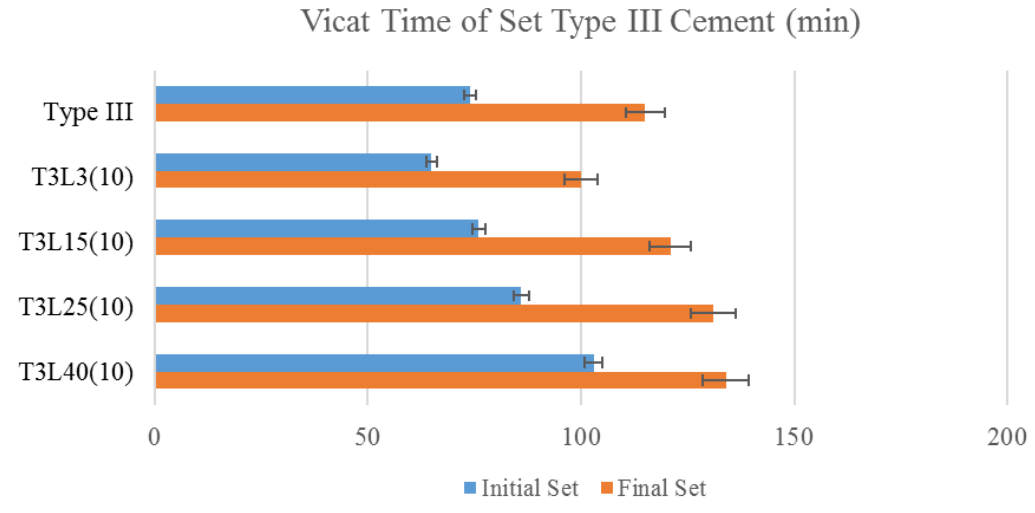

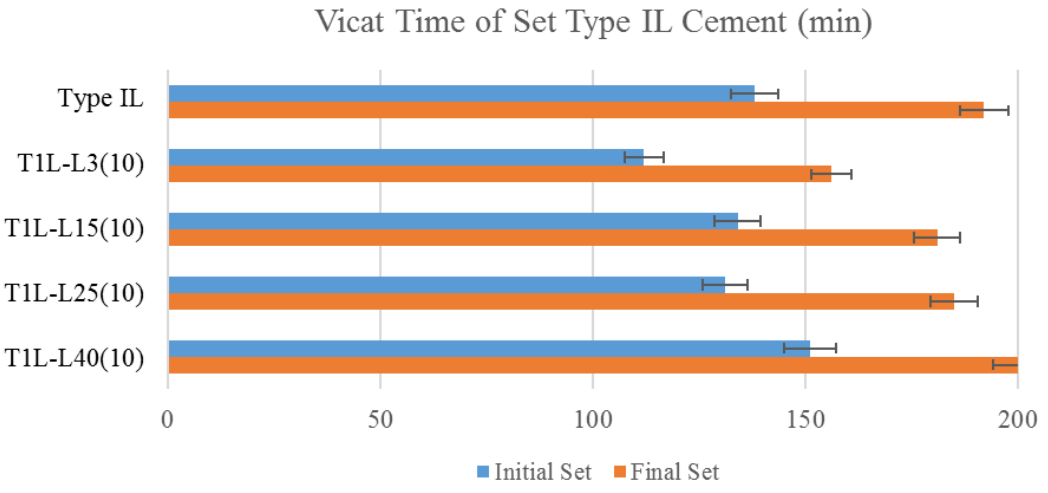

Figure 4-8: Vicat Time of Set with 10% limestone of varying median particle size

4.3.2.2 Effect of percent substitution by limestone powder

Figure 4-9 shows how limestone content affects initial and final set time as more limestone replaces cement. Similar to the dilution effect observed in the calorimetry study, for all cements, the initial and final time of set increases as the percentage of limestone powder increases. The initial set time appears to be more affected than the final set time, regardless of cement type. For Type III cement, for each additional 10% limestone powder added, the initial set is delayed around 13% and the final set is delayed around 8%. As more cement is replaced by a less reactive constituent, the water to cement ratio is effectively increased producing a wetter mix that takes longer for the cement paste to harden.

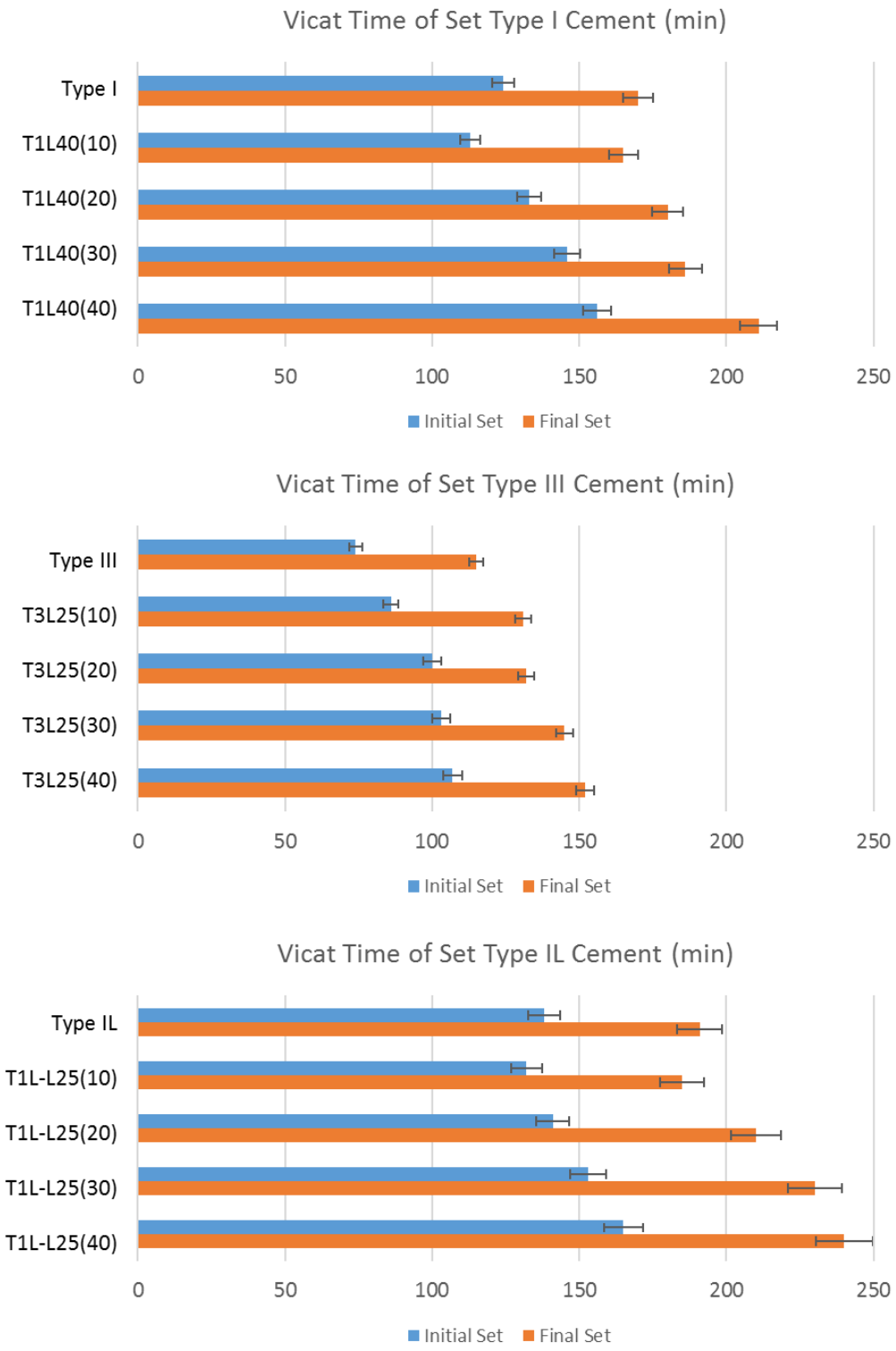

Figure 4-9: Vicat Time of Set with Increasing Cement Replacement

4.3.3 Vicat time of Set and Median Limestone Particle Size

In comparing the time of set of Type III with the varying percent limestone substitutions, the time of set follows a similar behavior to the cement hydration in that the effect of the 3 μm limestone powder is less pronounced that the effect of the 40 μm limestone powder. Figure 4-10 shows that substitutions of up to 30% of the 3 μm limestone powder *accelerates* initial and *delays* final set time of the paste by around 3% on average for every 10% cement replacement, whereas every 10% cement substitution of the 25 μm limestone powder *delays* initial and final set times by 11% and 8%, respectively. Cement substitutions of the 40 μm limestone powder delays initial and final set times of the Type III pastes by 35% and 32%, respectively. This delayed set time with the 40 μm limestone powder, if undesirable, can be modified using set accelerator admixtures.

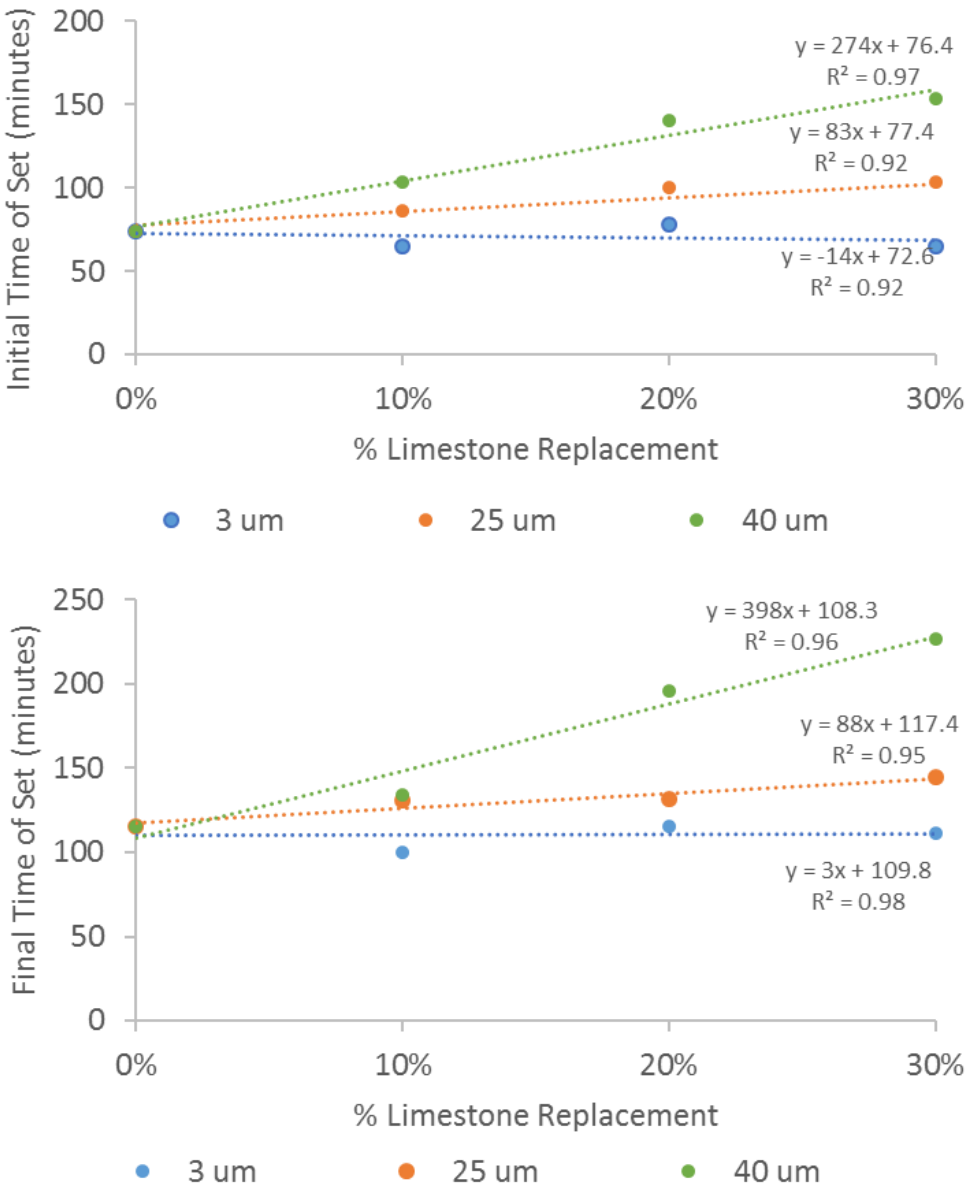

Figure 4-10: Time of Set with Type III cement replaced with varying percentages of 3, 25, and 40 µm limestone powders

4.3.4 Workability - Mini slump

Cement paste workability was evaluated from the spread diameter produced from lifting a mini slump cone and allowing the cement paste to spread freely on an acrylic surface. A greater spread diameter, D_f, indicates a lower yield stress and greater paste workability (Figure 4-11) [76].

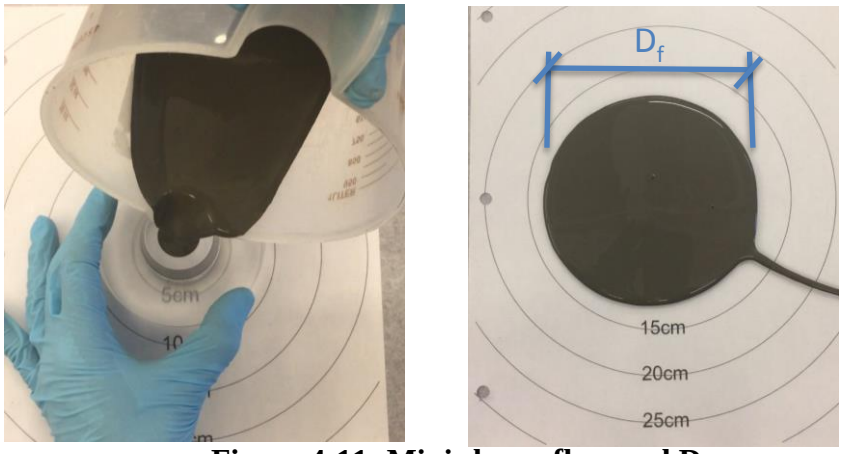

Figure 4-11: Mini slump flow and D_f

Figure 4-12 shows how the spread diameter of cement pastes varies with 10% substitutions of 3, 15, 25, and 40 μm limestone powders. Dashed lines represent the base cements without any limestone powder. It is worth noting that the spread diameter of the Type IL cement without any limestone powder replacement was significantly smaller than the other two cements. As seen in the graph, for all cement types, as the median particle size of the limestone powder increases (becomes coarser), the yield stress decreases, leading to improved workability. For the case of the Type III cements, the finer 3 μm limestone powder had a smaller spread diameter than the neat cement indicating more paste cohesion and less workability than the base cement paste without limestone. In the case of the Type IL cement, all limestone powders regardless of median particle size increased

spread diameter, indicating improved workability. For all three cements, the cement substitution of 10% of the 15 and 25 μm limestone powder had the most positive effect on workability. The cement substitution of 10% of the 3 μm limestone powder had a negligible effect for the Type I/II cements, a decrease in spread diameter for the Type III cement and a significant increase in spread diamter for the Type IL cement. There was very little difference in spread diameter between cement pastes prepared with limestone powders of median particle size of 25 μm and 40 μm. There appears to be an optimum median particle size around 15 to 25 μm where beyond that the workability stabilizes for all three cements. In Chapter 5 when looking at concrete mixes, this reduced yield stress sometimes leads to excessive bleeding and mix segregation.

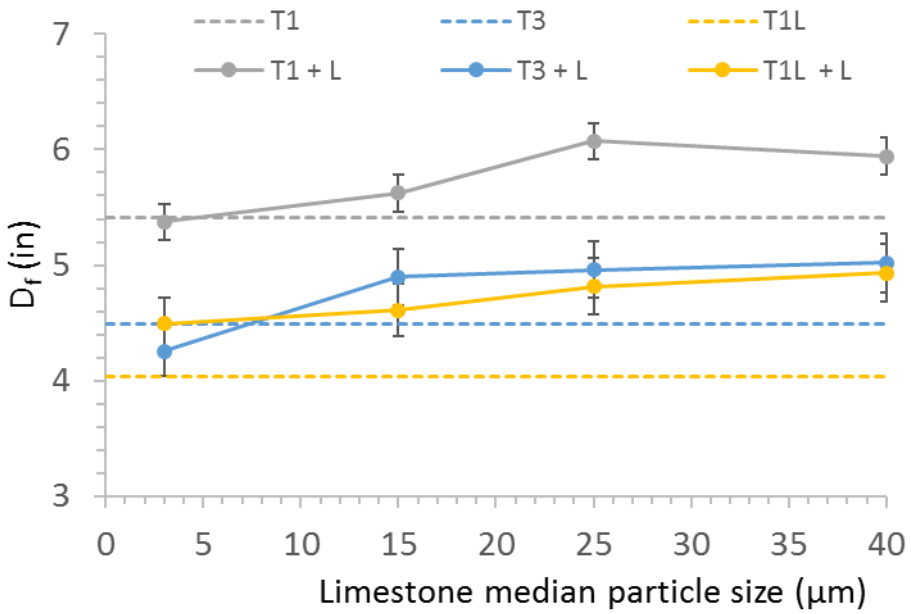

Figure 4-12: Cement paste spread diameter with 10% limestone replacement

Figure 4-13 shows the effect of replacing cement with varying percentages (0-25%) of 25 µm limestone powder. As previously noted, the particle size distribution of the 25 µm limestone powder is most like the Type III and Type IL cements. One would expect to see a greater dilution effect in these cements as the percentage of limestone powder increases. However, the dilution effect is most notable with the Type IL cement that already has 9% limestone powder, albeit ground finely. Therefore, it appears that intergrinding limestone powder and cement to make a Type IL cement, leads to increased cohesion and decreased workability. Increased workability for a Type IL cement requires the cement substitution of around 12% limestone powder to reach the same spread diameter of a Type III with the same percent limestone substitution. The yield stress of the Type I/II cement appears to be the least affected by increased limestone powder substitution rates.

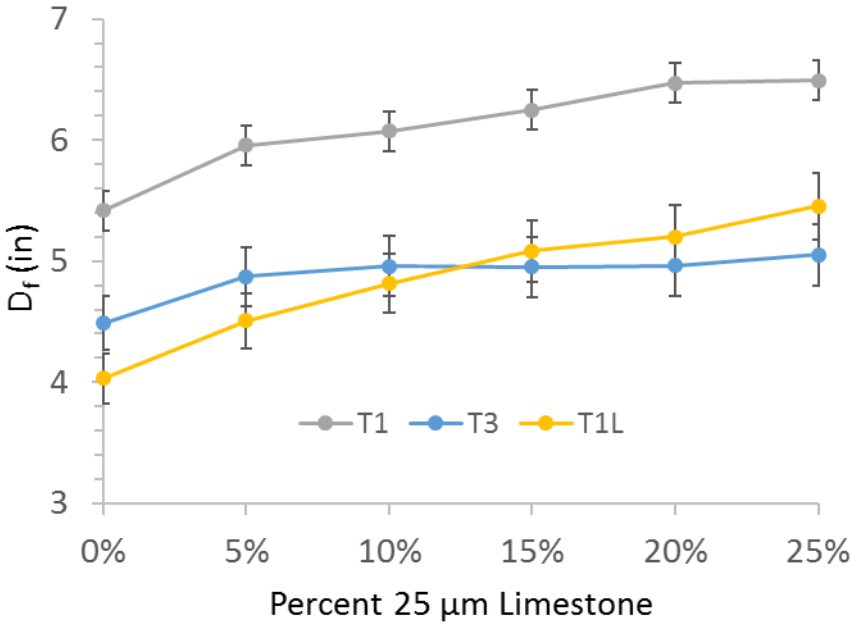

Figure 4-13: Cement paste spread diameter with varying percentage of limestone powder with 25 µm median particle size

4.3.5 Mini slump and limestone median particle size

Figure 4-14 shows how varying percentages (from 0 to 25%) of cement substitution of 3, 25, and 40 μm limestone powder affects the yield stress of Type III-limestone blended cement pastes. Adding either 25 or 40 μm limestone powders to Type III cement blends increases the spread diameter at any cement replacement values, which should lead to improved workability of concrete mixes. In the case of the 25 μm powder, the spread diameter remains fairly constant after 10% substitution and it is unclear how beneficial additional cement replacement would be to workability. On the other hand, the 40 μm limestone powder shows continuously increased workability as the percent cement replacement increases.

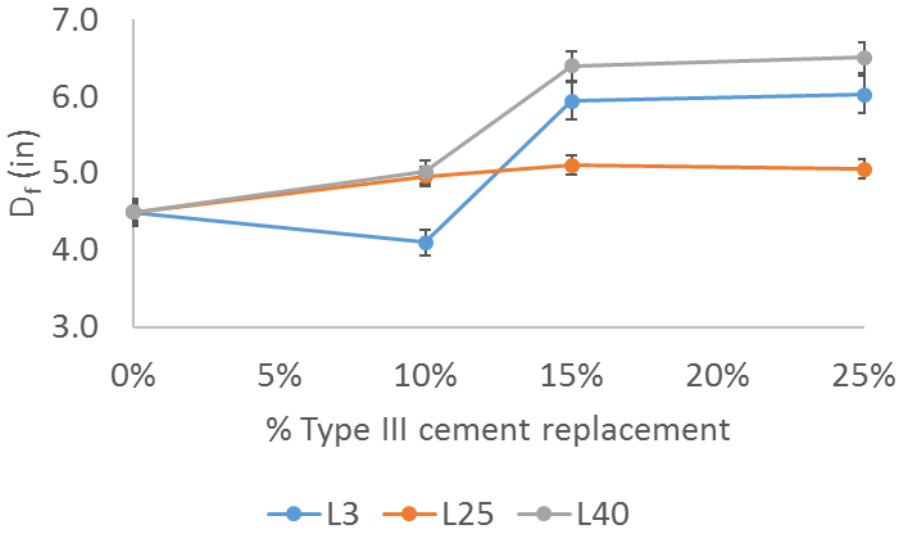

Figure 4-14: Mini slump yield stress of Type III cement with varying % limestone replacement

The substitution of the 3 μm limestone powder follows a slightly different trajectory. At low doses of cement substitution, the spread diameter decreases presumably

due to more agglomeration from the greater surface area of the finer limestone powder compared to the cement base. As the cement replacement increases and the paste become more diluted with limestone powder, spread diameter increases. Similar to the 25 μm powder, little change is observed after 15% cement substitution.

For proportioning concrete mixes, it would appear that when using a fine limestone powder (3 μm), cement substitutions up to around 15% are required to improve workability. When using coarser limestone powders (40 μm), any amount of cement substitution improves workability up to around 15% cement replacement. However, care must be taken with increased cement replacement, which may lead to less cohesive mixes and promote excessive bleeding and segregation.

4.4 Mortar Compressive Strength

The results of the mortar compression tests for Type I/II cements and Type III cement with 0, 10 and 20% limestone substitution and at varying limestone median particle size (3, 25, and 40 μm) at 7 and 28 days are shown in Figure 4-15 and Figure 4-16. All mixes had constant w/b ratio of 0.44.

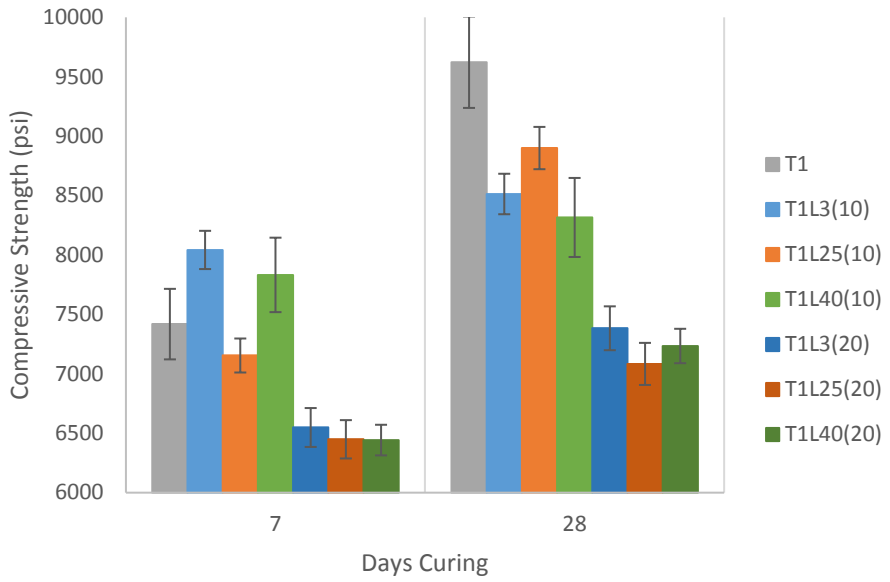

Figure 4-15: Mortar Compressive Strength – Type I/II and limestone powder

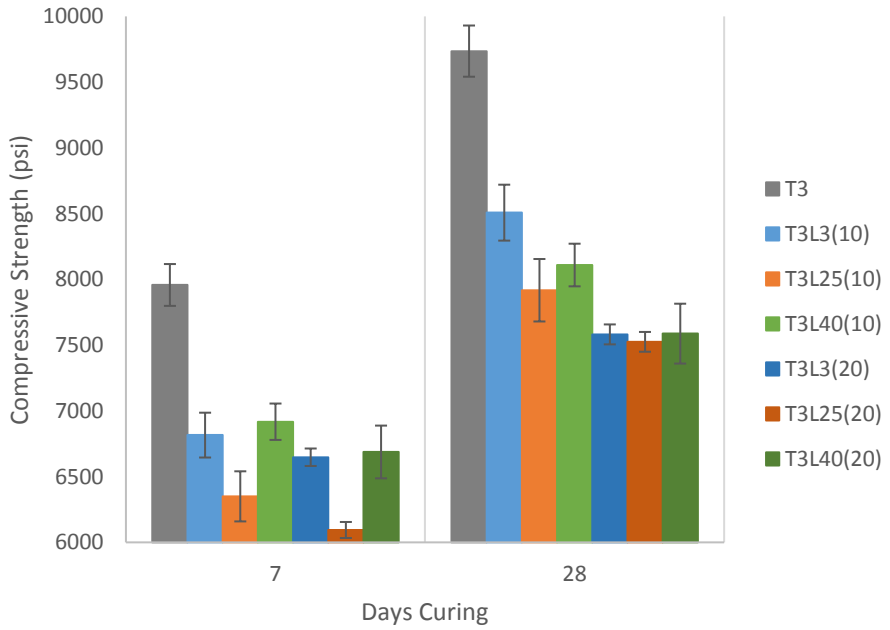

Figure 4-16: Mortar Compressive Strength – Type III and limestone powder

As expected, due to dilution effect, the mixes with only 10% cement replacement show greater strengths than the mixes with 20% cement replacement, regardless of the limestone median particle size. In general, the mixes made with the finer limestone powder (3 μm) show higher compressive strengths than the other two limestone powders (25 and 40 μm). Surprisingly, the mixes made with cement substitutions of the 25 μm limestone powder had lower compressive strengths than the 40 μm limestone powder regardless of the cement type. The one exception was the Type I/II mix with 10% cement substitution (T1L25(10)) at 28 days which has a higher compressive strength than the other powders. This reduced strength for the 25 μm limestone could be attributed to the similarities in particle size distribution between the limestone and the cements. The 40 μm limestone powder, however, has a wider particle size distribution and therefore may benefit from improved particle packing.

There was more variation in compressive strengths of mortars at 7 days than at 28 days and with mortars made with 10% cement replacement than with mixes having 20% cement replacement. For example, the three mortars made with Type I/II but with 20% limestone replacement showed similar 28-day strengths regardless of median particle size. Additionally, the difference in 28-day mortar compressive strength between the 10% cement replacement and 20% cement replacement was less significant with mortars made with Type III cement than with the Type I/II cement. The trends in mortar strength will be compared in later chapters where concrete mixes are evaluated.

4.5 Life Cycle Analysis

A life cycle analysis was performed using SimaPro Eco-indicator 99 in order to determine the environmental benefit of using limestone powder as a cement substitute. The cradle-to-gate comparison was performed between concrete mixes with a w/b ratio of 0.38 using only ordinary Portland cement (OPC) and two concrete mixes with either a 20% cement substitution of fly ash or a 25 μm limestone powder by mass, which is the what is currently used in Atlanta area precast plants. The scope of the study was contained within the production and transportation of cement from Holly Hill, SC, fly ash transported from Wilsonville, Alabama and limestone powder ground and transported from Marble Hill, GA for use in a precast concrete plant in Atlanta, GA. Included in the study was production energy associated with quarrying and grinding limestone powder supplied by Imerys Carbonates. Since fly ash is considered a waste materials, it has no production energy associated with it, but does include transportation energy.

The SimaPro analysis determines the environmental impact of many factors and scales them to a single score, Pt, defined as the impact one average European has in one year. As can be seen from Figure 4-17, the concrete mixes produced with a 20% cement substitution of either fly ash or limestone powder are comparable. When compared to the OPC concrete mix, the main environmental benefit comes from climate change (CO_2 emissions) and respiratory inorganics. The energy associated with transportation of material and grinding of limestone powder is negligible compared to the production energy and climate change potential required to produce Portland cement. This analysis, however, is limited to just the environmental effect of the mix constituents; it does not take into the environmental impact associated with the strength or durability of the concrete.

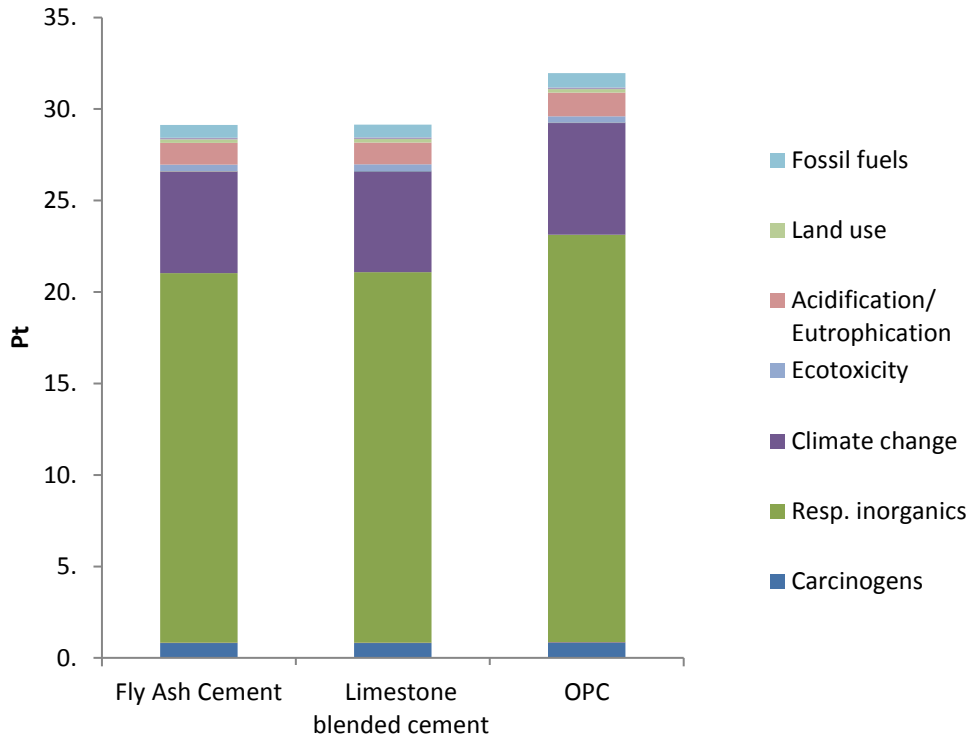

Figure 4-17: Comparison of concrete mixes with and without 20% cement preplacement of fly ash or 25 μm limestone powder

4.6 Conclusions and Discussions

Using limestone powder as a cement replacement is an environmentally friendly option that provides potential for tailoring concrete mixes to achieve prescribed performance goals. The fineness of the limestone powder replacing the cement affects hydration kinetics, time of set, workability and compressive strength. The finer the limestone powder, the faster the hydration occurs due to increased nucleation sites from the greater surface area. This trend was seen with both the accelerated hydration curves and Vicat time of set. An opposite trend was seen with results of the mini slump where the

coarser limestone improves workability and the finer limestone makes the mix more cohesive but less workable.

The trends for the mortar compressive strength are not as clear. In some instances, the mixes made with 3 μm powder produced the highest strength mortars, but in other cases, the 25 μm limestone powder did. In general, however, the lowest mortar compressive strengths were achieved using the 25 μm limestone powder as cement replacement, perhaps due to a less efficient particle packing when using a limestone powder with similar particle size distribution as the base cement. In addition, the reduction in compressive strength due to the dilution effect between 10% and 20% cement replacement is less significant when using Type III cement compared with Type I/II. This may prove useful to precast suppliers who tend to favour Type III cement due to its higher early strength.

The effect of cumulative heat gain at 48 hours is more affected by the median particle size of the limestone powder and less affected by the cement type. The smallest reductions in cumulative heat were seen when substituting cement with the limestone powder having the finest median particle size (3 μm) and the greatest heat reduction was seen with the 40 μm limestone powder. Due to the linear relationship of cumulative heat and percent limestone substitution rate, predictions can be made as to how much heat reduction will occur at each limestone substitution rate.

When used as cement replacement, the median particle size of the limestone powder affects the initial and final time of set of cement paste. In general, finer ground limestone powders accelerate both initial and final set times while coarser ground limestone take

longer to set. The percent limestone content and set time has a linear relationship depending on the median particle size of the limestone powder and can be used to predict initial and final set times of a given cement type.

The median particle size of the limestone powder used as cement replacement can greatly affect the workability of pastes made from cement limestone blends. The coarser the limestone powder, the larger the spread diameter and consequently better paste workability. An increase in limestone content in general improves workability, up to a point, depending on the median particle size of the limestone powder used. Each limestone median particle size appears to have an optimal range depending on the cement type. When using Type III cement and 3 μm limestone blends, substitutions above 15% are required to lower yield stress and insure adequate workability, whereas only 10% of the 25 μm limestone is optimal. Increasing cement replacements of the 40 μm appear to linearly improve workability of the Type III cement blends, but care should be taken when overly diluting the cement, which can lead to excessive bleeding and segregation.

CHAPTER 5. WORKABILITY AND SURFACE FINISH OF PRECAST CONCRETE MADE WITH LIMESTONE BLENDED CEMENTS

5.1 Introduction

As defined by ACI 237R, self-consolidating concrete (SCC) is a non-segregating highly flowable concrete that can flow under its own weight to fill formwork without the need for mechanical consolidation [45]. Precast suppliers use self-consolidating mixes to ensure proper filling of formwork and improve surface finish. SCC mixes are similar to conventional concrete mixes except that SCCs tend to have higher binder to aggregate ratios and maximum aggregate size limits to improve mobility [12]. Mixes with too high of fines are too viscous impeding mobility whereas mixes with too low of fines leads to bleeding and segregation. Until recently, precast suppliers used fly ash as a cost-effective partial cement replacement method to increase the fine content of flowing mixes. Due to seasonal supply limits of fly ash, precast suppliers have found that substituting a portion of the cement with limestone powder is also a cost-effective method to ensure a high enough powder content to reduce bleeding and segregation while still maintaining adequate workability.

An additional concern for precast suppliers is the presence of bug holes after removing formwork from precast members. Bug holes are imperfections on the surface of concrete due to entrapped air, oil and/or water on formwork surfaces that are generally more pronounced in high viscosity, low slump flow mixes [77]. Although they rarely

present a structural concern, their presence decreases production time due to required finishing and patching work thus increasing the cost of structural members.

Based on mini slump studies performed on blended cement pastes presented in Chapter 4, the addition of limestone powder can decrease the yield stress of cement pastes that may lead to greater workability in flowing concrete mixes. Cement pastes mixed with blends of a coarser limestone powder showed decreased yield stress than those blended with a finer limestone powder. Whether blending with a fine or coarse limestone, increasing the percent of cement replacement also lead to a decrease in yield stress.

Although there is extensive research on blending or interground limestone with Type I/II cements that are ground finer that the base cement [31, 37, 78, 79], there is limited research on blending coarser ground limestone with other cement types such as Type III, commonly used by precast suppliers. Additionally, current research using coarser ground limestone used varying water-to-binder ratios which do not isolate the effect of the limestone median particle size [80]. Inconsistencies exist in the literature among reported information regarding the workability of pastes, mortars and concrete mixes made with limestone powders [5, 31, 48, 80]. Isolating the influences of the limestone powder itself is further complicated due to experimental variations with water-to-binder ratios, varying dosages of high range water reducing admixtures (HRWRA), or whether limestone was used as a mix addition or cement replacement. Therefore, in order to isolate the effect of both median particle size and limestone content on fresh concrete properties of flowing concrete mixes, this chapter addresses the following two questions: what is the effect on fresh concrete properties of flowing concrete mixes with 0, 15, and 25% cement replacement by mass of limestone powder and how does the median particle size of the

limestone affect both workability and surface finish? Compressive strength, drying shrinkage, creep, and permeability will be discussed in Chapter 6.

5.2 Materials and Methods

Self-consolidating concrete mixes were developed at the Georgia Tech Structures Lab to study the fresh and hardened concrete properties of mixes with limestone powders. The basis for the concrete mixes investigated was on a mix from a local precast manufacturer which used a Type III cement blended with a limestone powder having a median particle size of 25 μm, achieved a slump flow of 20 inches and reached a compressive strength of 4,000 psi and 5,000 psi in 1 and 3 days, respectively, without accelerated curing. In the experimental mixes, the water content of the base mix was modified slightly to account for the moisture content of the aggregates used and the HRWRA dosage to achieve a 20-inch slump flow just after mixing when using the 25μm limestone powder to replace 15% of the cement.

Mixes with two types of cements, Type I/II and Type III, along with varying percent substitutions (0, 15, and 25%) of three limestone powders (3μm, 25μm, and the 40μm) were investigated. A companion Type IL SCC mix was also examined to understand the differences between interground limestone blended cements and SCC mixes with limestone powder added during the mixing process. The chemical composition (Table 3-1) and particle size distributions (Table 3-2) of the materials used are presented in Chapter 3. Concrete mixes with the 15μm limestone powder were not investigated since previous cement paste studies showed very similar behavior compared with the 25μm limestone,

and to get a wider range of properties that bracketed the fineness of the different cement types.

Table 5-1 shows the proportions of the fifteen concrete mixes studied. The naming nomenclature of the concrete mixes lists the type of cement followed by the limestone median particle size and percent limestone substitution. T3 is the Type III cement, T1 for Type I/II cement and T1L for Type IL cement. L3, L25, and L40 represent the median particle sizes of the 3 μm, 25 μm and 40 μm limestone powder. The number in parenthesis designates the percent cement replacement in the mix. Therefore, T3L3(25) represents a mix using Type III cement with a 3 μm limestone powder at a 25% cement replacement rate.

Table 5-1: Mix Proportions of SCC concrete mixes

		% limestone		
		0%	**15%**	**25%**
Cementitious Material ***lb/yd³***	cement	850	725	637
	limestone	-	125	213
	water	340	340	340
	w/b	0.40	0.40	0.40
Aggregate ***lb/yd³***	#67 stone	1724	1724	1724
	natural sand	1200	1200	1200
HRWRA	oz/yd^3	38-54	38-60	31-48
	oz/cwt	4.5-6.4	4.5-7.0	3.6-5.6

The high cement content was deemed adequate to achieve high early strength, to ensure that the effects of limestone substitution would be advantageous, to reduce bleeding and to achieve an appropriate level of workability. Additionally, to better isolate the influence of the median particle size and content of the limestone powder on each cement type, a constant water-to-binder ratio, and coarse and fine aggregate content was

maintained. The HRWRA (Glenium 3400) was modified slightly on mix T3L3(15), T3L40(25), T1L3(25), T1L40(25) and T1L to either achieve a 20 inch slump flow or to reduce bleeding.

Based on the results from the mini slump study discussed in Chapter 4, a different HRWRA dosage for the Type I/II and Type III concrete mixes was used since mixes with Type I/II cement could reach comparable final spreads with less HRWRA. An SCC mix was also cast using the Type IL cement with the a modified HRWRA so that mechanical property comparisons could be made between mixes with interground limestone and blended limestone cements of similar fineness. Long-term concrete property such as compressive strength results are discussed in Chapter 6.

Approximately 2 ft^3 of the fifteen concrete mixes were prepared in a 5-ft^3 revolving drum mixer per ASTM C192 [81]. Coarse and fine aggregate were added to the mixer and mixed until thoroughly blended. The cement and limestone powder, if used, were added next and mixed for a few minutes until the aggregate was fully coated by the cement blend. Next, the mixing water was added to the mixer and the timer started. The mixer would run for one minute followed by a brief pause when the HRWRA was added to the mix. Finally, the mixer was allowed to run for two additional minutes, followed by a 3-minute rest period and a 2-minute final mix.

5.2.1 Slump flow, flow rate, S-groove and VSI

In field applications, concrete suppliers use four main methods for determining workability, relative viscosity, self-healing and stability of self-consolidating concrete mixes – slump flow, flow rate, S-groove test, and the visual stability index, VSI. Slump

flow was determined according to ASTM C1611, where the SCC mixes were placed in a dampened inverted Abram's cone in one lift without vibrating or tamping resting on a dampened base plate [82]. After raising the cone 225 ± 75 mm (9 ± 3 in) in 3 ± 1 seconds using a steady upward movement with no lateral motion and allowing the concrete to spread freely, slump flow was determined as the average spread measured in two orthogonal directions. The total time from filling to lifting was under 2.5 minutes. A common acceptable slump flow for precast applications is 20 in. (500 mm). Flow rate, T_{20}, is the time it takes for the slump flow to reach a spread of 20 in. (500 mm) from the time of initial lifting of the cone. It is generally considered to be a measure of relative viscosity among the concrete mixes. The S-groove test was used to determine the self-healing ability of SCC mixes. During the test, an "S" was drawn into the concrete after measuring slump flow and flow rate, and a disappearing "S" indicates a self-healing mix (Figure 5-1).

Figure 5-1: S-groove test on SCC mix

Finally, the stability of the concrete mixes was determined using the VSI criteria of ASTM C1611 where the distribution of aggregate within the concrete mass, and mortar fraction and bleeding along the perimeter of the slump flow are visually noted as 0, 1, 2 or 3 [82]. A VSI equal to 0 indicates a highly stable mix with no indication of bleeding or

segregation; a VSI equal to 1 is a stable mix with no segregation, but slight bleeding; a VSI equal to 2 is unstable with a slight mortar halo and/or aggregate pile; and a VSI equal to 3 is highly unstable with clear segregation, a large mortar halo and/or large aggregate pile (Figure 5-2).

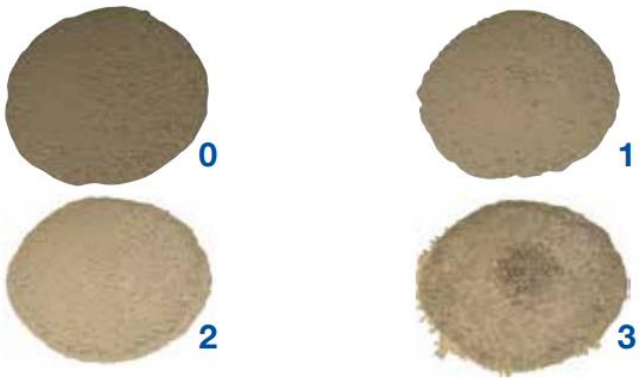

Figure 5-2: Visual Stability Index, VSI [65]

5.2.2 Surface Finish

The finished surface of precast elements is of great importance to precast suppliers. Post-production work such as patching bug holes and honeycombing costs valuable time and money. Therefore, self-consolidating concrete mixes that produce smooth surface finishes is beneficial to precast production rates. To quantify and compare the surface finish produced by the fifteen concrete mixes, the number and size of bug holes and imperfections were manually counted and compared between the different concrete mixes on six 3 in. x 3in. x 11 in. (76 mm x 76 mm x 280 mm) concrete prisms per concrete mix (Figure 5-3) [83].

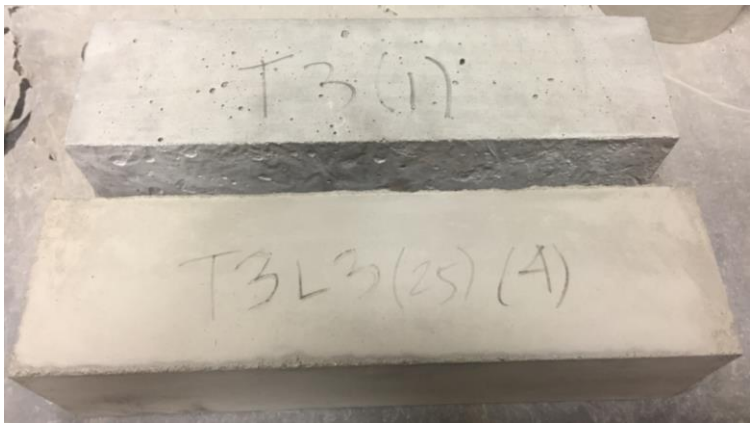

Figure 5-3: Bug hole variations in two concrete specimens

The surface imperfections were classified as either small (under 0.1 in. (2.5 mm), the size of a pinhead, or large (greater than 0.1 in. (2.5 mm), see Figure 5-4. The total number of bug holes on six specimens were tallied and the average was reported.

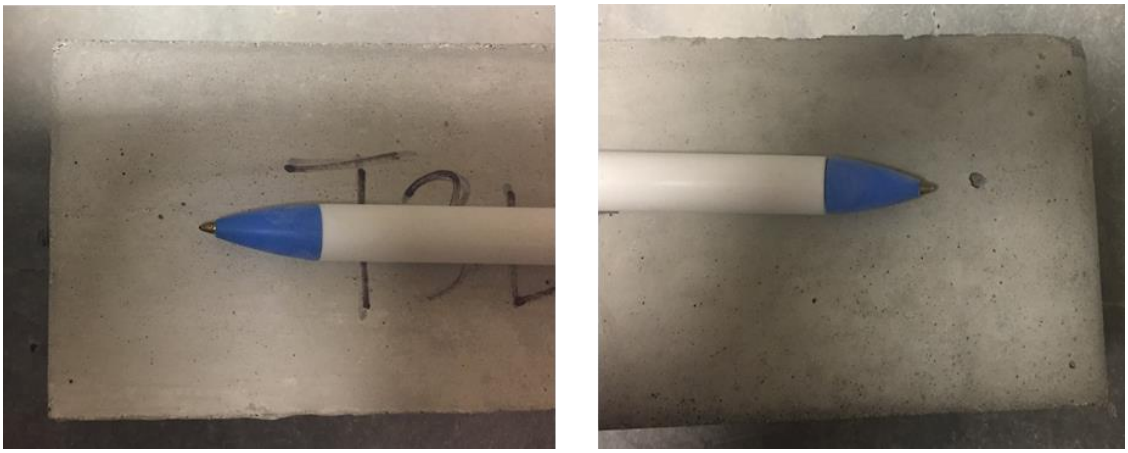

Figure 5-4: Image of small (left) and large (right) bug holes on concrete samples

5.3 Experimental Results

Workability of the fifteen concrete mixes was assessed by measuring the spread diameter of the mixes after lifting an inverted Abrams cone, by determining the time it took for the spread to reach 20 in., by performing an S-groove test and by visually inspecting the perimeter and center of the slump spread to detect signs of separation and bleeding.

5.3.1 Slump flow, flow rate, S-groove, and VSI

The results of the slump flow, flow rate, S-groove test and VSI measurements are listed in Table 5-2. In general, for the Type III mixes, the addition of limestone improved workability and the mixes with 25% cement replacement had greater slump flows than their 15% counterpart. Most blended cement mixes met the slump flow requirement of 20 inches, the T_{20} requirement of 5 seconds, an acceptable S-groove test and a VSI of 0 or 1. Non-self-healing mixes that did not meet the S-groove test also did not meet the slump flow requirement. Some mixes required adjustments to the HRWRA in order to meet a slump flow of 20 inches and an acceptable VSI index. The first mix attempt is noted as "A" and the adjusted mix is listed as "B" in the table. Mix T3L3(15)-A did not meet the required slump flow and was modified with additional HRWRA. Mix T3L40(25)-A had a large slump flow, but showed signs of bleeding and segregation. It had a VSI of 2 and was improved with less HRWRA.

The SCC mixes made with Type I/II-limestone blends were less predictable. Slump flow was reduced with additional limestone powder (25% vs 15%) having either 3 or 40 μm median particle size but improved with the addition of the 25 μm limestone powder. Although all mixes were cast indoors, the decreased slump flow for mixes T1L3(25) and

T1L40(25) could be explained by the cold outside temperatures on the day of casting which may have affected the indoor temperatures of the constituents and resulted in increased mix viscosity. These mixes were recast and noted as "B" in Table 5-2.

Although the mix using the Type IL mix with 9% interground limestone powder was cohesive and showed little signs of bleeding, the mix did not meet the slump flow, T_{20} or S-groove criteria. An increased dosage of HRWRA was needed to make it a viable flowing mix.

Table 5-2: SCC made with limestone powder of varying median particle size and varying percent cement substitutions

Mix	Slump Flow (in)	T_{20} (s)	S-groove	VSI	HRWRA oz/yd^3
T3-A	18	N/A	NO	0	48
T3-B	24	4	YES	0	54
T3L3(15)-A	16	N/A	NO	0	48
T3L3(15)-B	25	3	YES	0	60
T3L3(25)	26	3	YES	1	48
T3L25(15)	23	3	YES	0	48
T3L25(25)	27	3	YES	1	48
T3L40(15)	21	3	YES	0	48
T3L40(25)-A	24	3	YES	2	48
T3L40(25)-B	23	3	YES	0	40
T1	21	4	YES	1	38
T1L3(15)	20	4	YES	1	41
T1L3(25)-A	15	N/A	NO	0	38
T1L3(25)-B	20	4	YES	0	41
T1L25(15)	20	4	YES	0	38
T1L25(25)	25	4	YES	1	38
T1L40(15)	25	3	YES	0	38
T1L40(25)-A	16	N/A	NO	0	38
T1L40(25)-B	26	3	YES	1	31
T1L-A	14	N/A	NO	0	48
T1L-B	20	3	YES	0	54

Note: The HRWRA of T3L3(15), T3L40(25), T1L3(25), T1L40(25) and T1L were modified to meet slump flow of 20 inches and VSI index requirement of 0 or 1

5.3.2 Influence of Concrete Mixer

As previously mentioned, all concrete mixes were prepared in a 5-ft^3 revolving drum mixer. High shear mixers, however, are more common in precast plants. To compare the effect mixer type has on workability, two identical mixes were prepared with the same mix time on the same day. The high shear mixer used was an Eirich mixer with rotational speed of, see Figure 5-5.

Figure 5-5: Concrete mixers used to compare workability

Two 2ft^3 mixes of mix T3L25(15) were prepared. Both mixes had a VSI equal to 0 and acceptable S-groove measurements. Due to the difference in mixing speed and energy, the slump flow of the mix produced with the revolving mixer was 21 inches and the slump flow of the high shear mixer was 27 inches, indicating a 25% improvement in spread, see Figure 5-6.

Figure 5-6: Slump flow comparison of concrete mix made in revolving mixer (left) and high shear mixer (right)

5.3.3 Surface Finish

Visual inspections of concrete prisms cast with each of the fifteen SCC concrete mixes indicate that, in general, mixes with a larger quantity of limestone powder used as cement replacement produced in a revolving mixer, appear lighter in color, have fewer overall surface imperfections and have fewer large bug holes as seen in Figure 5-7. Additionally, mixes produced with Type I/II cement have fewer surface imperfections than those produced with Type III cement.

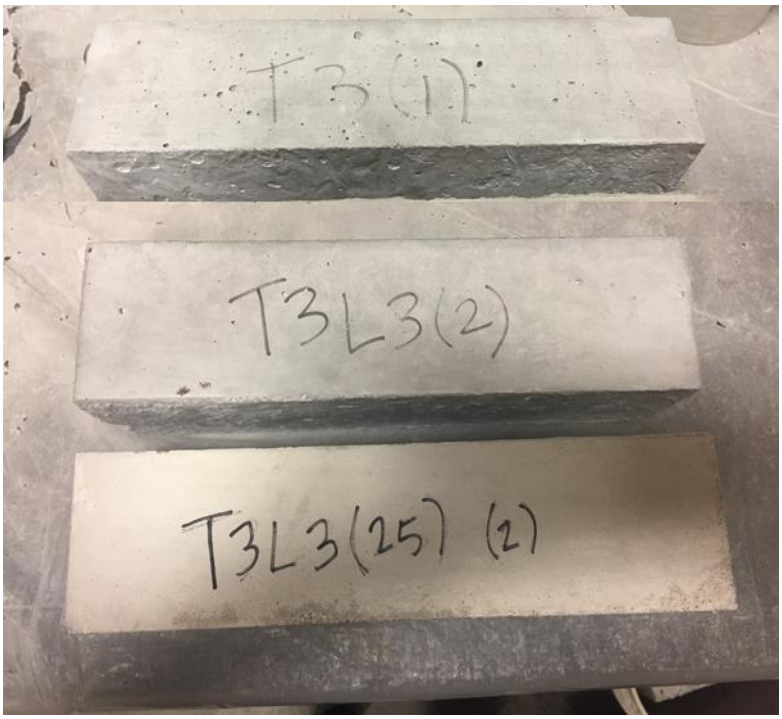

Figure 5-7: Surface finish comparison of concrete mix with no limestone (top) with 15% cement replacement (middle) and with 25% cement replacement (bottom)

Figure 5-8 shows the average number of small and large bug holes measured on the surface of samples made with each concrete mix. The SCC concrete mixes produced with Type I/II cement had fewer surface imperfections in general than the mixes produced with Type III cement. The surface finish of the neat Type I/II mix showed only small bug holes and no large bug holes. Due to the improved workability of mixes with higher limestone content, it was unexpected that the 3 and 40 μm mixes with the 25% percent limestone had a larger quantity of small bug holes compared to the 15% percent limestone of the same median particle size. Whereas the 25 μm limestone blends follow the more expected pattern that the higher percent cement substitution, the fewer surface imperfections.

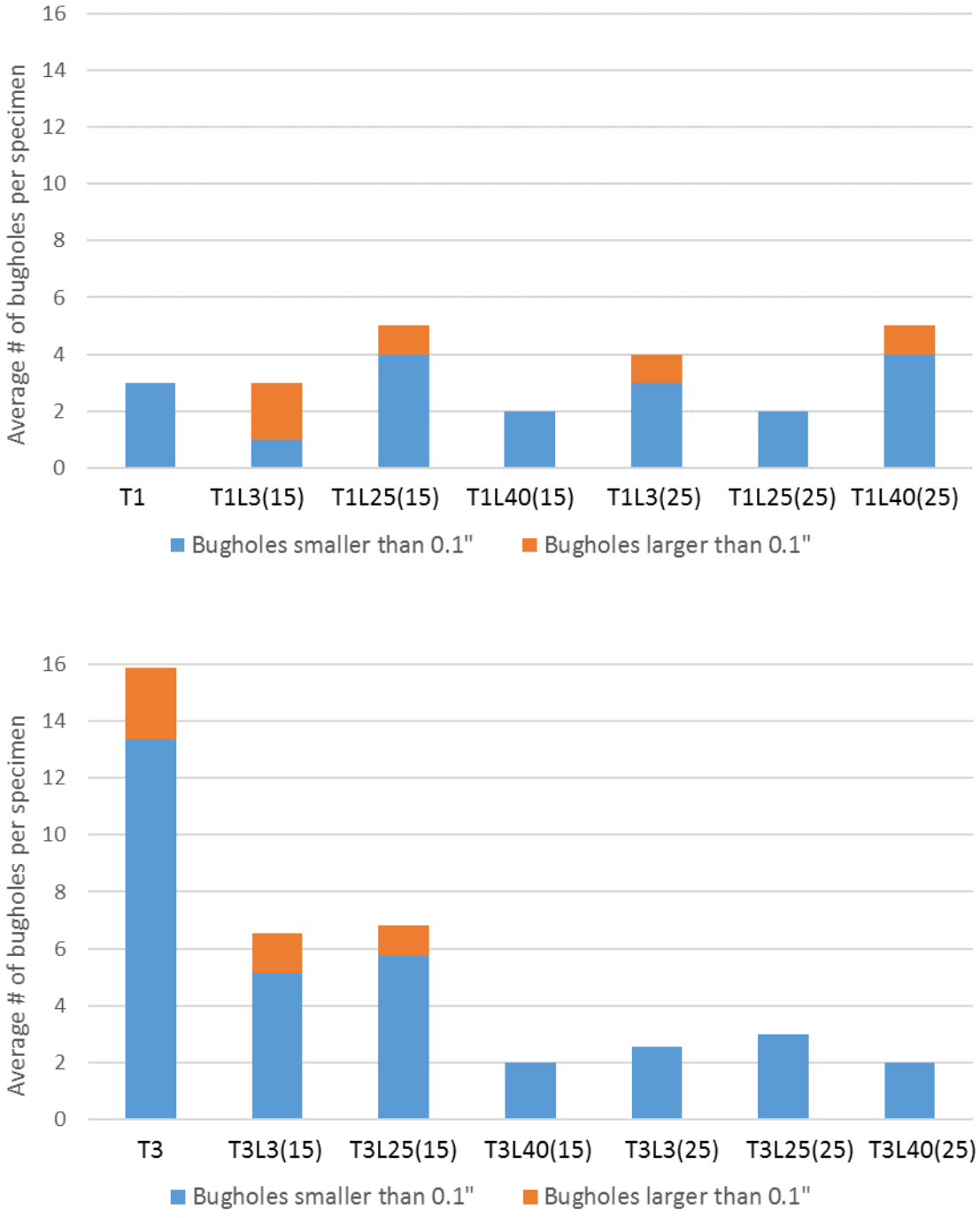

Figure 5-8: Quantity of small and large bug holes for SCC mixes made from Type I/II cement (above) and Type III cement (below)

The greatest number of large bug holes was found in the T1L3(15) mix. The maximum size bug hole was found in the T1L3(25) and T1L40(25) which measured 0.3 in. (7.5 mm) and 0.22 in. (5.5 mm), respectively.

For the SCC concrete mixes produced with Type III cement, the number of both small and large bug holes reduces as more limestone replaces cement. Additionally, mixes made with the 3 and 40 μm limestone powders had slightly fewer surface imperfections than the mixes made with the 25 μm limestone powder. This may be attributed to the more efficient particle packing in mixes with limestone powders with particle distributions that are more varied than the base cement. No large bug holes were found in the 25% limestone content mixes of the T3L3(25) and T3L40(25). The maximum size bug hole was found in the neat Type III mix, T3L3(15) and the T3L25(15) mixes and measured 0.33 in. (8.5 mm). All other bug holes in the other mixes were smaller than 0.122 in. (3.1 mm).

5.4 Conclusions and Discussion

Replacing cement with limestone powder is a viable option for improving viscosity, cohesion, stability and surface finish of SCC concrete mixes. For Type III cements, the use of a fine 3 μm limestone powder produces a cohesive mix, but better workability and surface finish is achieved at higher cement substitution rates (25% vs 15%). The blending of Type III cement with a 25 μm limestone powder at 15 and 25 % cement replacement produced workable cohesive mixes with minor improvements of surface finish with the higher cement substitution rates. The Type III cement mixed with the 40 μm limestone powder was stable at lower cement replacements (15%) but showed excessive bleeding at

the higher rate (25%), which required adjustment to the HRWRA. The surface finish of both T3L40(15) and T3L40(25) were comparable.

Blending of Type I/II cements with 3, 25, and 40 μm limestone powders showed slightly inconsistent results compared with the Type III cement. SCC concrete mixes using the 3 μm limestone at 15% cement replacement met the workability requirements, whereas mixes with 25% cement replacement were too cohesive and did not pass the S-groove test without additional HRWRA. Type I/II cements blended with 25 μm limestone powder showed good workability, stability and surface finish.

In general, with either cement Type I/II or III, when preparing SCC concrete mixes and considering only workability and surface finish, the finer ground 3 μm limestone powder should be used at higher cement replacement rates unless additional HRWRA is provided. The coarser ground 40 μm limestone should be used at lower cement replacement rates unless less HRWRA is provided. The medium ground 25 μm powder can be used at either 15 or 25% cement substitution to obtain adequate slump flow, self-healing ability, stability and surface finish.

CHAPTER 6. COMPRESSIVE STRENGTH, DRYING SHRINKAGE, CREEP, AND DURABILITY OF PRECAST CONCRETE MADE WITH LIMESTONE BLENDED CEMENTS

6.1 Introduction

Chapter 5 focused on the properties and workability of the concrete mixes in the fresh state, this chapter focuses on the mechanical properties of the hardened concrete. First, the compressive strength development over time is investigated, followed by a look at dimensional stability considerations such as drying shrinkage and creep, and finally tests to predict permeability are investigated.

Compressive strength is considered to be the single most important mechanical property for concrete designers [14]. Precast suppliers use strength development curves to determine the time concrete members can be removed from the setting beds and tensioned, so that the next batch of member can be produced. Designers use compressive strength to predict other mechanical properties such as modulus of elasticity and tensile capacity. Research shows that when limestone powder is interground with cement at limited quantities, generally around 10% cement replacement; compressive strength can match or exceed that of the neat cement concrete mix [38, 42, 84]. In precast plants, limestone powder is blended with Type III cement at the time of mixing rather than intergrinding to achieve a desired strength. There is limited research in how the particle size distribution of the blended limestone or the percent cement substitution affects the compressive strength evolution of these concrete mixes.

In addition to compressive strength, designers must be able to predict how much concrete members will shrink once curing has finished. Both unrestrained drying shrinkage and creep need to be addressed for precast member design. Concrete specimens undergo drying shrinkage as the concrete experiences a loss of moisture due to both evaporation and self-desiccation during hydration [14]. Failing to account for this unrestrained shrinkage could lead to concrete members not fitting correctly. Although some research exists on the drying shrinkage of limestone blended cements [43, 85, 86], developing a deeper understanding of how the median particle size of the limestone powder or the percentage cement substitution rate affects drying shrinkage is warranted. Additionally, being able to use existing drying shrinkage models to predict the unrestrained shrinkage of limestone blended cements would be useful to precast designers.

Under sustained load, concrete members experience deformations over time called creep. This time dependent deformation can be as large as six times greater than the instantaneous deformation when load is first applied. Many variables contribute to creep behavior, but the exact creep mechanism is not well understood. It is generally agreed that creep involves the movement of adsorbed water molecules between the CSH layers of the hardened cement paste [87]. However, factors including concrete age at loading and the restraining effect of aggregate also come into play. Understanding creep is important in predicting long-term effects such as cracking, stress redistribution, and buckling of members under sustained loads [88]. Creep can be of particular importance to the prestressed concrete industry where it is accountable for long-term stress relaxation of prestressed tendons and can lead to reduced capacity of prestressed members. The nonuniform nature of creep may lead to excessive cracking which in turn may promote

steel corrosion [87]. Excessive deflections can limit the service life and long-term durability of structures. As structures become larger and concrete stresses become greater, the adverse effects of creep become accentuated. Having an accurate creep prediction model for design engineers is essential in the design of long span bridges and prestressed members. Accurately predicting creep behavior, however, is challenging. Although researchers have looked at creep and shrinkage of various mixes which have been blended or interground with limestone powder to produce mixes of comparable strength levels, most have been limited to mixes using a single limestone powder and variable parameters [85]. Understanding the effect the median particle size of the limestone and percent cement substitution has on creep behavior would be useful to designers.

Finally, assessing the long-term durability of concrete members made with limestone blended cements is important. Concrete durability is most commonly classified by its permeability. Although there are many methods to determine permeability of concrete, all methods have their benefits and draw backs [89]. Some standard tests are time consuming and destructive, while others may be rapid but do not directly measure permeability. For comparing relative permeability of concrete mixes, two common tests methods are AASHTO T358 surface resistivity [90] and ASTM C1202/AASHTO T277 rapid chloride permeability test (RCPT) [91] [92]. Although neither method measures permeability directly, they use electrical resistance of concrete to give some predictor of how permeable and tortuous the concrete pore structure is. Surface resistivity measures the electrical resistance in a saturated concrete specimen using a Wenner probe, where four probes are placed equidistant apart across the concrete surface [89, 93]. The outer two probes produce a current while the inner two measure the potential. The main benefits to

this measurement is that it is fast and nondestructive. The RCP test measures ionic movement through a two-inch section of saturated concrete [89] [91]. Although this test has been criticized for measuring all ions passing, not just chloride ions; that poor-quality concretes fair worse than they should due to increased temperature; and that the high voltage does not allow a steady state to be achieved, the test is a rapid way to compare many concrete mixes in a short time period [89].

The main objective of this chapter is to investigate how the median particle size of limestone powder used in concrete mixes made with limestone cement blends affects compressive strength development, volume stability and durability. Additionally, drying shrinkage and creep models are compared with experimental results to determine if any can be used to accurately predict dimensional stability. Finally, the correlation of surface resistivity to compressive strength is investigated.

6.2 Materials and Methods

Concrete mixes were made from three cements supplied by LafargeHolcim and three limestone powders supplied from Imerys Carbonates. The three cements were made from the same base clinker and consist of a Type I/II and Type III conforming to ASTM C150, and a Type IL conforming to ASTM C595. The three limestone powders used were ground to median particle sizes of 3, 25, and 40 μm. See Chapter 3 for a more in-depth material characterization.

Fifteen concrete mixes were made at the Georgia Tech structures lab on a $5ft^3$ rotating drum mixer following the procedure outlined in ASTM C192 [81] having a consistent water-to-binder (cement + limestone) ratio of 0.4 and aggregate content (See

Table 6-1). The limestone cement blends had 15% or 25% cement replacement by mass of either 3, 25, or 40 μm limestone powders.

Table 6-1: Mix proportions of SCC concrete mixes

		% limestone		
		0%	**15%**	**25%**
Cementitious Material ***lb/yd³***	cement	850	725	637
	limestone	-	125	213
	water	340	340	340
	w/b	0.40	0.40	0.40
Aggregate ***lb/yd³***	#67 stone	1724	1724	1724
	natural sand	1200	1200	1200
HRWRA	oz/yd^3	38-54	38-60	31-48
	oz/cwt	4.5-6.4	4.5-7.0	3.6-5.6

The high cement content was deemed adequate to achieve high early strength of 4,000 psi at 1 day and 5,000 psi at 3 days, to reduce bleeding and to achieve an appropriate level of workability. The HRWRA (Glenium 3400) was modified slightly to either achieve a 20 inch slump flow or to reduce excessive bleeding. See Chapter 5 for a more in depth discussion on the modifications made to certain mixes.

6.2.1 Compressive Strength

Using ASTM C39, compressive strength was measured on 4 in. (100 mm) diameter x 8 in. (200 mm) tall concrete cylinders cast from the fifteen concrete mixes [94]. The cylinders were demolded 24 hours after casting and stored in a fog room at 100% relative humidity at 73.5 ± 3.5 °F at the Georgia Tech Structures Lab until time of testing. Three cylinders from each batch were tested at 1, 3, 7, 28, and 90 days, using a load rate of 26.4 kip/min. The results presented is the average of the three tests (see Figure 6-1).

Figure 6-1: Concrete cylinder in compression testing

6.2.2 Volume Stability

Volume stability describes the dimensional change experienced by concrete members as it dries out. Two experiments were performed to determine the dimensional stability of concrete mixes made with limestone blended cements – unrestrained drying shrinkage and creep.

6.2.2.1 Drying Shrinkage

Drying shrinkage was determined following the procedures of ASTM C157 on 3 in. (76 mm) x 3 in. (76 mm) x 11 in. (286 mm) concrete prisms with cast in place Humboldt gauge studs for a 10 in gauge length, but with a slight modification to the curing regime [95]. The standard requires that concrete samples be stored in limewater for 28 days before testing. Since precast members are generally demolded after 24 hours and tensioned shortly after, it did not seem representative of construction practices to cure the drying shrinkage specimens in limewater for 28 days. Additionally, the drying shrinkage behavior of small specimens is not entirely representative of large precast specimens. Nonetheless, since the main objective is to compare how drying shrinkage is affected with limestone substitution and fineness, two curing regimes were used to represent the worst and best-case scenarios that may occur at precast plants. For each concrete mix, six molds were cast with Humbolt gauge studs cast at the far ends of the specimen. The six specimens were covered and cured in their molds in a fog room at 100% relative humidity at 73.5 ± 3.5 °F and demolded after 24 hours. After 24 hours, three specimens were placed in a limewater bath at 73 ± 1 °F and remained undisturbed for 7 days. The other three specimens were allowed to air dry at 50 ± 4% relative humidity at 73 ± 3°F beginning at 24 hours. Change in length measurements were taken at 4, 7, 14, 28, 56, 112 and 224 days after initial curing, see Figure 6-2.

Figure 6-2: Drying shrinkage measurement on concrete prisms

6.2.2.2 Creep

Following the procedures of ASTM C512, four 4 in. (100 mm) diameter x 15 in. (279 mm) long creep cylinders and three companion 4 in. (100 mm) diameter x 8. in (200 mm) strength cylinders were cast to test creep and compressive strength, respectively [63]. Six mixes, deemed the most suitable for precast applications, were studied – two mixes made with 3 μm limestone powder – T3L3(15) and T3L3(25); two mixes made with the 25 μm limestone powder – T3L25(15) and T3L25(25) and two neat cement mixes made from Type III (T3) and Type IL (T1L) cements.

During concrete placement, four tree nuts were cast into the molds (two on each side) spaced at a 10 in. (254 mm) gauge length for measuring strain using a DEMEC device. The cylinders were demolded after 24 hours curing in the molds and placed in a fog room

at 100% RH at 73.5 ± 3.5 °F for 3 days. After 3 days, the concrete cylinders were removed from the fog room and 3 strength cylinders were tested to determine the compressive strength. Two of the four creep cylinders were installed in a creep frame. The cylinders were capped by steel plates and stacked one on top of the other, see Figure 6-3. The frame was compressed to 40% the compressive strength of the concrete and strain measurements were taken before loading, immediately after loading, and at periodic intervals afterwards. The load applied was measured at the same intervals as the strain measurements and confirmed to be within 2% of the original applied load. Throughout the duration of the experiment, the cylinders were kept in a room at 73^0F ± 3^0F with relative humidity of 50% ± 4%. The two remaining cylinders remained unloaded and were used to measure drying shrinkage. Strain measurements are taken daily for one week, weekly for one month, then monthly for one year. The strains of the loaded cylinders represent the total strain due to shrinkage and creep. Creep was calculated as the difference between the total strain of the loaded cylinders and the shrinkage strain experienced by the unloaded cylinders.

Figure 6-3: Cylinders loaded in creep frames

6.2.3 Permeability

Two test methods were employed to compare the permeability and consequently durability of fifteen concrete mixes produced with varying cement types and varying limestone powders – surface resistivity and rapid chloride permeability test (RCPT). Surface resistivity is a nondestructive test method that measures concrete resistivity and RCPT measures the one-way passage of ions through a concrete sample.

6.2.3.1 Surface Resistivity

Following the procedures of AASHTO T358-17, three 4 in. (100 mm) diameter x 8 in. (200 mm) tall cylinders were cast from each concrete mix [90]. The cylinders were

demolded after 24 hours and kept in a fog room at 100% relative humidity until ready to be tested. In order to be consistent with the compressive strength test method, fog room curing was performed rather than limewater curing. The cylinders were tested at 1, 3, 7, 14, 28, 56, and 90 days. Four measurements were taken on each of the three cylinders at 90 degrees from the previous measurement (Figure 6-4). The measurements were repeated twice per cylinder and the results were averaged. Depending on the value measured, the concrete is rated for OPC as having high, moderate, low, very low, or negligible permeability according to AASHTO T358-17 (see Table 6-2).

Figure 6-4: Measuring surface resistivity of a concrete cylinder

Table 6-2: Permeability classification according to AASHTO T358 surface permeability test

SR limits (kOhm-cm)	Chloride ion permeability
<12	High
12-21	Moderate
21-37	Low
37-254	Very low
>254	Negligible

6.2.3.2 Rapid Chloride Penetrability Test (RCPT)

Following the procedures in ASTM C1202/AASHTO T277, a 2 in. (50 mm) thick section was wet saw cut from the top portion of a 4 in. (100 mm) diameter x 8 in. (200 mm) concrete cylinder [91] [92]. The section was allowed to air dry before applying an epoxy coat along the round surface of the section to allow for one-way movement of ions across the section. After allowing the epoxy to cure, the sections were vacuumed for 3 hours and then saturated in de-aired water for 18 hours before being placed into an apparatus for testing where one end of the specimen is exposed to a 3.0% NaCl solution and the other end is exposed to a 0.3M NaOH solution (Figure 6-5). The specimen is subjected to a 60 V applied DC voltage for 6 hours and the total charge passed is determined. The results reported are the average of three specimens for each concrete mix. Depending on the total charge passed, the concrete is rated for OPC as having either high, moderate, low, very low or negligible permeability (see Table 6-3).

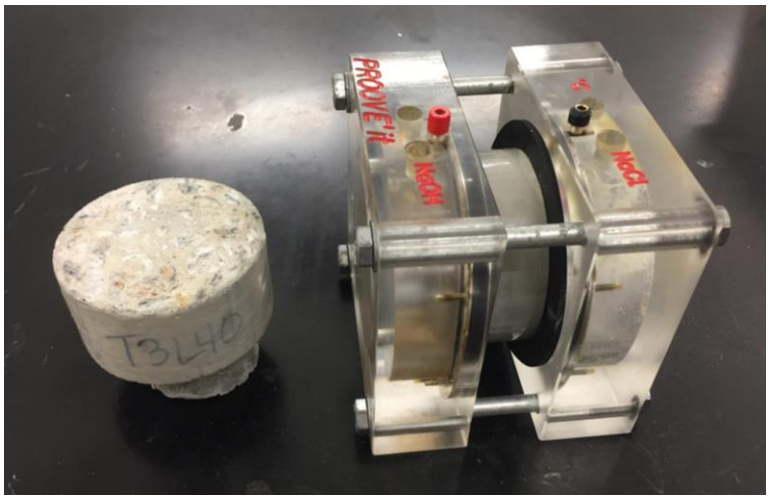

Figure 6-5: Epoxy coated specimen and specimen loaded in holder exposed to NaOH solution on one end and NaCl solution on other ready for voltage application

Table 6-3: Permeability classification of concretes tested according to ASTM C1202/AASHTO T277 Rapid Chloride Permeability method

Charge Passed	Chloride ion permeability
>4000	High
2000-4000	Moderate
1000-2000	Low
100-1000	Very low
<100	Negligible

6.3 Experimental Results

To fully understand the role both limestone particle size and percent cement substitution rates have on the mechanical properties of self-consolidating concrete mixes, compressive strength development, drying shrinkage, creep, surface resistivity and rapid chloride penetration were investigated. For the case of volume stability, results were compared with existing models to evaluate which model best represents the behavior of concrete mixes made with limestone blended cements. The two predictors of durability

were compared, and correlations were made between surface resistivity and compressive strength.

6.3.1 Compressive Strength

Effect of cement type: The compressive strength development of the concrete mixes produced with the Type I/II, Type III, limestone cement blends and the Type IL are shown in Figure 6-6 and Figure 6-7. The Type IL concrete mix with approximately 9% interground limestone experienced statistically similar compressive results to the Type III cement with no limestone substitution. Due to their high specific surface area, the Type III and Type IL neat cements have higher 1 day compressive strengths than the Type I/II. By 3 days, the Type I/II cement mix has the same compressive strength as the other two and by 7 days, is 4% stronger.

At 1 and 3 days, the substitution of cement with limestone has a much more significant effect on the Type I/II blends compared with the blends made with the Type III cement. The blends made with the Type III cement had similar compressive strength values at 3 days, varying by less than 8%, regardless of median particle size or percent replacement. At all ages, the substitution of 25% cement with the 25 μm limestone significantly reduced the compressive strength of the concrete (by approximately 30%), whereas the 25% cement substitution by the 3 μm limestone was less pronounced (15%). A close comparison between companion mixes made with Type I/II versus Type III cements (i.e. T1L3(15) vs T3L3(15)) show that the compressive strength at 90 days varied by less than 3%. Table 6-4 shows the compressive strength values for each concrete mix and the percent change relative to the neat cement.

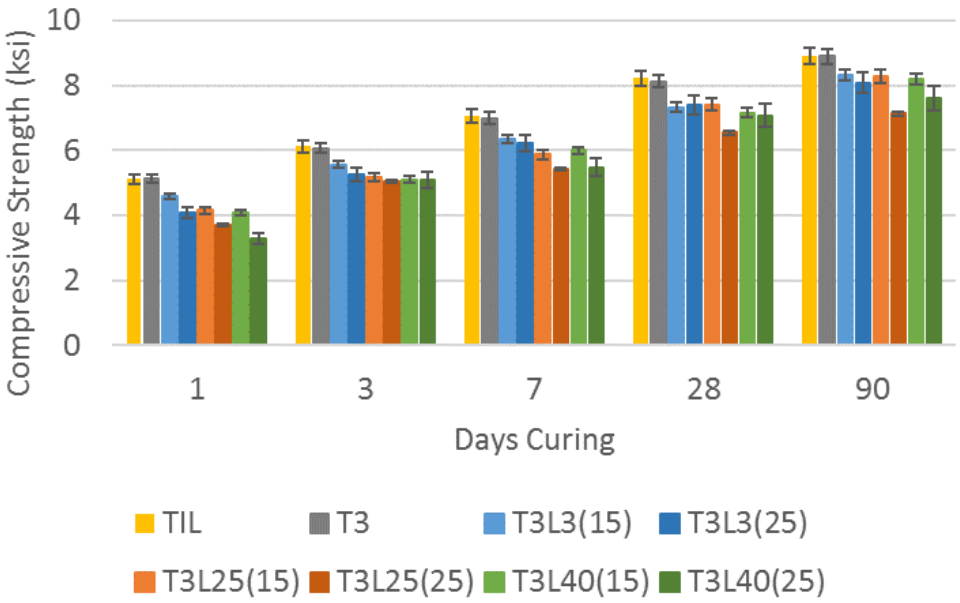

Figure 6-6: Compressive strength development of Type IL and Type III cement blended with various limestone powders

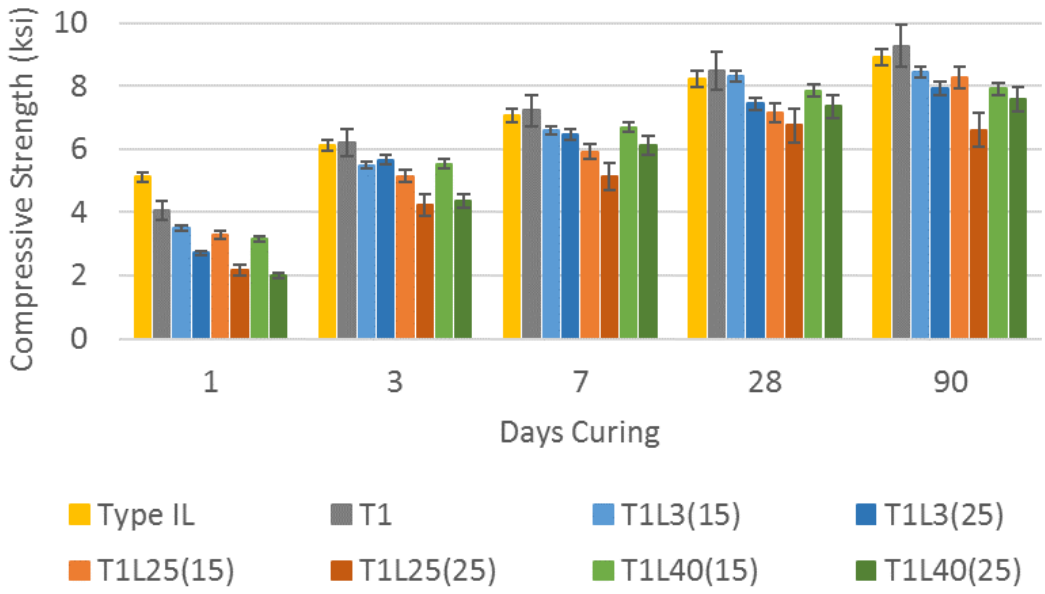

Figure 6-7: Compressive strength development of Type IL and Type I/II cement blended with various limestone powders

Table 6-4: Compressive strength development (ksi) of concrete mixes with and without limestone powder and percentage difference from neat cement mixes

	Days curing and % decrease from neat cement									
Mix	**1**	**%**	**3**	**%**	**7**	**%**	**28**	**%**	**90**	**%**
Type III	5.13	-	6.07	-	7.00	-	8.13	-	8.89	-
T3L3(15)	4.59	11%	5.56	8%	6.33	10%	7.32	13%	8.32	6%
T3L3(25)	4.07	21%	5.25	14%	6.22	11%	7.39	12%	8.08	9%
T3L25(15)	4.17	19%	5.16	15%	5.89	16%	7.41	12%	8.28	7%
T3L25(25)	3.72	28%	5.05	17%	5.43	22%	6.54	26%	7.13	20%
T3L40(15)	4.10	20%	5.10	16%	6.00	14%	7.16	16%	8.21	8%
T3L40(25)	3.28	36%	5.10	16%	5.47	22%	7.08	17%	7.60	15%
Type I/II	4.07	-	6.20	-	7.22	-	8.50	-	9.28	-
T1L3(15)	3.50	14%	5.17	17%	6.61	8%	8.33	3%	8.46	9%
T1L3(25)	2.72	33%	5.67	9%	6.47	10%	7.44	17%	7.93	15%
T1L25(15)	3.29	19%	5.16	17%	5.92	18%	7.16	22%	8.28	11%
T1L25(25)	2.17	47%	4.23	32%	5.14	29%	6.76	28%	6.61	29%
T1L40(15)	3.16	22%	5.54	11%	6.70	7%	7.85	11%	7.92	15%
T1L40(25)	2.00	50%	4.37	29%	6.11	15%	7.35	19%	7.59	18%
Type IL	5.12	-	6.12	-	7.05	-	8.22	-	8.91	-

Effect of limestone median particle size: All Type III conrete mixes, except the 25 and 40 μm limestone powders at 25% cement replacement levels, achieved a compressive strength of 4,000 psi at 24 hours (Figure 6-6 and Table 6-4). At 3 days, all mixes reached an average compressive strength of 5,000 psi and showed similar strengths regardless of limestone fineness or percent substitution. Mixes produced with the 3 μm limestone powder showed the highest early age compressive strength and outperformed the 25 and 40 μm limestone mixes even at higher cement substitution rates. For example, at 7 days, both mixes T3L3(15) and T3L3(25) had compressive strengths above 6,000 psi. But by 28 and 90 days, at 15% cement replacement, all three limestone powders showed similar strength. At 25% cement replacement, the dilution effect becomes more pronounced especially for the 25 μm limestone powder mixes at later ages, showing a 20% strength reduction compared

with 9% for the 3 μm limestone and 14% for the 40 μm compared with the neat cement mix. Of note is that the Type III and 25μm limestone powder have similar specific surface areas and particle size distributions. At later ages, all mixes, except T3L25(25), showed similar compressive strengths even between the 15 and 25% cement replacement regardless of limestone fineness, and much higher strengths than what would be expected with the reduced w/c ratio of the cement substitution mixes. This may indicate that there is improved particle packing when cements are blended with limestone powders having a more varied particle size distribution than the base cement.

Effect of percentage cement replacement: Compressive strength is directly proportional to the water/cement (w/c) ratio of concrete mixes. In these concrete mixes, the water-to-binder (cement + limestone) was held constant at 0.4, which produces an effective w/c ratio of 0.47 and 0.54 for the mixes with 15 and 25% cement replacement, respectively. At these reduced w/c ratios, it would be expected that the concrete strength at 28 days would reduce by 14.3% and 27.8%, repectively, compared with the neat cement mix [96]. At early ages – 1 and 3 days – the average strength reduction due to dilution effect, matched that of reduced w/c ratios, but began improving by 7 days of curing. A compilation of all results is shown in Table 6-4. For the Type III cement blends, at 15% cement replacement, concrete strengths reduced on average 13% at 28 days and less than 10% by 90 days (Figure 6-6). At 25% cement replacement, concrete strengths reduced on average by 16% and 15% at 28 and 90 days, respectively, indicating a higher than expected strength due to increased nucleation sites, better dispersion of cement particles, and improved particle packing.

6.3.2 Drying Shrinkage

As previously mentioned, drying shrinkage was measured on concrete specimens to determine the effect that varying limestone fineness, percentage cement substitution, and varying cement types has on dimensional stability. Additionally, the mixes underwent two curing regimes. Half of the specimens were cured in a limewater bath for 7 days after initial curing for 24 hours at 100% RH in their molds and the other half began air drying immediately after the 24 hours of initial curing.

Effect of curing regime and percent cement replacement: Figure 6-8, Figure 6-9, Figure 6-10, and Figure 6-11 show the results of the concrete mixes that were limewater cured for 7 days before being allowed to air dry and those that were air drying staring at 1 day. At 15% cement replacement the drying shrinkage profile for the T3L3(15) mix is similar to that of the Type III neat mix with no limestone replacement. The two mixes made by replacing 15% of the cement with either 25 or 40 μm mixes showed a similar profile to each other at early ages and then differing by no more than 13% at later ages. These two mixes experienced approximately 45% more shrinkage than the neat cement and 3 μm mix at later ages, starting at around 63 days of air drying. Of note is the similar shrinkage behavior of the mixes with 25% cement replacement, which varied by less than 5%, regardless of limestone fineness.

For limewater cured specimens, all mixes except the T3L3(15) experienced more drying shrinkage than the neat cement mix, even though the mixes had less cement content. This may be attributed to having fewer hydration products and therefore less tightly bound water which allows them to dry more rapidly.

For the air-cured specimens, the drying shrinkage results showed less variation among different limestone particle size regardless of fineness (Figure 6-9). This is especially true for the mixes with 25% cement replacement, which varied by less than 20% at early ages and 5% at later ages. Of note, the mixes with 15% cement replacement showed slightly more overall shrinkage than their 25% counterpart, which may be attributed to the balance between lower stiffness of the former, producing more shrinkage, and the lower cement content of the latter, producing less shrinkage. Upon careful inspection, between 14 and 100 days, the concrete mixes with 15% cement replacement experience greater shrinkage compared with their 25% cement replacement counterpart. This trend did not occur with the limewater cured specimens where the 15% replacement mixes experienced less shrinkage than their 25% counterparts.

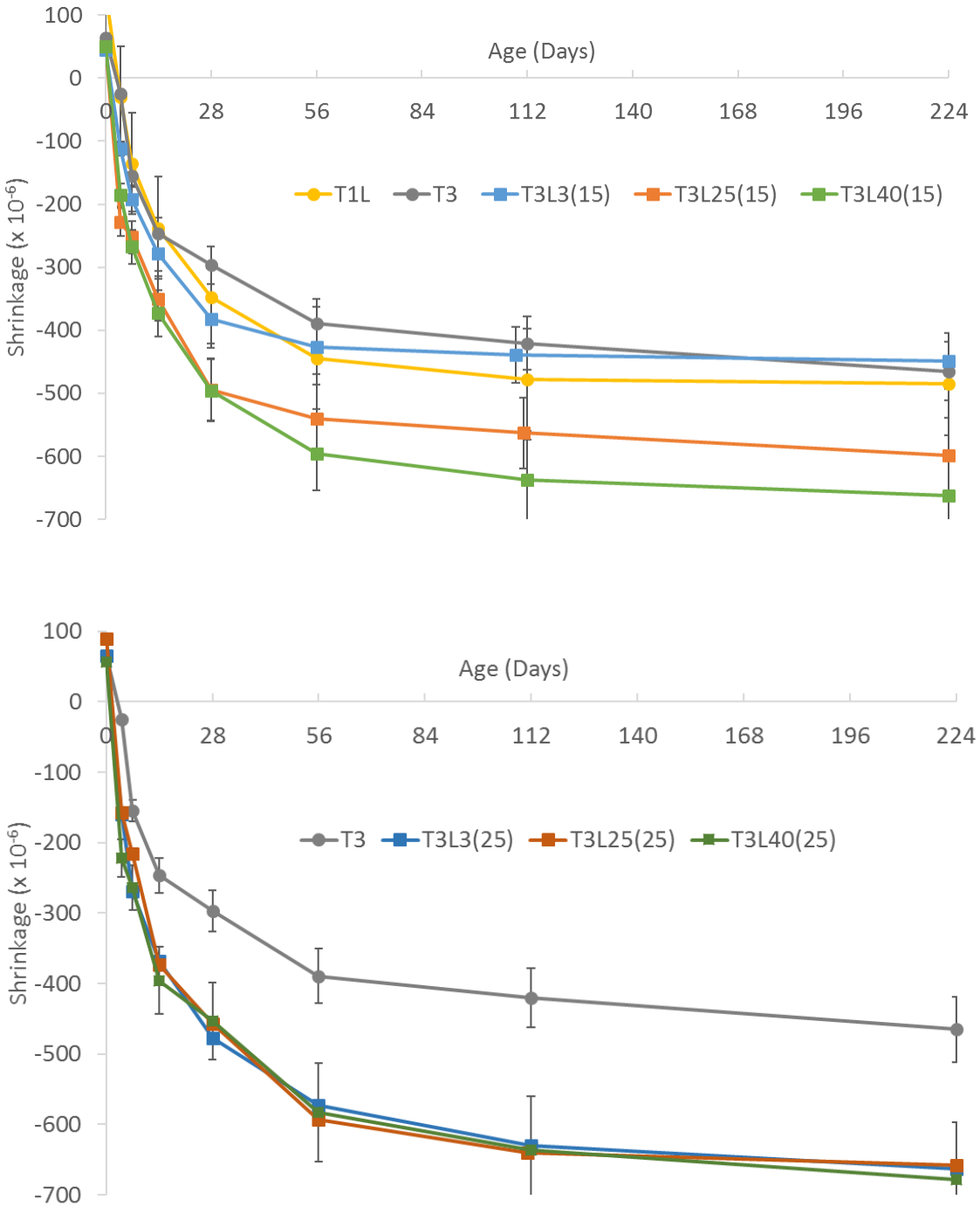

Figure 6-8: Drying shrinkage results for 7-day limewater cured concrete mixes made with Type IL and Type III cement blended with varying limestone powders (a) at 15% and (b) 25% cement replacement

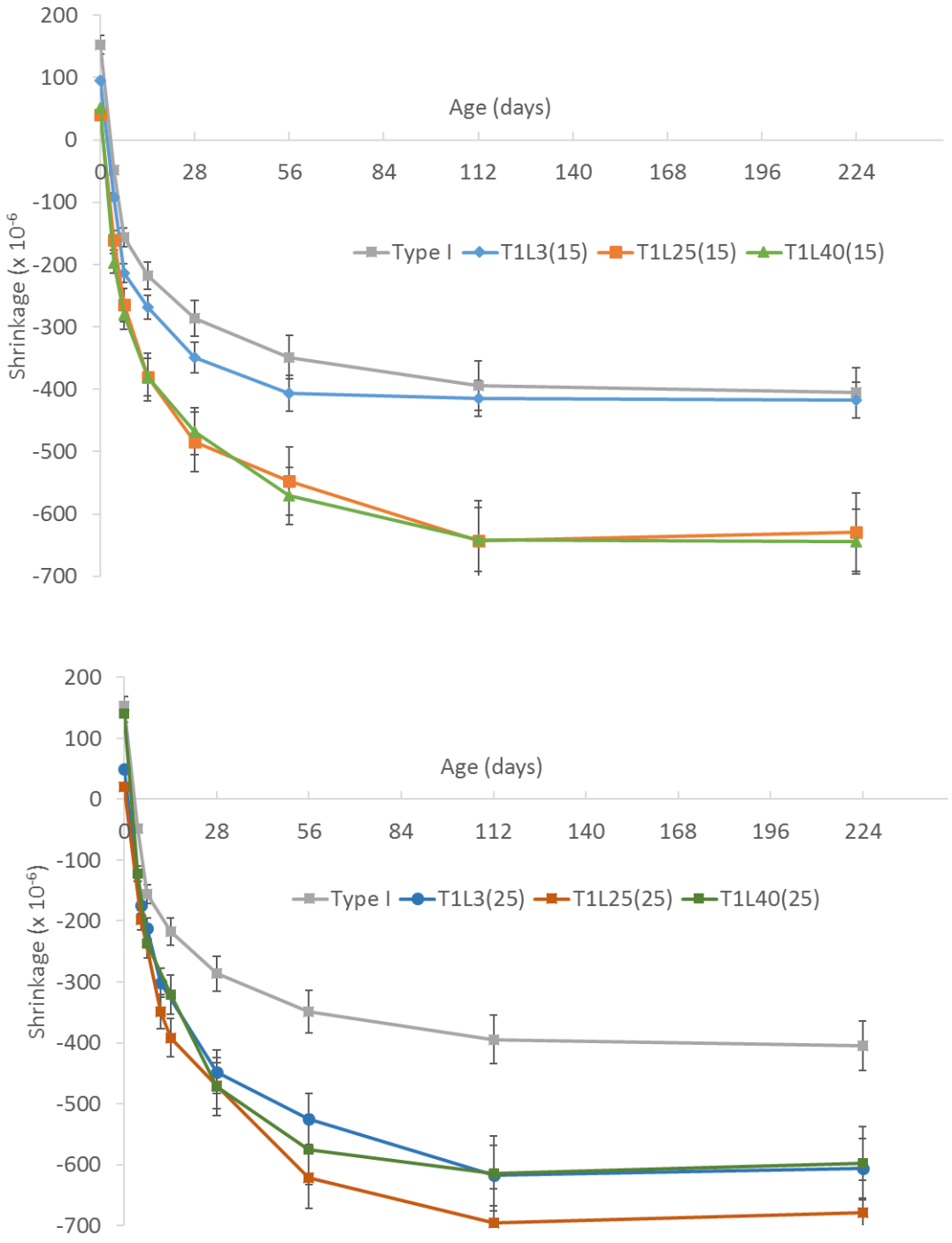

Figure 6-9: Drying shrinkage results for 7-day limewater cured concrete mixes made with Type I/II cement blended with varying limestone powders at (a) 15% and (b) 25% cement replacement

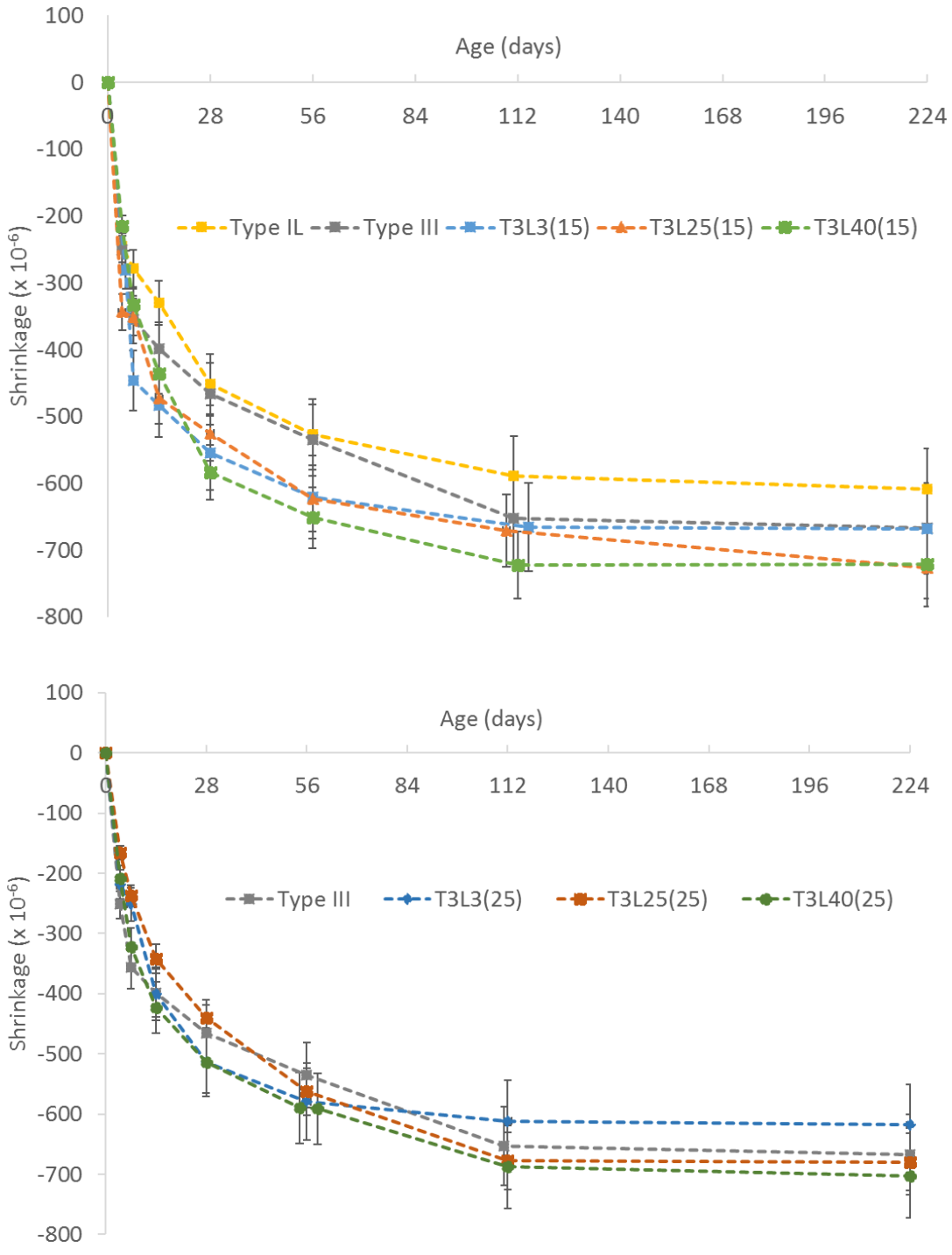

Figure 6-10: Drying shrinkage results for air cured concrete mixes made with Type III cement blended with varying limestone powders (a) at 15% and (b) 25% cement replacement

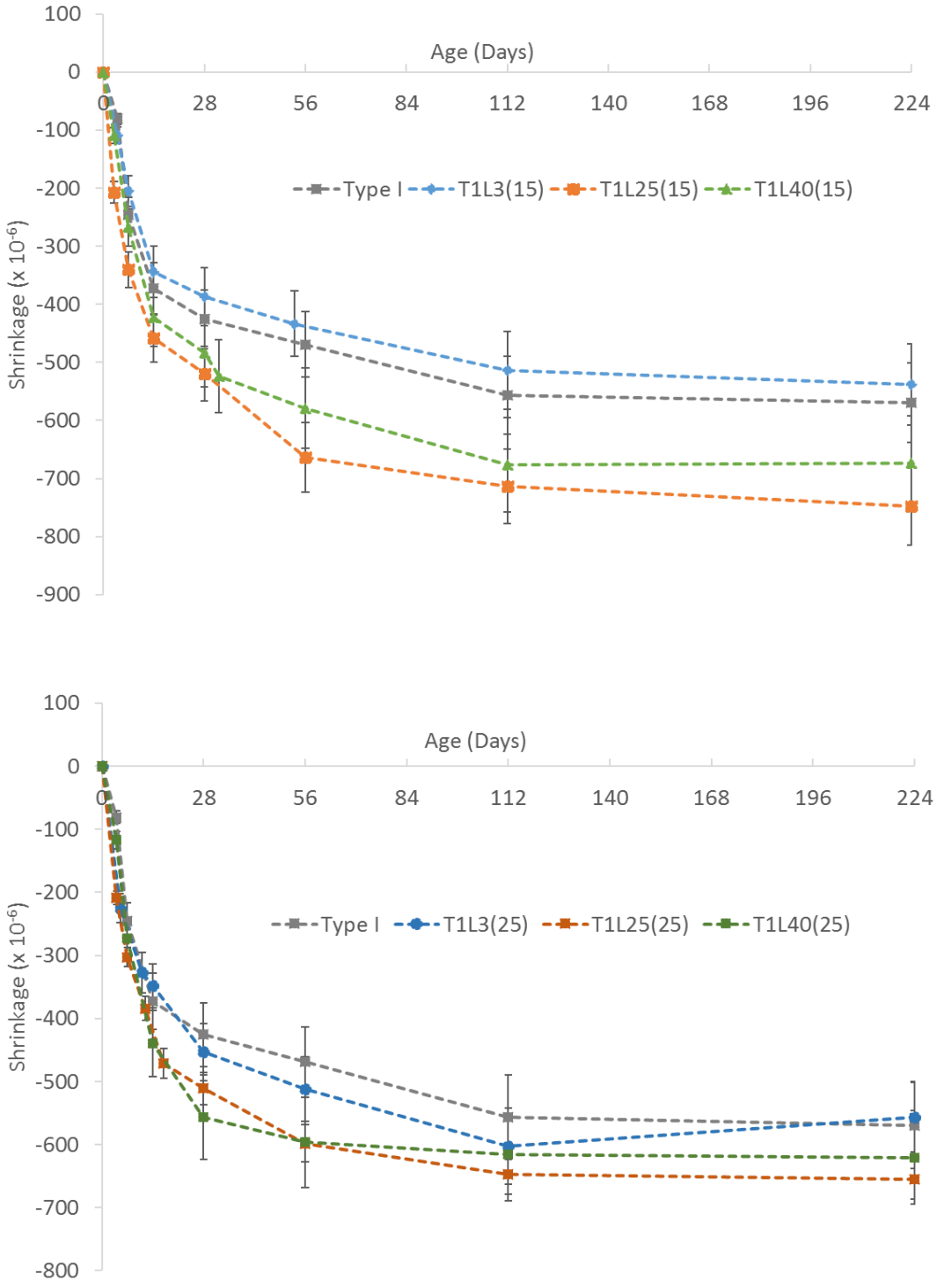

Figure 6-11: Drying shrinkage results for air cured concrete mixes made with Type I/II cement blended with varying limestone powders (a) at 15% and (b) 25% cement replacement

Effect of cement type: The graph shown in Figure 6-12 compares the drying shrinkage of concrete mixes made with either Type III (shown in color) or Type I/II (shown in gray) cements blended with limestone powders of varying median particle size. The graphs show remarkable similartites, regardless of curing regime, indicating that there was no substantial difference between the drying shrinkage of concrete mixes made with Type I/II or Type III cements.

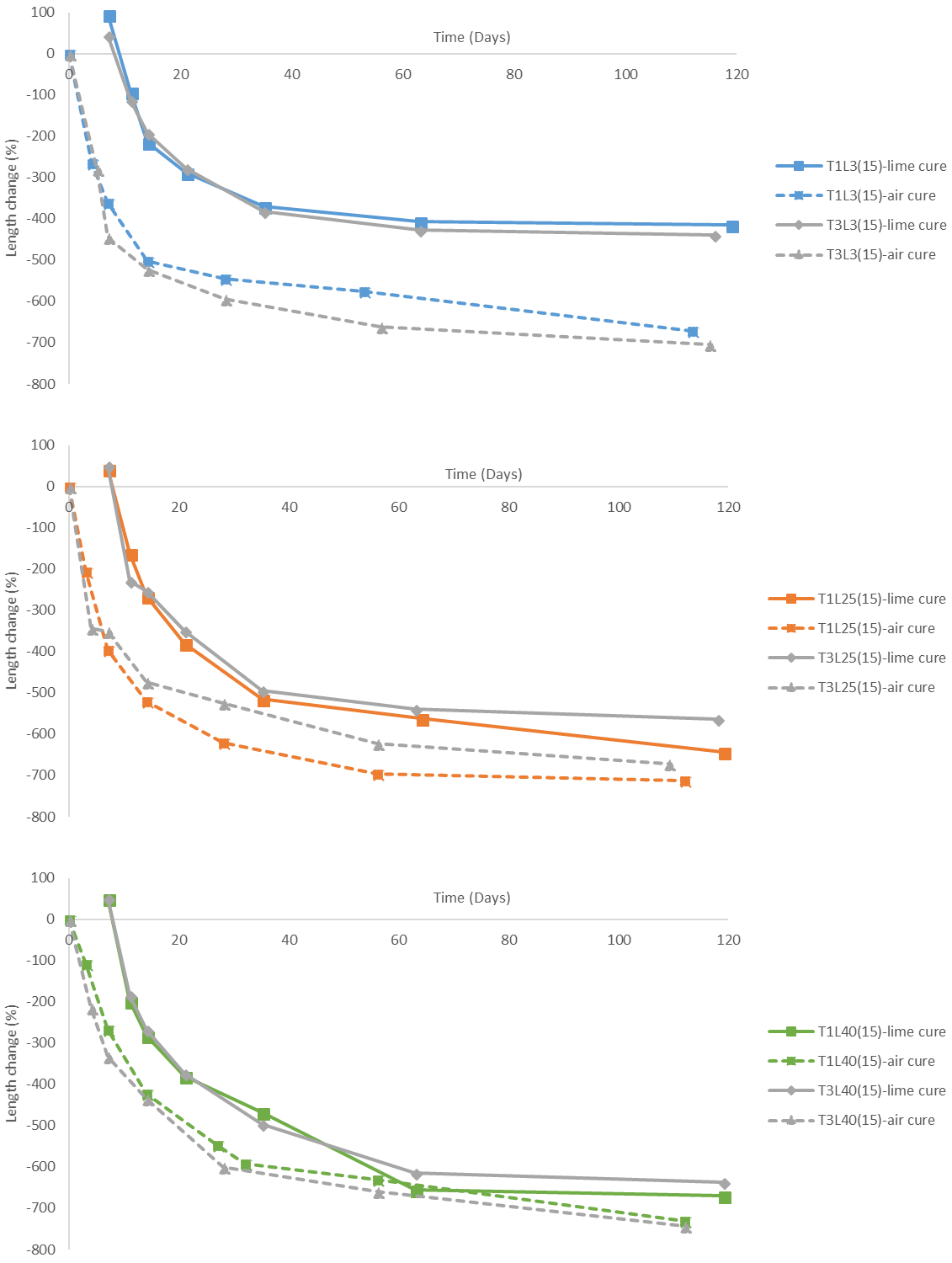

Figure 6-12: Comparison between drying shrinkage of concrete mixes made with Type III and Type I/II limestone blended cements

6.3.3 Drying shrinkage prediction models

In CHAPTER 2Chapter 2, five commonly used drying shrinkage models were presented – ACI 209R, Bažant B3 model, CEB MC90-99, the GL2000 and AASHTO-LRFD. The experimental results reported in the previous section were compared with these models to see if one model could be used to predict the drying shrinkage behavior of self-consolidating concrete made with limestone blended cements. Figure 6-13 shows the drying shrinkage results for the concrete mix T3L25(25), with and without limewater curing, compared with the five drying shrinkage models.

For the case with limewater curing, the CEB MC90-99, ACI, and AASHTO models under predict shrinkage strains while both the GL2000 model and the B3 model showed the best fit to the experimental data. For the case without limewater curing, which may be closer to what is experienced in a precast plant, the CEB model under predicts shrinkage strains, the ACI model under predicts strains less than 84 days, but then over predicts strains at later ages. Similarly, the AASHTO model under predicts strains earlier than 224 days, but over predicts strains after 224 days. For this curing regime, the Bažant B3 slightly over predicts the shrinkage strains. The GL2000 models showed good fits with the experimental data for both limewater and air cured specimens (see Figure 6-14).

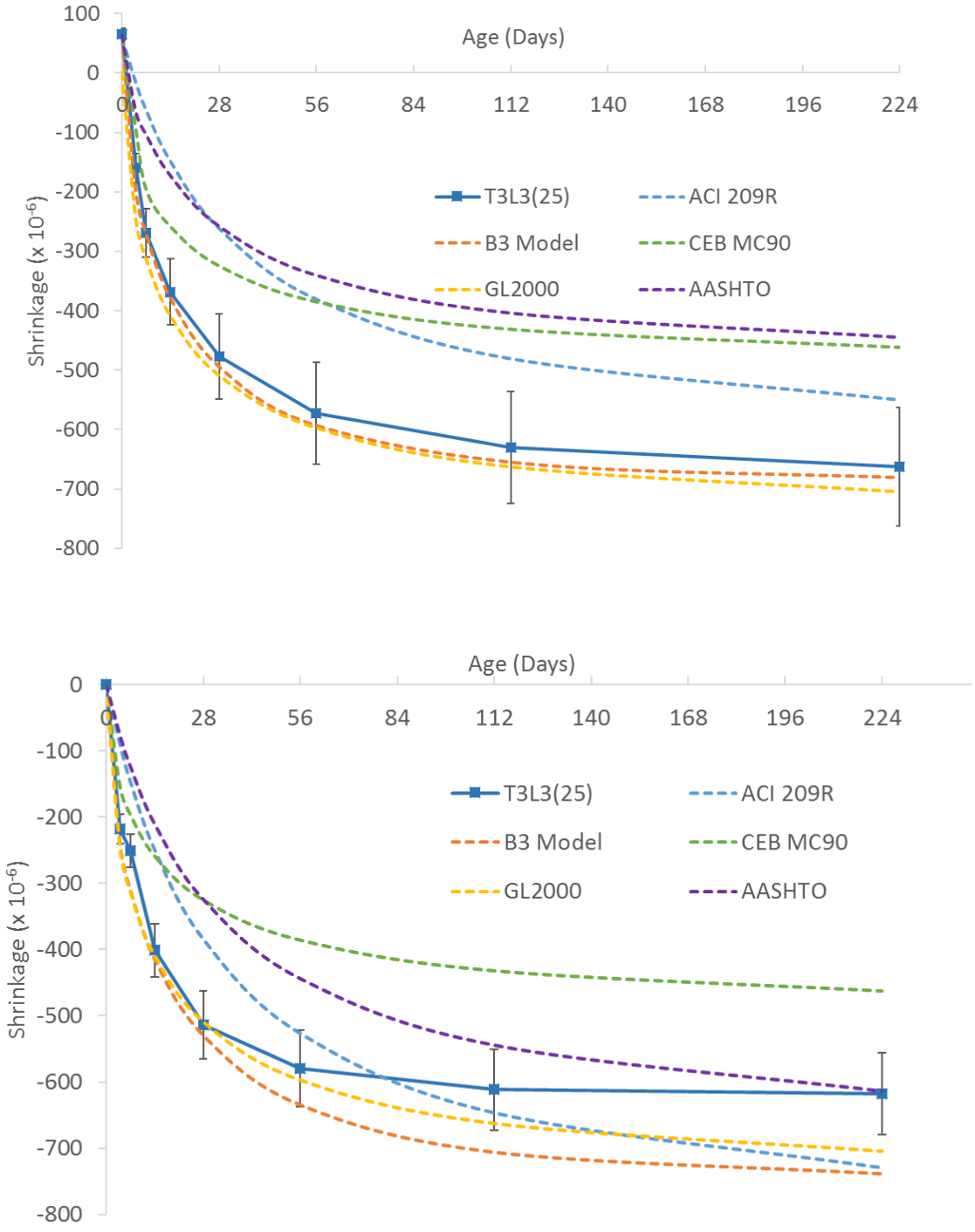

Figure 6-13: Drying shrinkage comparison of T3L3(25) with (upper) and without limewater curing (lower) and five prediction models

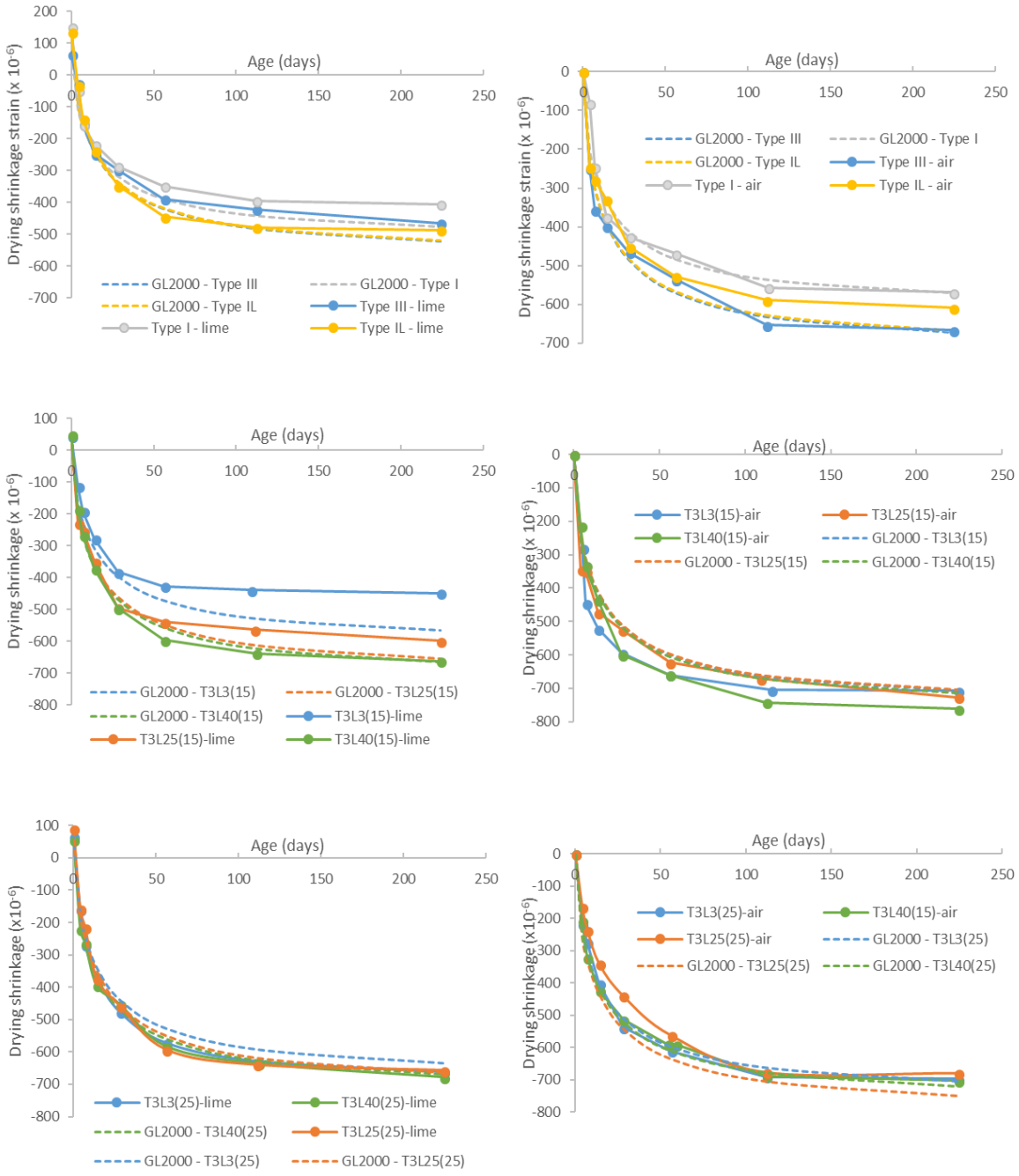

Figure 6-14: Drying shrinkage comparison of concrete mixes with limewater curing (left) and without limewater curing (right) and the GL2000 drying shrinkage model

The GL2000 model appears to be the best model to predict drying shrinkage behavior of this cement type for either with or without limewater curing. This model was chosen and compared with the fifteen concrete mixes and the results are shown in Figure 6-14. The equation for drying shrinkage first presented in Section 2.6.4 is copied again below:

$$\varepsilon_{sh}(t,t_c) = 900k\left(\frac{4350}{f_{cm28}}\right)^{1/2} \times 10^{-6}\beta(h)\beta(t-t_c) \qquad 6\text{-}1$$

where the *k* term in the above equation is taken as 1.0 for Type I cements and 1.15 for Type III cements. For the Type IL cement and the limestone blended cements, the best fit was found when *k* was taken as 1.15, even if blended with Type I/II cement.

One reason for the good predictor of the GL2000 model may be due to the fact that the model uses concrete strength rather than cement content to predict drying shrinkage behavior used in both the ACI 209R and Bažant B3 models. For limestone blended cements, the effect of the limestone is not well defined by the term cement content, since limestone acts as both filler and binder. If the total cement plus limestone amount is used as cement content, drying shrinkage is overestimated, but if only the cement portion is used, the drying shrinkage is underestimated. The GL2000 eliminates ambiguity by relying on compressive strength rather than cement content.

6.3.4 Long-term creep

The cylinders loaded in the creep frames undergo recoverable elastic strain due to the low initial load application, drying shrinkage strains from being in a room at 50%± RH and creep strains, while the unloaded cylinders experience only drying shrinkage strain. Creep strains are determined by subtracting the elastic strain and drying shrinkage strain from the total strain. Since all cylinders were loaded with different compression loads depending on their compressive strength, comparison between mixes are normalized by the applied pressure. This normalized creep value is referred to as specific creep.

Figure 6-15 shows the total strains of the loaded cylinders along with shrinkage strains from the unloaded concrete mixes. For visual clarity, the results are presented in two graphs. The total strains of all mixes varied by less than 6%, with the Type III and Type IL mixes experiencing the largest total strains and the two mixes with 15% cement replacement experiencing the smallest total strains. The shrinkage only strains of the six unloaded concrete mixes showed more variations of around 16%. The largest shrinkage strains were observed in the Type III cement mix and the two mixes blended with the 3 μm limestone, while the Type IL mix and the two 25 μm limestone mixes experienced the smallest shrinkage.

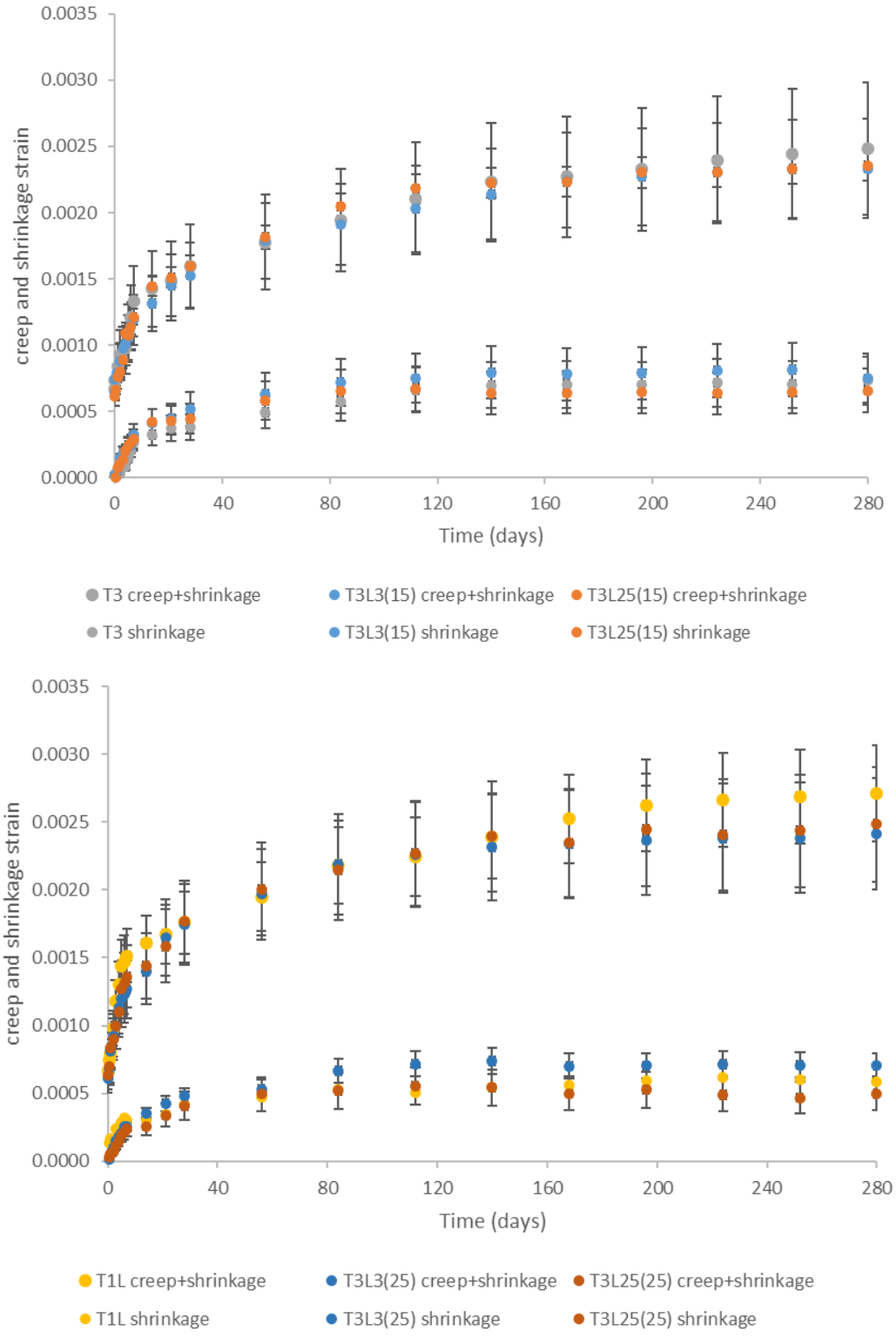

Figure 6-15: Total creep and shrinkage strains for concrete mixes with 15% limestone replacement (top) and 25% limestone replacement (bottom)

The specific creep is the amount of creep strain that has been isolated from the shrinkage strain and normalized by the applied stress. More variation (between 20-30%) is seen in the results for the specific creep shown in Figure 6-16 than in the previous results for total strain and drying shrinkage strain of the different mixes. The concrete mix made with neat Type III cement and the T3L3(15) mix experience the smallest specific creep while the T3L25(25) mix experiences the largest. It is worth noting that specific creep is a somewhat arbitrary value since there rarely exists a condition where creep occurs in the absence of drying shrinkage.

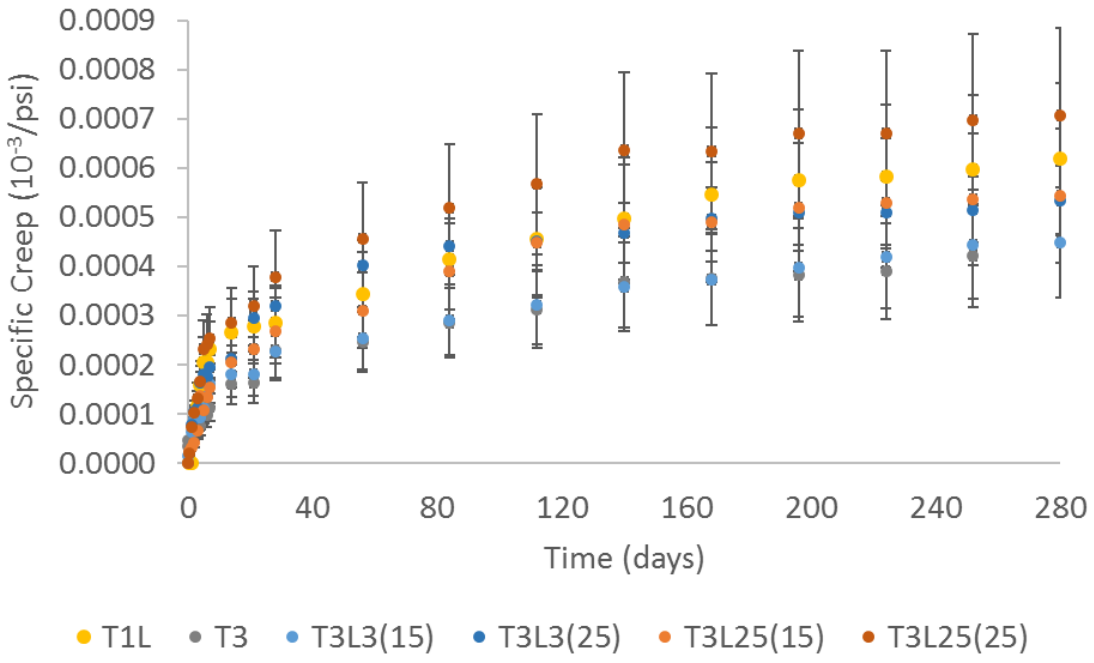

Figure 6-16: Specific creep of concrete mixes made with blended limestone cements

6.3.5 Creep prediction models

The creep and shrinkage behavior of the six concrete mixes were compared with five prediction models – ACI 209R, Bažant B3 model, CEB Mc90-99, the GL2000 model, and the AASHTO-LRFD model. A thorough discussion of these models is presented in Section 2.7. As seen in Figure 6-17, when considering shrinkage strains only, the ACI 209R, the Bažant B3, and the GL2000 models showed good correlation with the experimental results. For the total creep and shrinkage induced strains, however, the two AASHTO and CEB MC90-99 models under predict strains while the Bažant B3 and GL2000 over predict total strains. For these limestone blended mixes loaded at 3 days, the ACI 209R shows the closest correlation to the experimental results for both the shrinkage strains and the total creep plus shrinkage strains. Only the T3L25(25) mix is shown here; the other models are presented in Appendix G. Figure 6-18 shows the close correlation of the ACI 209R model with the for the specific creep experimental data.

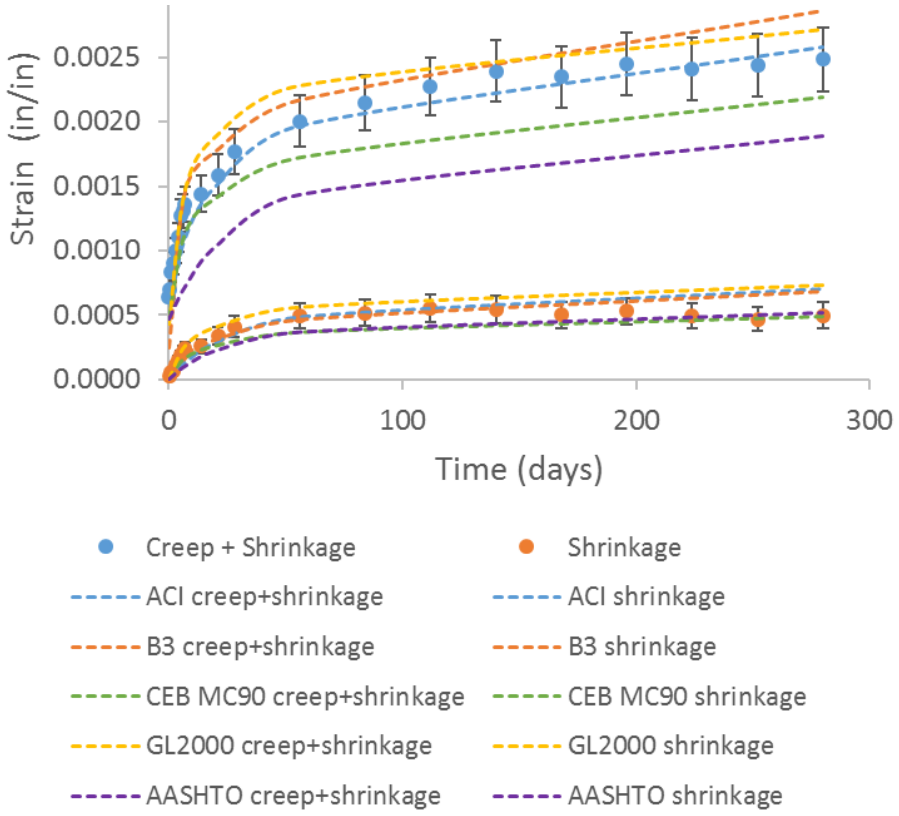

Figure 6-17: Comparing experimental total creep and shrinkage strains with five prediction models for mix T3L25(25)

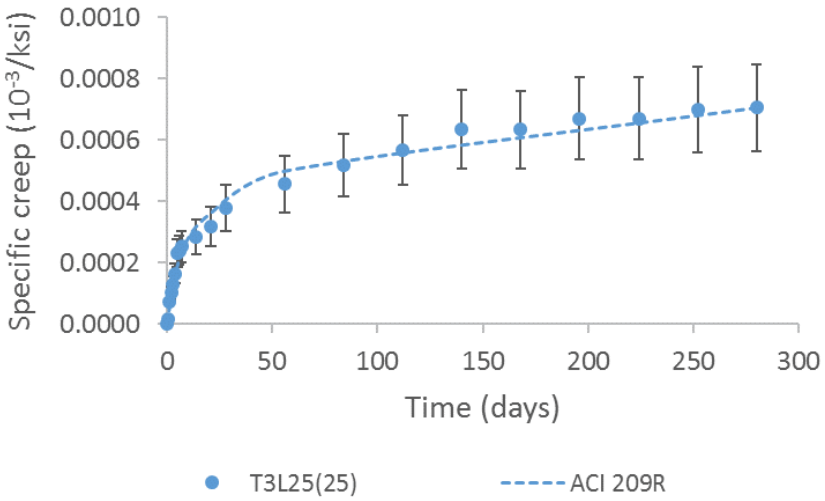

Figure 6-18: Specific creep comparison of ACI 209 and AASHTO creep prediction models with experimental T3L25(25) data

The best correlations for both total strains and drying shrinkage strains are with the ACI 209R model. The equations are presented again below. The ACI model showed the best correlation when the calculated E_{cmt0} using equation 2-20 was used rather than that obtained experimentally at load transfer and when the default values of 10 and 0.6 were used for coefficients d and ψ, respectively, in equation 6-4. ACI provides an option of setting ψ = 1.0 and calculating d from an equation based on the volume to surface ratio of the concrete member but doing so overestimated the total combined strains.

$$J(t,t_0) = \frac{1 + \varphi(t,t_0)}{E_{cmt0}} \qquad 6\text{-}2$$

$$E_{cmt0} = 33\gamma_c^{1.5}\sqrt{f_{cmt0}} \qquad 6\text{-}3$$

$$\varphi(t,t_0) = \frac{(t-t_0)^{\psi}}{d + (t-t_0)^{\psi}}\varphi_u \qquad 6\text{-}4$$

6.3.6 Surface Resistivity

The results of the surface resistivity measurements taken over a period of 90 days is shown in Figure 6-19 and Figure 6-20 for the Type III and Type I/II cements and cement blends, respectively. Most concretes fell right within the resistivity limits of moderate to high permeability set by AASHTO T358.

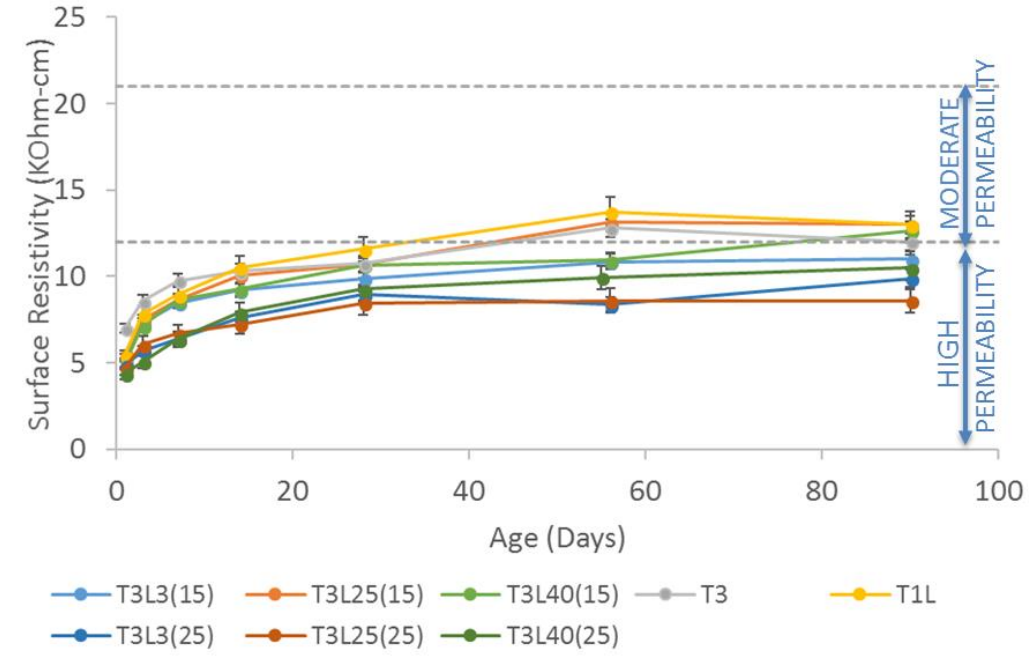

Figure 6-19: Surface resistivity measurements of Type IL and Type III blended limestone cements with varying percentage cement substitution and limestone fineness

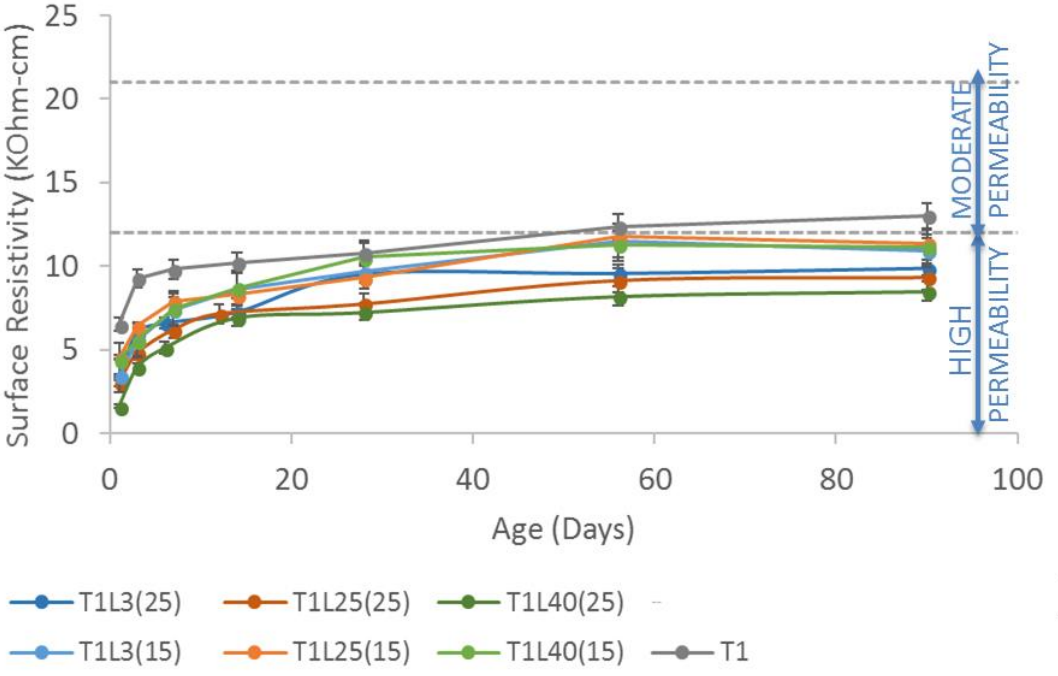

Figure 6-20: Surface resistivity measurements of Type I/II blended limestone cements with varying percentage cement substitution and limestone fineness

As a general trend, the concrete mixes made with the neat cements have higher surface resistivity, indicating lower permeability, than the mixes where limestone powders replace a portion of the cement. The concrete mixes with 25% cement replacement have slightly lower surface resistivity than the neat mixes and their 15% cement replacement counterparts. Interestingly, the T3L25(15) and T3L40(15) mixes showed surface resistivity comparable to the Type III and Type IL mixes, which is inconsistent with compressive strength results.

6.3.7 Rapid Chloride Permeability Test (RCPT)

Results from the RCP test are shown in Figure 6-21 and Figure 6-22. The amount of charge that passes through the concrete in 6 hours is used to classify the permeability of the concretes. The concrete mixes made with Type IL and Type I/II cements had the lowest charge passed, indicating the lowest permeability. This result correlates with the surface resistivity study that showed the Type IL cement had the highest surface resistivity. The graphs show that all the T3 concrete mixes fell within the moderate permeability range as classified according to AASHTO T277 (see Table 6-3). The T3L25(25) unsurprisingly had the highest permeability. The T1 concrete mixes showed greater permeability than their T3 counterparts and were mostly on the border between high and moderate. The T1 mixes made with 40 μm limestone blends showed the highest permeability.

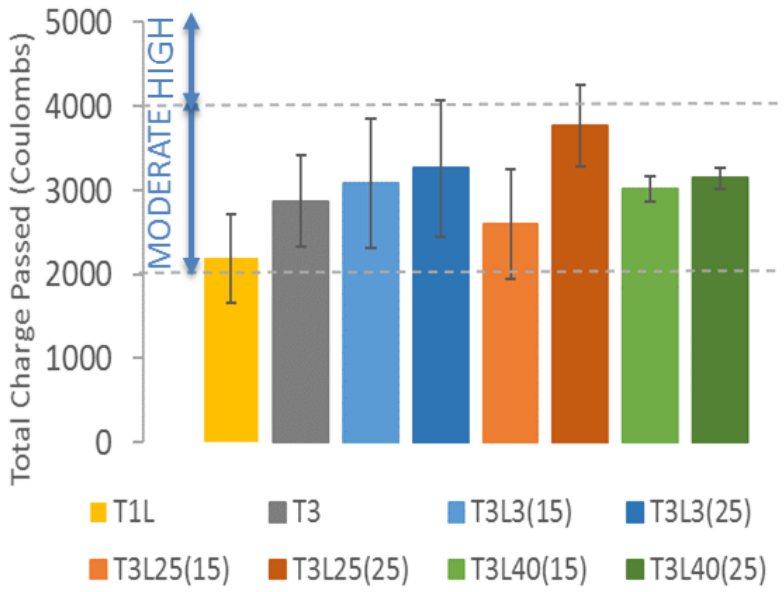

Figure 6-21: RCPT results for Type IL and Type III blended limestone cements

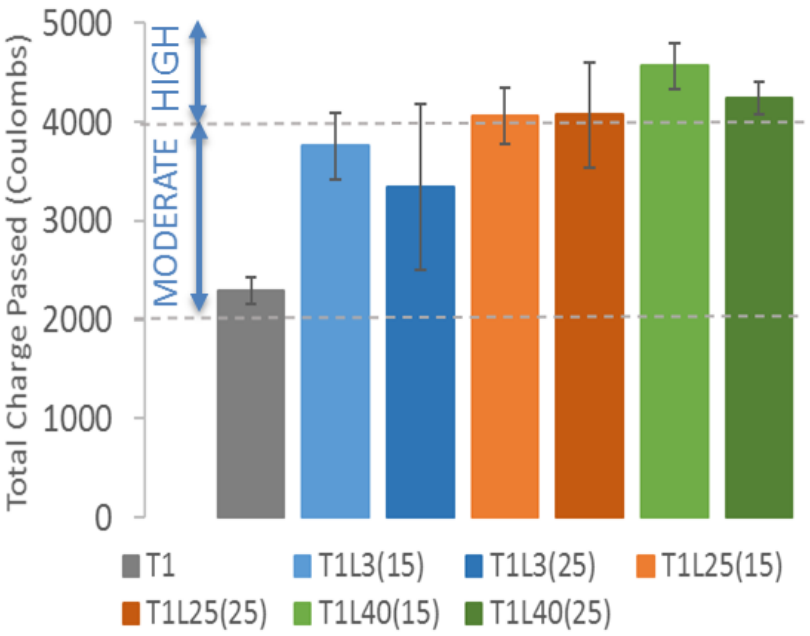

Figure 6-22: RCPT results for Type I limestone blended cements

Interestingly, the T3L25 mix with 15% cement replacement of the 25 μm powder showed less permeability than the other limestone powders, similar to surface resistivity, while the 25% cement replacement of the 25 μm powder showed the most permeability, again similar to the surface resistivity results. In all cases for the Type III cement blends, regardless of limestone fineness used, the 15% limestone replacements showed less permeability than their corresponding mixes with 25% cement replacement while the opposite was true for the Type I/II blends where permeability remained unchanged or improved with increased limestone powder substitution percentages. Lastly, the Type I/II cement was more affected by limestone replacement than the Type III cement. The permeability of concrete made with limestone blends of the Type I/II cements were between 46-100% greater than the neat cement while limestone blends with the Type III were 5-30% greater.

6.4 Comparison of SR and RCPT

Both surface resistivity and the rapid chloride permeability test indirectly measure permeability through an applied electrical current. In the case of the former, the electrical current is used to measure resistivity and in the case of the latter, the current is used to measure charge. Resistivity and current are inversely proportional to each other and researchers have found correlations between the two [91, 97, 98]

Figure 6-23 shows the relationship between surface resistivity and RCPT for the Type III, I/II, IL, the Type III limestone blends, and the Type I/II limestone blends. The dashed line represents a best fit curve from comprehensive research conducted by Rupnow based on concrete mixes at all ages [99].

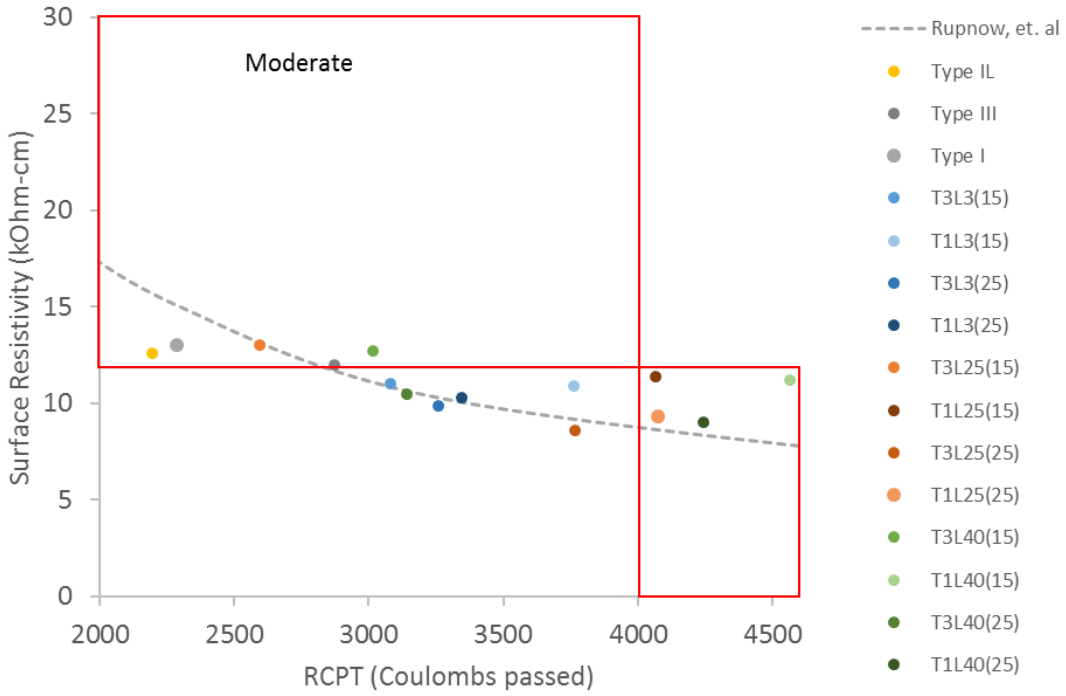

Figure 6-23: Relationship between surface resistivity and rapid chloride permeability test for limestone blended cements

As can be seen, all mixes fall within a narrow range of results, just at the border between moderate and high permeability. The neat cement mixes and the two blends T3L25(15) and T3L40(15) all fall in the moderate permeability zone. The four mixes made with Type I cement and either 25 or 40 μm limestone powder were classified as high permeability mixes, whereas the Type III cement blends were classified as moderate permeability. It appears that blending limestone powders with Type III cements has less of an impact on permeability than the equivalent blends made with Type I cement.

6.5 Correlation of Permeability Indices and Compressive Strength

Since the same parameter which affects compressive strength also affect permeability, mainly porosity, researchers have investigated the correlation between

compressive strength and permeability through measured tests [100, 101]. Al-Amoudi et al. found that certain durability indices, such as RCP results, could be correlated to compressive strength via the equation below:

$$DI = \frac{a}{(f_c')^b} \qquad 6\text{-}1$$

where *DI* is the durability index, f_c' is the compressive strength and *a* and *b* are empirical constants [100]. For the fifteen concrete mixes, the RCP test was performed only at 91 days, which provided a limited number of data points and therefor showed very little correlation with compressive strength (Figure 6-24).

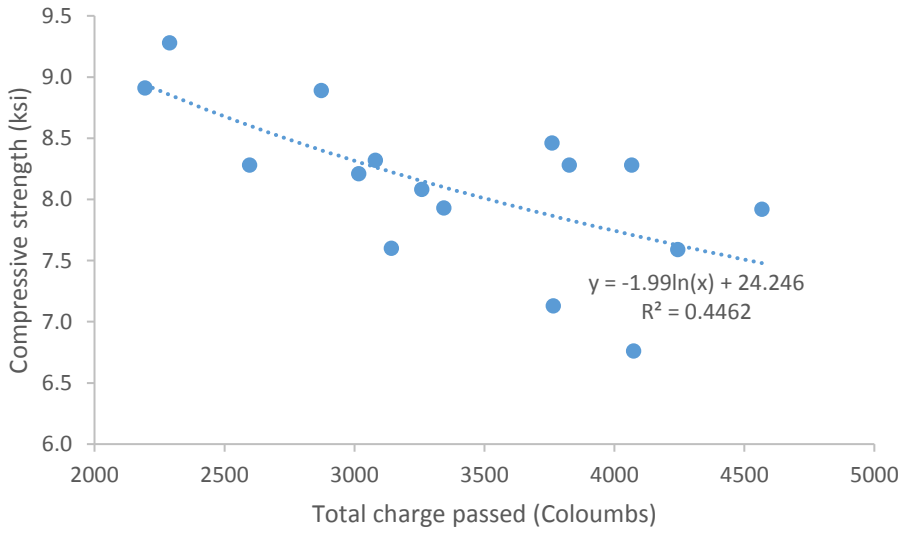

Figure 6-24: Correlation between RCPT results and compressive strength for all concrete mixes (Type III neat, Type I/II neat, Type IL, Type III limestone blends, and Type I/II limestone blends)

Surface resistivity on the other hand was measured at the same intervals as compressive strength several times over a period of 91 days for each concrete mix. With more data points, a strong correlation was found between the two. Interestingly, although research by Vosoughi et al. [101] found a logarithmic correlation between surface resistivity and compressive strength, it appears that the Type III neat cement mix and the Type III mixes with 15% cement replacement of 3, 25, and 40 μm limestone powder correlate best with an exponential equation (Figure 6-25). While the mixes made with Type I/II cement, Type IL cement and Type III blends with 25% cement replacement of the 3, 25, and 40 μm limestone follow the more typical logarithmic correlation (Figure 6-26). In both studies, they found that cement type was the most important indicator in establishing correlations between compressive strength and durability parameters, which this research would concur.

The difference in graph curvatures implies that for the Type III neat cement mix and the Type III with 15% cement replacement, the compressive strength develops faster than the development of the surface resistivity. This may be explained by the increased cement fineness of the Type III cement coupled with an accelerated hydration due to additional nucleation sites provided by the limestone powder. At higher cement replacement rates, however, the limestone powder dilutes the effectiveness of the cement contributing to a higher effective w/c ratio, counterbalances the nucleation and filler effect, and manifests as a slower compressive strength development compared with the surface resistivity development.

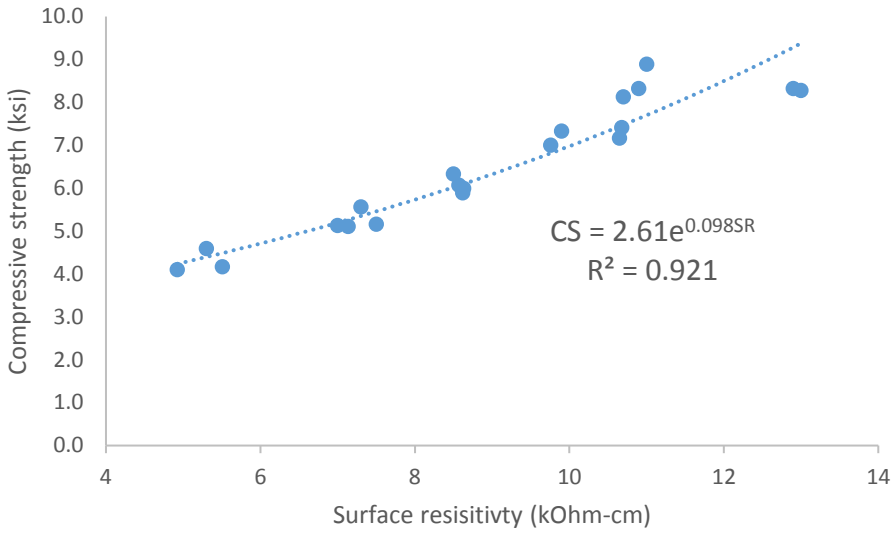

Figure 6-25: Correlation between Type III neat and Type III limestone blends with 15% cement replacement during first 91 days

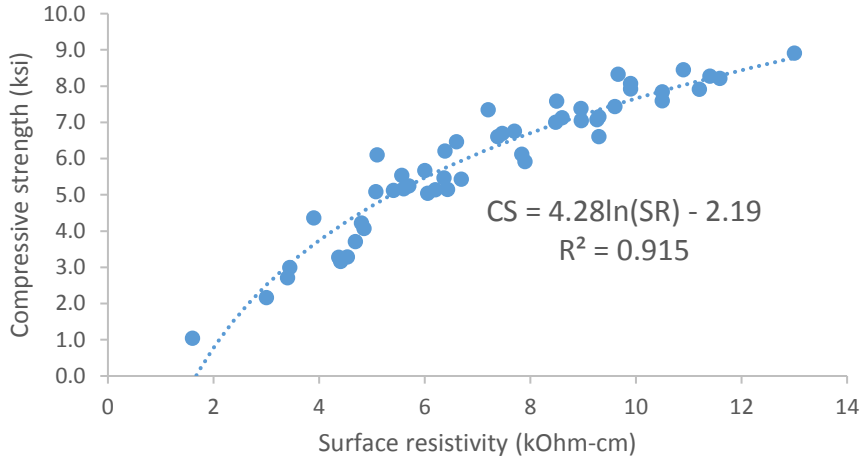

Figure 6-26: Correlation between TypeI/II neat, Type I/II limstone blends, and Type III limestone blends with 25% cement replacement during first 91 days

When using surface resistivity as a means to estimate compressive strength, care should be taken as to what cement type and percentage limestone replacement was used in the concrete mix. For example, if a surface resistivity reading of 8.0 kOhm-cm is measured, the compressive strength estimate for the Type I/II mix would be 6,700 psi, whereas it would only be 5,700 psi for Type III mixes and low cement replacement Type III limestone blends.

6.6 Conclusion and Discussion

Here, the long-term mechanical properties of hardened concrete were investigated. This chapter focused on compressive strength development over the first 90 days, dimensional stability of both drying shrinkage and creep over 9 months, and durability assessed by surface resistivity and rapid chloride permeability test. Additionally, existing drying shrinkage and creep models were investigated to determine whether they could be used to predict concrete behavior.

Some observations include:

Compressive strength:

- Compressive strength results show that in most cases, limestone blended cements produce concretes with compressive strengths far greater than what would be expected due to the reduction in cement quantity and consequent increase in effective w/c ratio.

- For the limestone blends made with Type III cement, after 3 days of curing, there was very little difference in concretes made with 15% cement substitutions of either 3, 25, or 40 μm limestone powder.
- At 25% cement replacement, the most significant compressive strength decrease was experienced by the concrete mixes made with 25 μm limestone powder blended with either Type I/II or Type III cement.

Volume stability:

- In general, lime cured concrete specimens experience more drying shrinkage strains than the neat cement mix. Air cured specimens increase comparable drying shrinkage strains to the neat cement.
- There was little difference in drying shrinkage strains between mixes made with Type I/II and Type III limestone cement blends
- Due to the prediction model being based on compressive strength rather than cement content, the GL 2000 model showed good correlation to the measured drying shrinkage strains when using $k = 1.15$ for the cement type coefficient.
- The neat Type III concrete and concrete mix T3L3(15) experienced the least amount of specific creep. In general, the mixes with 25% cement replacement experienced more specific creep than their 15% counterpart.
- The best correlations between creep models and experimental data were when using the MC90-99 or ACI models. When using the ACI model to predict creep of limestone blended cement concrete mixes, the best correlation was achieved with the default ACI values of ψ and d were used.

Durability:

- The measured surface resistivity of concrete mixes made with 25% cement replacement of concrete mixes was less than the 15% cement replacement counterpart, indicating greater permeability.
- Blended limestone cements made with Type I/II cement showed much greater ion passage than the neat Type I/II cement, indicating significantly greater permeability. Blended limestone cements made with Type III cement showed far less variability from the neat Type III mix.
- Surface resistivity and compressive strength are well correlated. However, for most mixes, the best-fit curve is logarithmic. However, when using Type III cement and Type III limestone cement blends at 15% cement replacement, the correlation is exponential.

CHAPTER 7. PREDICTING LONG-TERM CREEP OF PRECAST CONCRETE FROM NANOINDENTATION CREEP STUDIES

7.1 Introduction

In the previous chapter, long-term characteristics of limestone blended cements were evaluated. Many of the experiments reviewed, such as drying shrinkage and creep, required daily or weekly measurements of at least one year. Not only is it often impractical to conduct such long-term experiments, it also requires careful control of temperature and humidity in order to acquire reliable results. In a study conducted by Zhang et al., creep studies on cement paste lasting only a few minutes were conducted at the microscale and correlated with year-long creep studies performed on concrete specimens [60]. Indentation creep studies of cement pastes differ from the long-term creep studies in a few significant ways. Recall that creep is associated with the movement of water molecules within the hardened cement paste. Even without any moisture exchange with the outside, a loaded cylinder will undergo creep, called basic creep [14]. Specific creep is considered the sum of basic creep and drying creep, which is the additional strain which occurs when the relative humidity falls below 100% [14]. Due to the rapid loading and duration of the indentation test, there is not enough time for drying creep to occur, so only basic creep is being measured. In addition, with the indentation study, creep measurements are taken of the cement paste only and results must be upscaled to the level of the concrete.

In Zhang's study, the concrete samples used for measuring long-term creep were wrapped with self-sealing aluminum paper to limit the transfer of moisture to the

environment and avoid drying creep. With this configuration, she was able to obtain a strong correlation between upscaled basic creep results performed at the microscopic level with long-term concrete creep performed at the macro level. Since the creep test outlined in the previous chapter performed according to ASCTM C512 included drying creep, the question arises as to whether micro indentation creep studies performed on cement paste could be correlated with this more common test where cylinders have moisture exchange with the environment and total creep reported is the sum of basic and drying creep.

To this aim, this chapter compares the results of a nanoindentation creep study performed on cement paste with companion long-term creep measurements performed on the six concrete mix designs previously discussed: T3, T1L, T3L3, T3L3(25), T3L25(15) and T3L25(25). As both a validation of the long-term creep study as well as a possible alternative to a yearlong creep study requiring specialty equipment, the studies were conducted on cement paste made from the same water-to-binder ratios as the long-term creep study.

7.2 Theoretical Background of Indentation Techniques

Many researchers have used indentation as a technique to measure the mechanical properties of materials [102] [103] [104]. Indentation machines can not only measure deformations during loading and unloading to obtain Young's modulus and hardness of various materials, but more recently have been used to measure indentation depth during a sustained load, i.e. creep [102, 103, 105]. A typical indentation curve is shown below where the load is slowly applied at a constant rate, followed by a hold time and lastly an unloading stage again performed at a constant rate. During the experiment, the depth of

the penetration, h, is continuously measured. The load-displacement curve such as the one shown in Figure 7-1 can be used to establish the mechanical properties of the material.

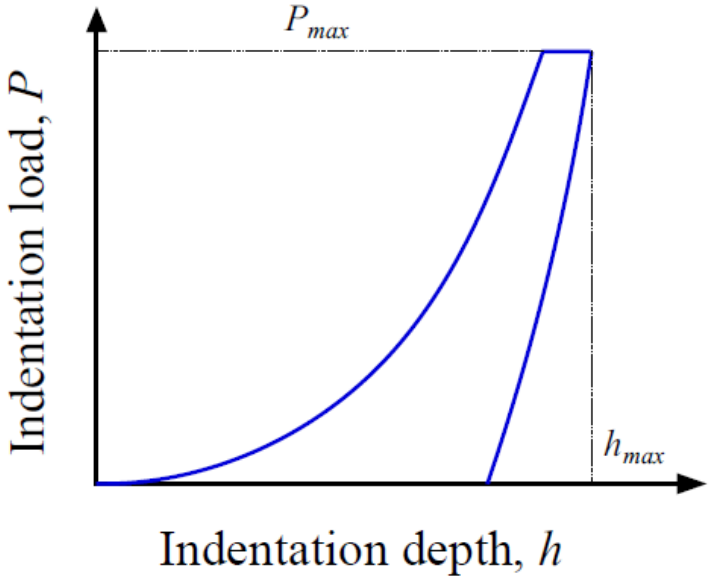

Figure 7-1: Load displacment curve for indentation experiements [106]

Figure 7-2 below shows the schematic representation of what occurs during loading by an indenter. When a load P is applied to a material, the indenter penetrates the material to a depth, h. Due to deformations of the surface profile, the max depth which remains in contact with the indenter is h_c and the contact surface has a radius, a. The indentation which remains once the load is removed is depth h_f.

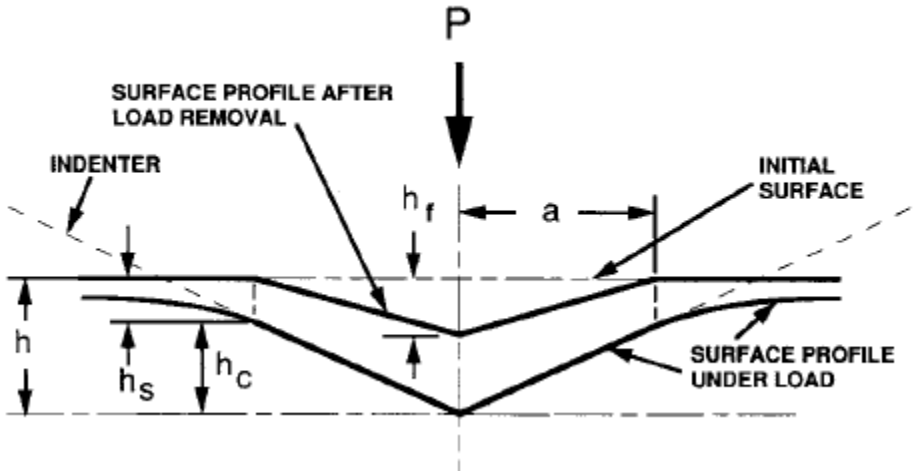

Figure 7-2: Schematic representation of indenter [107]

There are several variations of indenter tips – spherical, conical or pyramidal – and associated contact surface areas associated with the different indenter tips. In this study, a three-sided pyramidal indenter called a Berkovich indenter tip was used. The contact area, *A*, is tip specific and is theoretically defined for the Berkovich tip by the equation below [107]:

$$A = 3\sqrt{3}h_c^2 tan^2\theta \qquad 7\text{-}1$$

where θ is the semiangle of the tip and is equal to 65.27° for a Berkovich tip. Oliver-Pharr found, however, that the above equation must be modified due to tip bluntness and must be calibrated for the individual machine and tip. He described a method of determining the contact area specific for machine and indenter used [107]. The contact area, *A*, is required to get the contact radius, *a*, which is used to determine contact creep compliance, defined shortly. With knowledge of the contact area *A* and the maximum load applied P_{max},

the mechanical properties of hardness H and reduced modulus E_r can be determined with the following equations:

$$H = \frac{P_{max}}{A} \quad 7\text{-}2$$

$$E_r = \frac{dP}{dh} x \frac{2\sqrt{\pi}}{\sqrt{A}} \quad 7\text{-}3$$

where dP/dh is the contact compliance and the reduced modulus E_r is the modulus of the entire system, meaning material and indenter.

While investigating the behavior of cement pastes, Vandamme and Ulm found that cement pastes which behave logarithmically during microindentation loading will produce concretes which creep logarithmically, and likewise cement pastes which creep deviatorically during microindenation will produce concretes which creep deviatorically [60]. They derived an expression for contact creep compliance, $L(t) - L(0)$, based on the rate of penetration during the hold phase [60]:

$$L(t) - L(0) = \frac{2a_u \Delta h(t)}{P_{max}} \quad 7\text{-}4$$

where a_u is the contact radius determined from the contact area A, P_{max} is the maximum load applied, and $\Delta h(t)$ is the change in penetration depth at each time step. Creep compliance represents the indentation depth normalized by the amount of material in

contact with the indenter tip and the applied load. It is similar to concrete creep compliance $J(t,t_0)$.

7.3 Materials and Methods

Cement pastes, matching the proportions used to make the concrete specimens of Chapter 6, including the HRWRA dosage, were prepared and placed into ¾-inch diameter molds and sealed. The sealed molds were rotated for 24 hours to avoid segregation. After 24 hours, the samples were demolded, wrapped with moistened paper towels, placed in a sealed container at 100% relative humidity, and placed in an environmental chamber at 73.5 ± 3.5 ^{0}F for three days, similar to the fog room curing regime of the concrete mixes. After 3 days, the cement pastes were removed from the chamber and prepared for loading. Recall that the concrete specimens were loaded into creep frames at age of 3 days.

The preparation steps to produce a specimen able to be loaded into the nanoindenter are significant. A ½-inch diameter disk was saw cut from the center of the hardened cement paste using a diamond edge blade lubricated in isopropyl alcohol. The surface to be indented was ground and polished using six gradually finer grits and three surface polish treatments of gradually finer grits. In between grinding and polishing, the specimens were sonicated to remove unwanted debris. According to Miller, cement paste samples used for nanoindentation must have smooth surfaces and be polished to the point that they reflect light [108], see Figure 7-3. After preparing the surface, the sample was loaded into a Micro Materials Ltd Nanoindenter with a Berkovich indenter tip, see Figure 7-4.

Figure 7-3: Polished cement paste samples ready for loading into nanoindenter

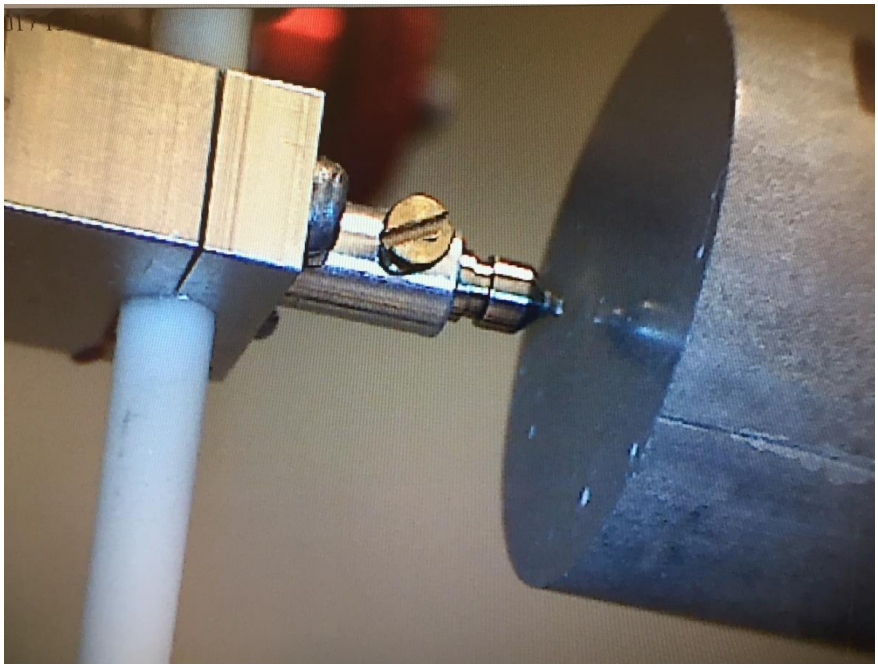

Figure 7-4: Cement paste loaded into nanoindenter. Notice the reflection of the indenter tip on the polished surface of the cement paste.

All six samples were loaded at a rate of 5 mN/s to a maximum load of 475 mN (the maximum capacity of the machine), the load was held constant for a period of 180 seconds (3 minutes) during which time the penetration depth was recorded. A long dwell time can lead to thermal drift of the apparatus [61]. Vandamme found, however, that a 180 second

hold time for nanoindentation using a Berkovich tip deviated by only 5% [61]. Due to the variability of the cement paste microstructure and in order to ensure a representative sample of cement paste, 144 measurements were taken in a 12x12 grid, spaced 150 μm apart [109, 110]. The results presented are the average of the depths at each time step and have a coefficient of variance ranging between 11-18% at each time step. The lowest coefficient of variance among average depth values at each time step were from the T3L25(15) and T3L3(25) mixes and the largest variation was from the T3L25(25) and T1L mixes. Neither the limestone fineness nor the percent limestone substitution appears to be a factor in the measured variations.

7.4 Experimental Results

Nanoindentation creep studies were conducted on six cement pastes to investigate how cement pastes creep over time and to compare results with long term creep studies being conducted on concrete specimens made from the same cements and limestone cement blends at the same water-to-binder ratio.

7.4.1 Nanoindentation Creep

The results from the nanoindenation analysis are summarized in Table 7-1. As can be seen the neat cement paste, T3, had the highest value of hardness and reduced modulus, which resulted in the smallest contact radius between the material and indenter, i.e. the indenter is penetrating less into the material. This cement paste made from a neat Type III paste also had the indentation point with the smallest penetration depth h_{min}. Unsurprisingly, the T3L25(25) limestone cement blend had the lowest measured hardness and reduced modulus, the largest contact radius and indentation grid point with the largest

depth h_{max}. Recall from the compressive strength results of Chapter 6 that the concrete mix made with Type III cement plus 25% cement substitution of the 25 μm limestone powder had the lowest measured compressive strengths.

Table 7-1: Summary of results from nanoindentation

Mix	Hardness *GPa*	E_r *GPa*	a_u *μm*	h_{max} *nm*	h_{min} *nm*
T3	0.449	21.03	18.86	11850	4944
T3L3(15)	0.309	17.51	22.80	11287	5838
T3L3(25)	0.289	16.99	23.48	11573	5767
T3L25(15)	0.326	17.79	21.95	10357	6058
T3L25(25)	0.216	14.41	27.73	15823	6265
T1L	0.294	16.22	24.23	15278	5695

Of the 144 indentations taken for each cement paste, the results of each time step were averaged and normalized by the amount of material in contact with the indenter and the applied load according to equation 7-4. This normalized data, creep compliance, was plotted over the hold time and shown in Figure 7-5. As can be seen in the graph, even at the nano level and at a 3-minute hold time, the logarithmic behavior of creep can be well captured. The graphs with the steeper slope represent pastes with a faster creep rates than the graphs with a shallower slope. Following a similar pattern to the results for hardness and reduced modulus, the slowest creep rate is observed for the neat Type III cement paste (T3) and the fastest rate is observed for the T3L25(25) mix where 25% of the cement has been replaced with 25 μm limestone powder.

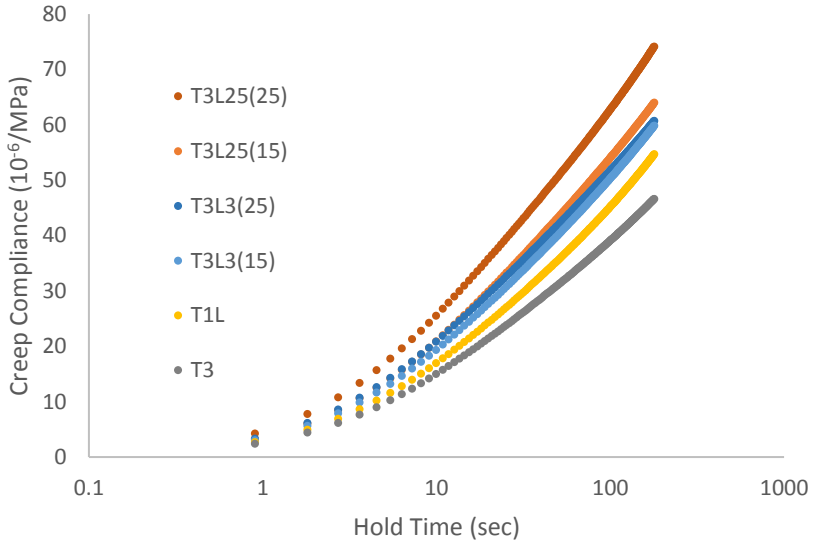

Figure 7-5: Nanoindentation creep results of cement paste

7.5 Comparison of creep compliance and specific creep

A visual comparison of the results from nanoindentation and those from the long-term creep study show that the specific creep of concrete follows a similar logarithmic behavior as the cement past, see Figure 7-6. Specific creep is the total creep due to basic and drying creep normalized by the applied load. In comparing the two graphs, it can be observed that the cement paste with the steepest slope T3L25(25) corresponds with the steepest slope of the concrete mix and that the cement paste with the shallowest slope T3 corresponds with the shallowest slope of the concrete. The other mixes fall in between these two mixes. In the following section, the two-part upscaling process to directly compare the cement paste and concrete creep functions is presented.

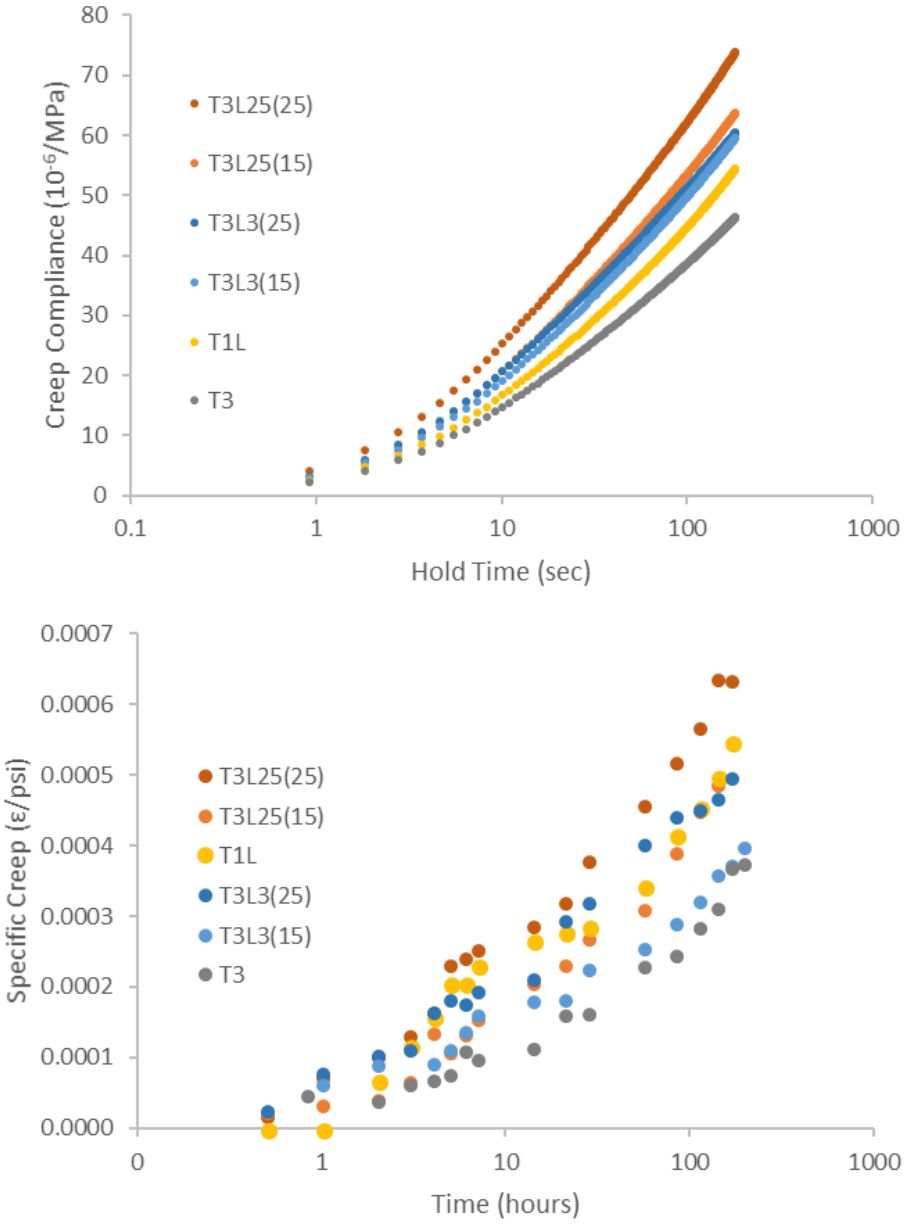

Figure 7-6: Comparison of nanoindenation creep (above with) concrtete creep (below)

7.6 Upscaling from Paste to Concrete

Comparing the creep rate of the cement paste with the concrete creep rate requires the calculation of the contact creep modulus, C_i, obtained from the cement paste and the uniaxial compression creep modulus, C_u, obtained from the concrete results. The nanoindenation creep compliance data on cement paste was fitted with:

$$L(t) - L(0) = \frac{\ln(\frac{t}{\tau_i} + 1)}{C_i} \qquad 7\text{-}5$$

While the concrete specific creep data was fitted with:

$$J(t) - J(0) = \frac{\ln(\frac{t}{\tau_u} + 1)}{C_u} \qquad 7\text{-}6$$

where τ_i and τ_u represent the time at which logarithmic behavior begins for the paste and concrete, respectively. The nanoindentation creep compliance results can be used to determine the contact creep modulus, C_i, of each cement paste and the long-term creep results can be used to determine the uniaxial creep modulus, C_u, of each corresponding concrete mix. Figure 7-7 shows the data and curve fit for the mix made with Type III cement and 15% cement replacement of 25 μm limestone powder (T3L25(15)). The parameters used for the curve fit are shown in Table 7-2.

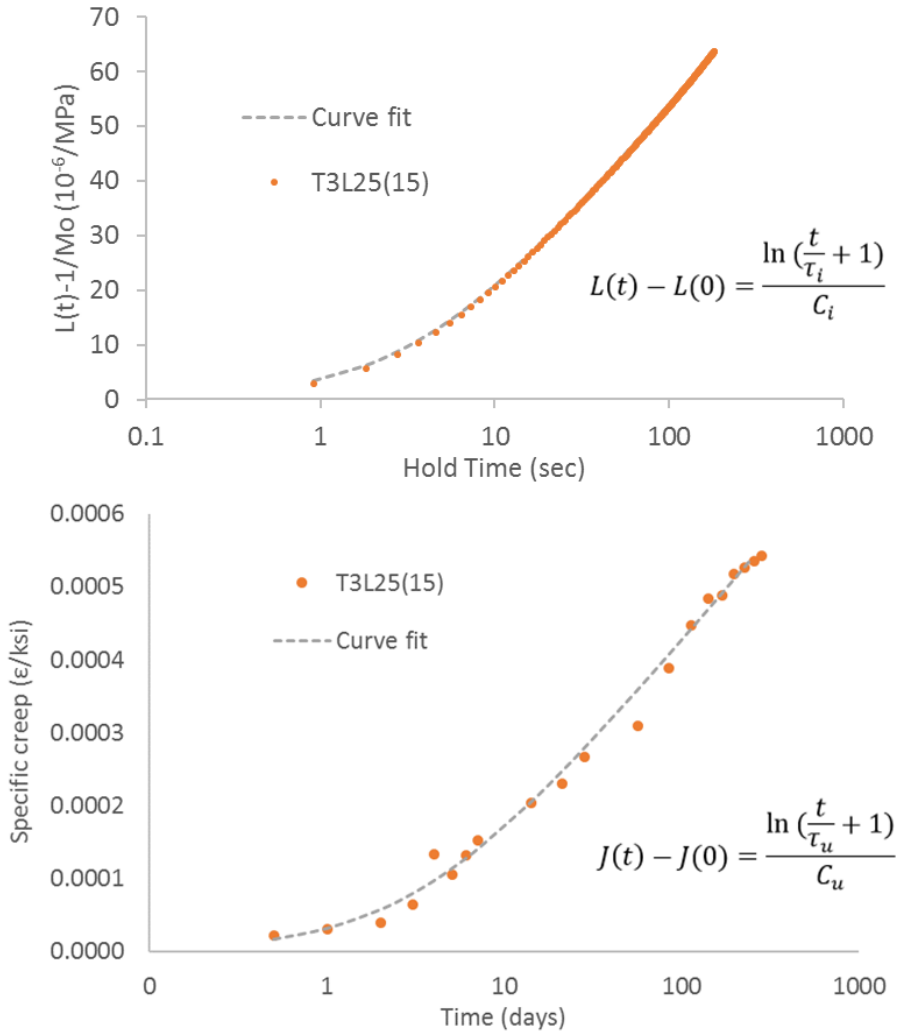

Figure 7-7: Example of curve fit data using equations 7-5 and 7-6 for mix T3L25(15) made with cement paste (above) and concrete (below)

Table 7-2: Results of curve fit

Mix	$C_{i,paste}$ *GPa*	τ_i sec	$C_{u,con}$ *GPa*	τ_u *days*
T3L25(25)	53.8	3.5	51.7	1.5
T3L25(15)	60.6	3.9	55.2	3.4
T3L3(25)	65.8	3.4	72.4	1.0
T3L3(15)	63.7	4.2	68.9	5.3
T1L	66.2	5.2	56.4	2.1
T3	80.6	4.4	82.7	1.8

The second step in the process is upscaling the cement modulus C_i to the level of the concrete, $C_{i,con}$. To upscale from the level of the cement paste to the level of concrete, one of two schemes can be used. The scheme proposed by Mori-Tanaka estimates the concrete creep moduli, $C_{i,con}$, from the cement paste creep moduli based on the volume fraction of aggregate, f_{agg}, in a concrete mix [60]:

$$C_{i,con} = C_i \frac{2 + 3f_{agg}}{2(1 - f_{agg})} \qquad 7\text{-}7$$

The second scheme proposed by Vu et al. estimates the concrete creep moduli, $C_{i,con}$ from the cement paste moduli based on the volume fraction of aggregate, f_{agg}, and the critical volume fraction of aggregate, [62]:

$$C_{i,con} = C_i\left(1 - \frac{f_{agg}}{f_{agg,m}}\right)^{-1.43} \qquad 7\text{-}8$$

The aggregate fraction f_{agg} for the neat cements, 15% cement replacement and 25% cement replacement cements are 0.646, 0.639, and 0.635, respectively. The critical volume fraction $f_{agg,m}$ was taken as 90% [60]. With these values, the paste moduli were upscaled to the level of the concrete using the two homogenization schemes. The results are shown in Table 7-3.

Table 7-3: Upscaling results using Vu et al. and Mori-Tonka schemes

Mix	$C_{i,paste}$ *GPa*	Vu, et al. $C_{i,con}$ *GPa*	Mori-Tonka $C_{i,con}$ *GPa*	Creep $C_{u,con}$ *GPa*
T3L25(25)	53.8	288	309	51.7
T3L25(15)	60.6	329	356	55.2
T3L3(25)	65.8	352	378	72.4
T3L3(15)	63.7	346	374	68.9
T1L	66.2	368	404	56.4
T3	80.6	449	492	82.7

As can be seen by the table, the upscaled modulus do not match closely to the concrete creep values, unlike the results achieved by Zhang [60]. This discrepancy can be explained by three differences between the cement paste and the concrete experiments. First, due to the rapid loading of the nanoindentation experiment, drying creep does not have time to occur and therefore only basic creep is being measured. Second, although the creep data is normalized by applied load, the concrete specimens were loaded at varying loads based on their concrete strengths, whereas the cement pastes were all loaded at the same load. This second effect should be accounted for during the load normalization of creep, but a more accurate comparison would have been to adjust the nanoindenter load based on the cement strength as is done with concrete specimens. Third, the modulus of the cement paste is different from the modulus of the concrete, which is not accounted for in the geometric upscaling.

Nonetheless, a plot of the data comparing $C_{u,con}$ calculated from the concrete specimens and $C_{i,con}$ calculated from either the Vu et al. scheme or the Mori-Tonka scheme show that there is a strong linear correlation between the two values even if the correlation is not 1.0 (Figure 7-8). This upward shift from the expected trend can be attributed to the

fact that the rate of creep being measured for the concrete is greater due to the inclusion of drying creep. It would appear that either method of upscaling from the level of the cement to the level of the concrete gives a good estimate of the creep rate of the concrete and that nanoindenation creep measurements on cement paste can be used to estimate the creep rate of concrete, including drying shrinkage.

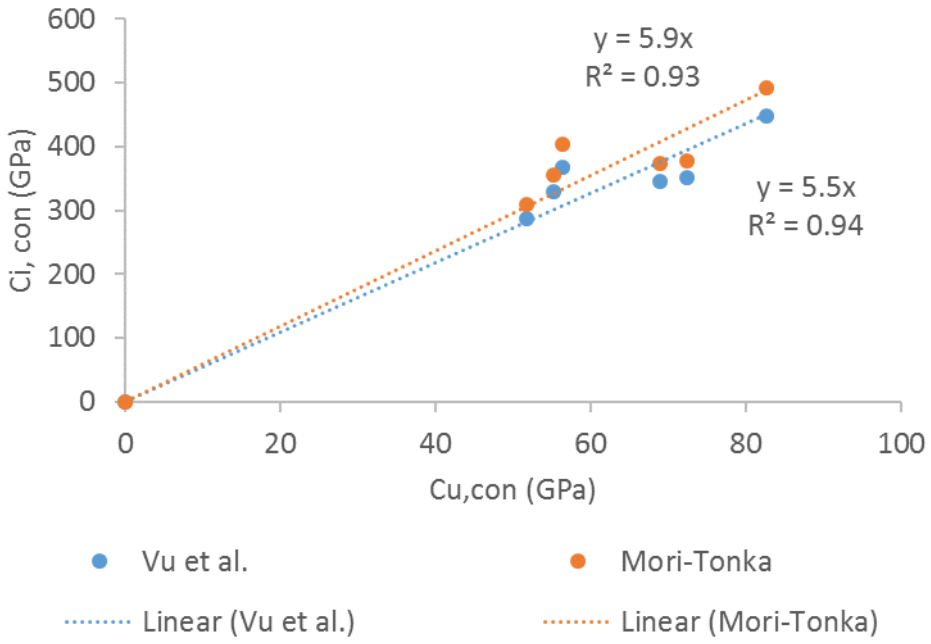

Figure 7-8: Relationship between $C_{i,con}$ upscaled from the level of cement paste and $C_{u,con}$ obtained from a long-term concrete creep study

Thus, using the Mori-Tonka upscaling equation, the creep rate $C_{u,con}$ of Type III limestone blended cement concrete mixes with water-to-binder ratio of 0.4 loaded at 40% compressive strength at 3 days subject to both sustained load and relative humidity below 100% can be approximated from the nanoindenation creep modulus C_i by:

$$C_{u,con} = 5.9C_i \frac{2 + 3f_{agg}}{2(1 - f_{agg})} \qquad 7\text{-}9$$

where f_{agg} is the volume fraction of aggregate in the concrete mix. The 5.9 factor accounts for the difference in modulus between cement paste and concrete, and the difference between drying and basic creep. Neville et al. determined the ratio between drying creep and basic creep for Type I concrete mixes with varying w/c ratios of 0.6 and 0.73, loaded at 3 days to 40% compressive strength to be 1.28 and 1.97, respectively, when measured after 100 days of loading [111]. His findings along with those by L'Hermitage [112] indicate that the ratio of drying creep to basic creep is mix specific suggesting further studies would need to be conducted in order to validate the ratio used.

7.7 Conclusions and Discussion

This study showed that creep results measured from the nanoindentation of cement paste over a 3-minute hold time could be used to predict the creep rate of concrete made with the same cement blends. Although past research showed correlations between basic creep studies performed on cement paste and concrete, the results here indicate correlations can also be drawn between cement paste and specific creep performed on concrete specimens where drying creep is also included. The main benefits of conducting nanoindentation studies to determine creep moduli and creep rate rather than yearlong concrete creep studies is in the time savings and reduced need to lock up equipment for large stretches of time. Rather than obtaining results in one year, results can be determined in a matter of days. Within weeks, various cement pastes can be sampled and compared.

The data indicates that the neat concrete or cement paste with the Type III cement shows the lowest creep rate, while the T3L25(25) mix made with 25% cement replacement of the 25 μm limestone powder had the highest rate of creep. The other mixes – Type IL neat (T1L), Type III + 15% cement replacement of either 3 or 25 μm limestone powder (T3L3(15) or T3L25(15)), and the Type III cement + 25% cement replacement of the 3 μm limestone powder (T3L3(25)) showed similar creep rates both at the cement paste and concrete levels. Recognizing the limited number of mixes run, there was no clear trend regarding effect of limestone powder or percent cement replacement. In the case of the T3L25(25) mix, however, it appears that this particular limestone fineness has much more of a dilution effect than the 25% cement substitution mix made with 3 μm limestone powder and that concrete made with this blend would creep significantly more than the neat Type III cement.

CHAPTER 8. CONCLUSIONS AND DISCUSSION

8.1 Conclusions

The main objectives of this study were to investigate how the median particle size of limestone and the percent cement substitution by mass of limestone powder affects the early age and long-term properties of concrete mixes made with limestone blended cements. The use of limestone powder to replace a portion of cement is becoming increasingly more prevalent. Limestone has the benefit of being readily available and more cost effective than other common cement replacements. Although it does not hydrate in contact with water like other cement replacements such as fly ash or slag, it has other characteristics that make it beneficial. Up until now, research mainly focused on creating limestone cement blends that produced the same compressive strength as a Type I/II cement, which was mainly achieved by intergrinding the limestone and cement together to make a more finely ground powder. In precast construction, where the use of self-consolidating concrete is more prevalent, the use of limestone is becoming more prevalent do to the improved workability and surface finish of concrete with limestone blends.

The addition of limestone powder affects early age properties through a combination of often competing effects by (a) dilution due to less hydrating cement being present in the matrix, (b) improved particle packing present if the limestone powder varies in size from the cement and (c) additional nucleation sites due to presence of limestone powder between cement particles.

Early age properties of cement paste heat evolution during hydration, set time, and workability were discussed in Chapter 4. The workability and surface finish of fifteen concrete mixes made with limestone blended cements of varying limestone median particle size and percent cement substitution by mass were discussed in Chapter 5 and slump flow, flow rate, S-groove, VSI, and surface finish were evaluated. In Chapter 6, compressive strength development, dimensional stability and durability were assessed for the same fifteen concrete mixes. Dimensional stability was evaluated through a drying shrinkage study with two curing regimes and a yearlong creep study. The durability of the mixes was indirectly measured using surface resistivity measurements and the rapid chloride permeability test. The limestone powders studied had median particle sizes that were finer than, similar to, and coarser than the median particle size of the base cement. It appears that the effect of cement replacement and limestone fineness has more impact on the early age properties than the long-term ones, except for the blends of Type I/II and Type III cement with the 25% cement replacement of the 25 μm limestone powder. This combination showed significant decreases in strength and increases in permeability and creep.

Additional studies were conducted to investigate whether existing drying shrinkage and creep models could be used to predict the behavior of concretes made with limestone blended cements. Experimental comparisons with these prediction models showed that drying shrinkage could be modeled with the existing GL 2000 model and that creep was best fitted with the ACI 209R model with minor modifications. Finally, results show that nanoindenation tests run on cement pastes show a promising future in being able to predict

long-term concrete creep rates made with the same water-to-binder ratios and cured with the same regime. Specific results and a more extensive discussion follows.

8.1.1 Effect of limestone median particle size

As previously mentioned, cement pastes and concrete mixes were made with Type I/II and Type III cements blended with a 3 μm limestone powder with smaller median particle size and larger specific surface area of the two cements; a 25 μm limestone powder with similar specific surface area to the cement Type III; and a 40 μm limestone powder with larger median particle size than the two cements. The results show that:

- Due to improved particle packing and enhanced nucleation sites, the finest limestone median particle size (3 μm) accelerated hydration and had the greatest amount of cumulative heat released in the first 48 hours of hydration compared with the coarser limestone powders. At 10% cement replacement by mass of the 3 μm powder accelerated time to peak hydration by 16, 24 and 15% from the neat Type I/II, III and IL cements, respectively. In comparison, the other limestone powders decreased time to peak by less than 8%. For all cement types, the cumulative heat for blends with the 3 μm were greater than the neat cements until around 12 to 16 hours. This accelerated hydration was also seen in the blended cement paste set times where a 10% cement substitution by mass of the 3 μm limestone increased set time by 25, 12, and 19% from the neat Type I/II, III and IL cements, respectively. Likewise, concrete mixes made with limestone cement blends with 15% cement replacement by mass of the 3 μm limestone powder showed high early strength, reduced drying shrinkage and creep rate than mixes made with coarser

limestone powders and has moderate durability as classified by AASHTO. On the other hand, the high specific surface area leads to enhanced paste cohesion, which meant a less workable mix with higher paste yield stress, smaller slump flow and more surface imperfections than the other mixes. Workability can be improved with additional HRWRA or increasing the percent substitution.

- Due to the similarities in median particle size and specific surface area to the neat cements, the 25 μm limestone powder showed more dilution dominated effects than the other limestone powders, especially at later ages. This dilution effect is most noticeable with the Type III cements blends at 25% cement replacement by mass that leads to a 20% reduction in both peak heat during hydration and cumulative heat at 48 hours, compared to the neat cement. The Vicat initial and final set times for this combination are 35% and 15% slower, respectively, than the neat cement. For the Type III blend with 25% replacement of the 25 μm limestone, compressive strength at 28 days is 25% less, whereas the other limestone powders show less than a 17% reduction. Of the concrete mixes studied for creep, this combination experienced the highest creep rate and had the worst performance for the durability tests performed. On the other hand, the mix showed great workability and surface finish.
- Blends made with the 40 μm limestone powder showed signs of dilution dominated effects competing with improved particle packing due to its diverse particle size distribution. Dilution effects were more prevalent with the Type I/II cement and less so with the Type III cement. This result is consistent with previous observation in that the specific surface of the 40 μm limestone powder is most similar to the

Type I/II cement then the Type III. During early hydration, limestone blended cements made with the 10% cement substitution of the 40 μm limestone showed a 17% reduction in both peak hydration and cumulative heat of hydration at 48 hours compared with the neat cement. The durability measures of surface resistivity and permeability also showed that the 40 μm limestone powder performed worse than the 3 and 25 μm limestone powders when blended with the Type I/II cement, but better results with the Type III cement blends. On the other hand, cement pastes made with blends of this coarser ground limestone powder had lower yield stresses and produced more workable mixes with few surface imperfections. Although care needs to be taken to avoid excessive mix segregation when the 40 μm limestone powder replaces 25% of the cement by mass.

8.1.2 Effect of limestone percent replacement

Early hydration of cement pastes was studied with percent cement substitutions up to 30% and concrete mixes were investigated with cement substitutions up to 25% by mass. The results show that:

- Regardless of the median particle size of the limestone or cement type, as more limestone powder replaces cement, the mix becomes more diluted showing a lower maximum heat of hydration and lower cumulative heat gains during hydration. The reduction in cumulative heat gain at 48 hours was shown to be linear with a slope specific to the median particle size of the limestone, regardless of cement type. For each 10% cement replacement of 3, 25, and 40 μm limestone powder, the cumulative heat at 48 hours decreases 5, 7, and 9 %, respectively.

- Due to the dilution effect, as the percent cement replacement of any of the limestone powders increased, the time of both initial and final set of all cement pastes increased linearly.
- Unsurprisingly, the compressive strength at all ages decreased as the percentage of cement decreased with increasing limestone content. Interestingly, for the Type III cement, by 28 days, there was very little difference in compressive strength between the mixes with 15% cement replacement regardless of limestone median particle size perhaps due to enhanced particle packing and increased number of nucleation sites. Generally, due to the dilution effect, the 15% cement replacement mixes had greater strengths than the 25% cement replacement mixes. The compressive strengths, however, were far greater than what would be expected from the reduced equivalent water to cement ratio indicating some benefit to the increased nucleation sites provided by the limestone powders and beneficial particle packing.
- At 25% cement replacement, the dilution effect is most pronounced for drying shrinkage where very little difference was seen in drying shrinkage of concrete mixes made with 25% cement replacement of 3, 25, or 40 μm limestone powder.
- On the other hand, workability improved and yields stress decreased as the amount of cement being replaced by the cement increased. For all limestone median particle size and cement types, increasing the limestone percentage improved fluidity and decreased yield stress of cement pastes. The yield stress of cement pastes made with Type IL limestone blends was most affected by percent limestone replacement, while the Type I/II cement blends showed the least change in yields

stress as the cement replacement increased. This phenomenon appears to be related to the yield stress of the neat cement. The Type IL cement had a very high initial yield stress whereas the Type I/II neat cement was far lower.

- Concerning durability, surface resistivity results showed higher permeability of concrete mixes made with 25% cement replacement compared with 15% mixes. RCPT on the other hand showed inconsistent results for the Type I/II mixes but showed the more expected result for the Type III cement where permeability increases with cement replacement.

8.1.3 Modelling drying shrinkage and creep of limestone blended cements

To predict drying shrinkage and creep, five existing models were compared with the experimental results – the ACI 209R, Bažant B3, CEB MC90-99 and GL2000 models. For drying shrinkage, the fifteen blended cement mixes with two varying curing regimes were best modelled by the GL2000 drying shrinkage model. This empirical model used the 28-day compressive strength as the main parameter to determine measurements rather than cement content, which is ambiguous for limestone blended cements since the limestone powder, behaves not quite like a cement but more than a filler. For limestone blended cements, however, it is recommended to use a k factor of 1.15 regardless of cement type used, even though it should be 1.0 for Type I/II cements.

Creep modelling results show that the ACI 209R is the best model to use to approximate the drying shrinkage and creep strains of loaded specimens. Additionally, the model best matched experimental results when E_{m0} was calculated using the empirical

equation rather than the actual value obtained experimentally and when the default values of coefficient values d and ψ were used.

8.1.4 Upscaling of nanoindentation cement paste creep to concrete creep

Nanoindentation creep experiments were performed on cement pastes matching the cement blends and curing regimes of concrete mixes used to study the long-term concrete properties. This study showed that the creep modulus calculated from the cement paste mixes and upscaled to the level of the concrete showed a linear trend between concrete creep rate and upscaled cement paste creep rates. An equation is proposed correlating the two creep rates:

$$C_{u,con} = 5.9 C_i \frac{2 + 3 f_{agg}}{2(1 - f_{agg})} \qquad 8\text{-}1$$

Although the correlation between the two creep rates was different to the expected value of 1.0, the difference can be explained in that the cement paste is measuring basic creep only due to the short duration of loading. The concrete mixes, on the other hand, were maintained at 50%± relative humidity experiencing both basic creep and drying creep. The correlation coefficient observed is similar to results found in research but is most likely mix specific and warrants additional investigation.

8.2 Recommendations for Practice

For precast concrete applications, specifically, where high early compressive strength, good workability and surface finish, are required coupled with good durability

and dimensional stability, the best results were achieved with either the 3 μm limestone powder at 15% or 25% cement replacement. The 15% cement replacement mixes had accelerated hydration and set time, high early compressive strength, good durability, and the lowest drying shrinkage and creep rates. At 15% cement replacement, however, the concrete mix was less workable and additional super plasticizer would need to be added to achieve target slump flows. Of slight concern with the 25% replacement is the slower set time, but mixes showed improved workability and great surface finish.

The 25 μm limestone powder currently being used should be monitored carefully. Although workability and surface finish are good and results made with 15% cement replacement are promising, higher cement replacements, especially with the Type III cement, showed considerable less durability, 28-day compressive strengths and higher creep rates than mixes with other limestone powders.

The 40 μm limestone powder would be useful where heat generated during hydration is of concern and where high early strength is not as important. Care should be taken when designing mixes with this limestone powder and Type I/II cements especially if the median particle size and/or specific surface area are similar.

When predicting drying shrinkage and creep of concrete mixes made with limestone blended cements from existing models, drying shrinkage was best predicted using the GL2000 model where the 28-day compressive strength is the basis for the empirically derived shrinkage formulas while the ACI 209R appears to be the best match when predicting creep strains.

8.3 Recommendations for Future Work

In order to try to isolate the influence that median particle size of limestone powders and percent cement replacement rates have on concrete mixes, consistent mixes were used throughout this research. For example, all cement pastes and concrete mixes were made using a water-to-binder ratio of 0.38 for the cement paste experiments and 0.4 for the concrete mixes. Investigating mixes with other combinations of water-to-binder ratio would be useful in determining whether that has any effect on concrete properties. Additionally, to further the research in this field, several possibilities for future research include:

- Performing a transfer and development length test of prestressing strands of loaded beams to ensure proper bond exists between the concrete and the tensioning cables. Although research shows very little difference in bond behavior of prestressing strands between neat cement concrete mixes and limestone blended cement concrete mixes, performing a test would be prudent, especially at higher cement substitution rates and for the concrete mixes most affected by limestone median particle size and cement type.
- The nanoindenation creep study performed for this research was limited to only six mixes. Nanoindenation of cement pastes could be performed and compared with existing creep data to investigate whether other factors such as water-to-binder ratio, applied load causing creep strain, and age of loading impact the drying creep to basic creep ratio proposed.
- Being able to predict the behavior of limestone cement blends based on the proportions of each component used would be very useful to designers. In

Appendix A, many investigations into doing so are presented. Blends of limestone and cement blended by median particle size, an area multiplier, and blends of specific surface areas using rule of mixtures were all investigated. In most cases, the rule of mixtures worked well to predict behavior of limestone blended cements of the 25 and 40 μm limestone powders blended with various cements, but the blends with the 3 μm limestone never quite fit the experimental results. There is opportunity in continuing this research to establish a good relationship between blends and experimental values.

- Given the varied results from the surface resistivity and RCP test, a more accurate measure of permeability such as ponding, formation factor, or freeze-thaw should be considered. Many of the results indicated that the durability classification according to AASHTO falls into the moderate to high permeability range. For members exposed to aggressive environments decreasing the permeability would be beneficial. Investigating if there are any benefits to blending also with fly ash, slag or metakaolin should be considered.
- Finally, creating a limestone blended cement guide for designers similar to the PCA Design and Control of Concrete Mixtures would be an ambitious but necessary goal. The objective would be to have a prescriptive outline of how to create concrete mixes with the required properties to assist designers in tailoring concrete mixes. For this, many more experiments with much more varying parameters would need to be investigated.

APPENDIX A: BLENDED D_{50}

Limestone and cement blends were used for making pastes and mortars. The properties of the blends were determined using Equation A-1 where the blended property is determined using the rule of mixtures as the property of the cement multiplied by the volume fraction of the cement plus the property of the limestone powder multiplied by the property of the limestone powder:

$$Blended\ D_{50} = fD_{50}^{cement} + (1-f)D_{50}^{limestone} \qquad \text{A-1}$$

and show the ratio of the specific surface area of the blends to the specific surface area of the cement combined with varying percentages of limestone powders with median particle size of 3, 15, 25, and 40 μm. As seen in the figures, the 3 μm powder has the highest blended specific surface area ratio and increases more rapidly with increasing percent cement substitution than the other blends. The blended surface area ratio of the 40 μm limestone powder with the Type I/II cement is fairly constant even with increasing cement replacement. This can be attributed to the similar specific surface area of the Type I/II cement and 40 μm limestone powder (Table 3-2). The blended surface area of the 40 μm limestone powder with the Type III cement shows a decreasing trend with increasing amount of cement substitution. The blended surface area of all limestone powders regardless of median particle size increase relative to cement Type I/II. With cement Type III, only the 3 and 15 μm limestone powders show an increase in the blended surface area.

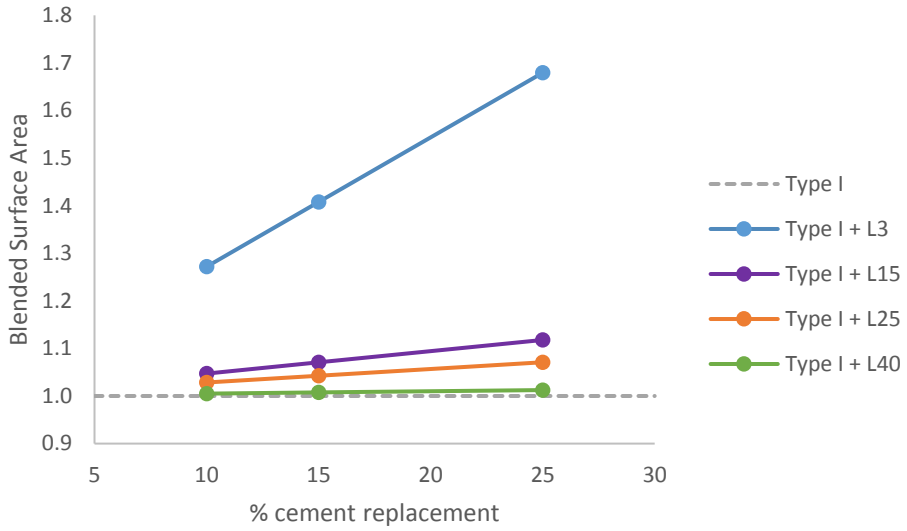

Figure A-1: Blended surface area of Type I/II and limestone

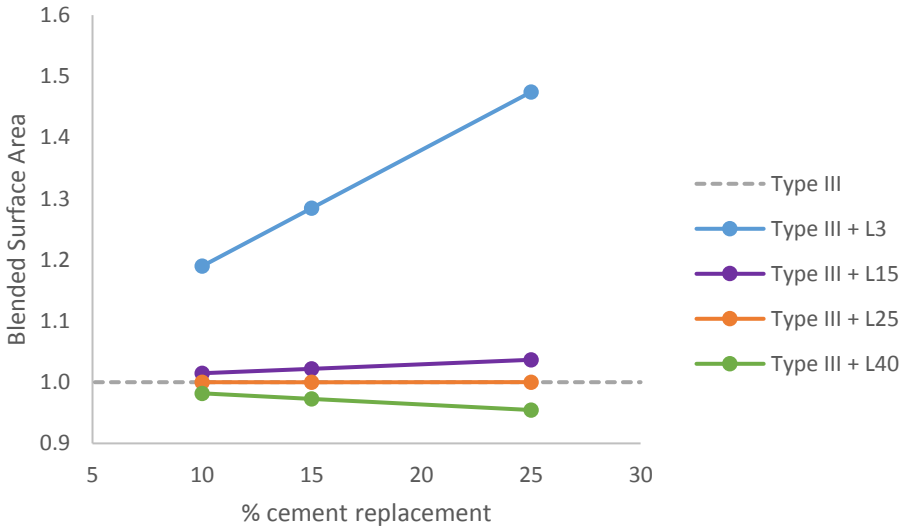

Figure A-2: Blended surface area of Type III and limestone

As previously mentioned, being able to predict and quantify the effects of limestone cement blends would be useful to concrete suppliers. Although other researchers found correlations with between various parameters such as blended packing density, β and blended specific surface area, the best correlations for the data previously presented were with the blended D_{50} values, obtained by rule of mixtures. The blended D_{50} values are

plotted against the peak hydration of a wide variety of cement-limestone blends. It is clear that each cement behaves differently and is affected independently of limestone powder

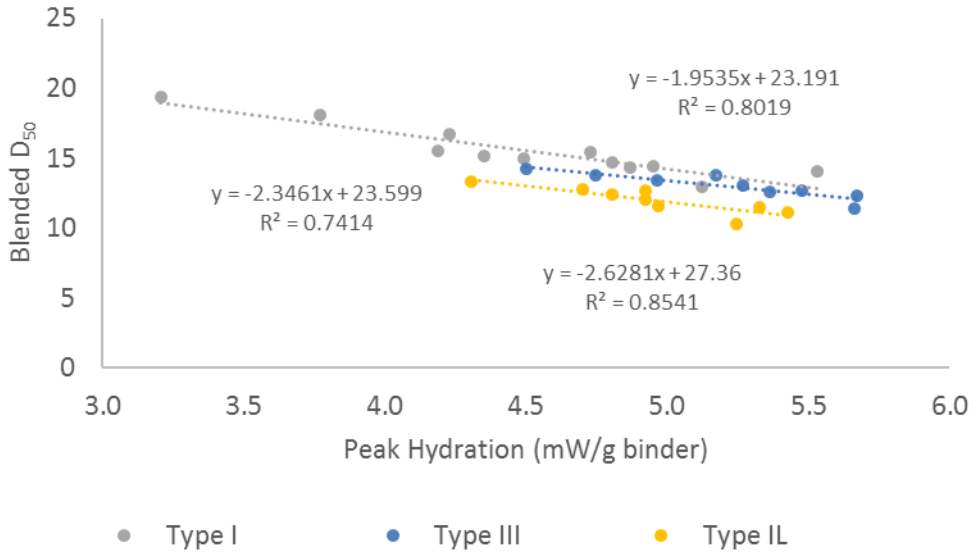

Figure A-3: Relationship between peak hydration and blended D_{50}

The blended D_{50} values of the limestone-cement blends were also correlated with the Vicat initial and final time of set. As seen in the initial and final set varies for each cement type. The Type I/II and Type III show similar trends to the Type IL cement.

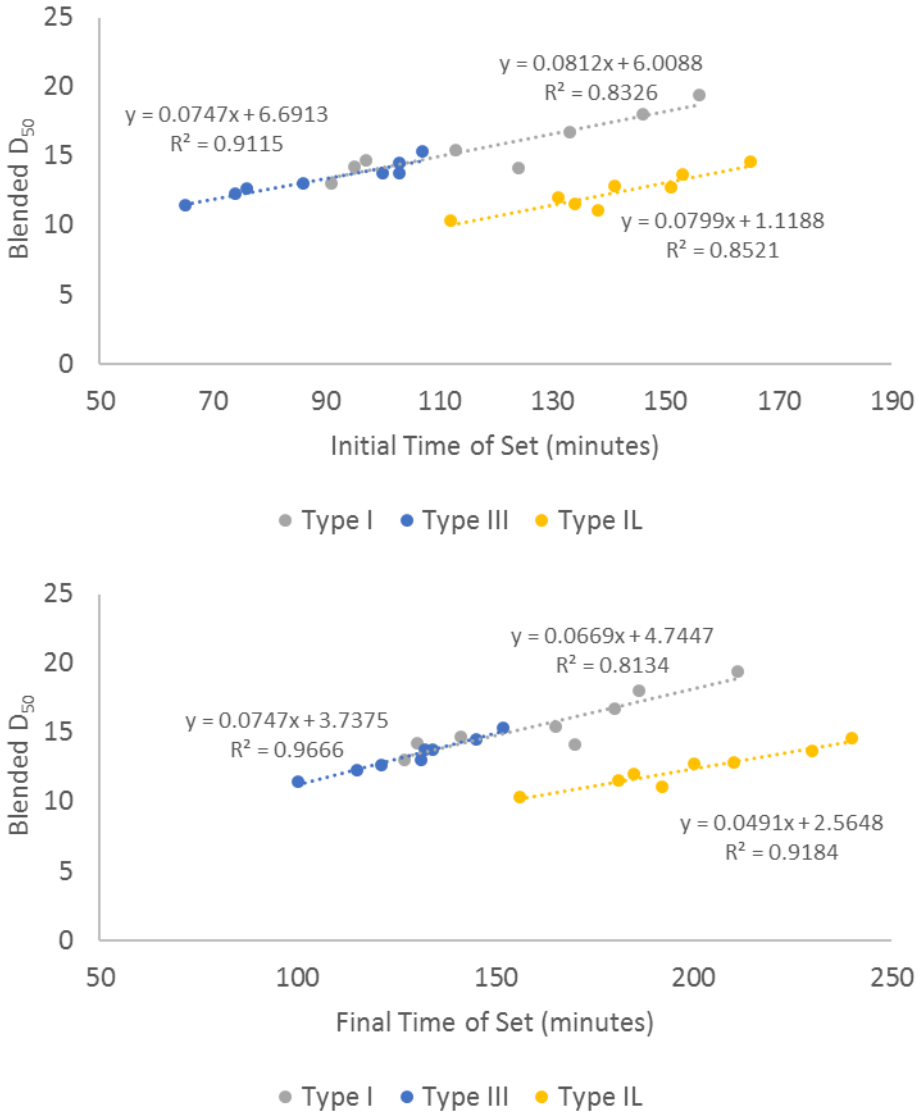

Figure A-4: Relationship between time of set and blended D_{50}

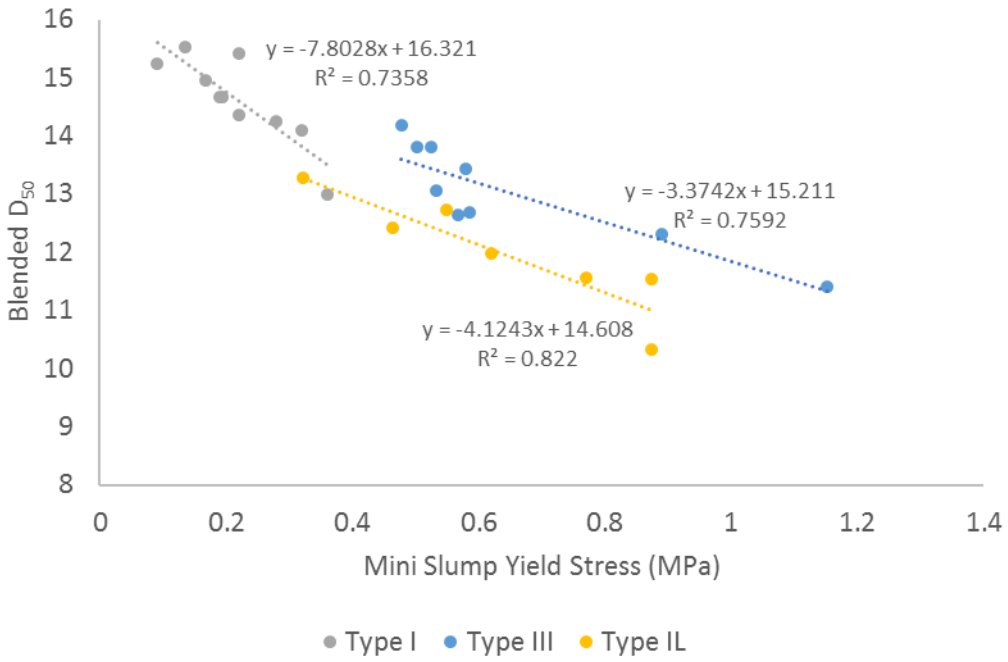

Figure A-5: Relationship between mini slump yield stress and blended D_{50}

APPENDIX B: SLUMP FLOW AND VSI PHOTOS OF MIXES

Figure B-1: Unacceptable S-groove

Figure B-2: Insufficient slump flow

Figure B-3: Bleeding and segregation due to too much HRWRA

APPENDIX C: DRYING SHRINKAGE DATA

Table C-1: Drying shrinkage data for limewater cured specimens

	Days drying				
Mix	**7 Days**	**28 Days**	**56 Days**	**112 Days**	**224 Days**
Type III	-154	-297	-389	-421	-465
T3L3(15)	-192	-383	-426	-439	-449
T3L3(25)	-269	-477	-573	-630	-663
T3L25(15)	-253	-494	-540	-563	-598
T3L25(25)	-216	-457	-593	-640	-657
T3L40(15)	-268	-496	-595	-637	-662
T3L40(25)	-264	-453	-583	-637	-679
Type I/II	-156	-286	-349	-394	-405
T1L3(15)	-214	-350	-407	-415	-417
T1L3(25)	-212	-448	-524	-618	-606
T1L25(15)	-265	-484	-548	-643	-629
T1L25(25)	-270	-470	-622	-695	-679
T1L40(15)	-281	-468	-571	-641	-644
T1L40(25)	-237	-472	-575	-614	-598
Type IL	-136	-348	-444	-479	-486

Table C-2: Drying shrinkage data for air cured specimens

	Days drying				
Mix	**7 Days**	**28 Days**	**56 Days**	**112 Days**	**224 Days**
Type III	-356	-466	-535	-653	-667
T3L3(15)	-446	-554	-621	-666	-669
T3L3(25)	-251	-514	-579	-611	-618
T3L25(15)	-351	-525	-623	-671	-727
T3L25(25)	-237	-440	-563	-678	-680
T3L40(15)	-332	-584	-651	-723	-722
T3L40(25)	-323	-513	-590	-688	-702
Type I/II	-245	-426	-469	-556	-569
T1L3(15)	-205	-387	-433	-514	-538
T1L3(25)	-225	-453	-512	-603	-556
T1L25(15)	-340	-519	-664	-713	-747
T1L25(25)	-303	-511	-598	-647	-654
T1L40(15)	-268	-484	-579	-676	-673
T1L40(25)	-273	-557	-596	-616	-620
Type IL	-278	-451	-527	-589	-609

APPENDIX D: CREEP DATA

Table D-1: Total creep + shrinkage strains

Days	T3	T3L3(15)	T3L3(25)	T3L25(15)	T3L25(25)	T1L
4	0.00098	0.00101	0.00114	0.00109	0.00110	0.00130
5	0.00109	0.00106	0.00120	0.00108	0.00127	0.00144
6	0.00121	0.00114	0.00123	0.00114	0.00131	0.00147
7	0.00133	0.00119	0.00127	0.00121	0.00136	0.00152
14	0.00143	0.00132	0.00140	0.00144	0.00144	0.00161
21	0.00148	0.00145	0.00165	0.00151	0.00159	0.00167
28	0.00160	0.00153	0.00175	0.00160	0.00177	0.00176
56	0.00178	0.00179	0.00197	0.00182	0.00201	0.00195
84	0.00195	0.00192	0.00219	0.00205	0.00215	0.00218
112	0.00211	0.00203	0.00226	0.00218	0.00227	0.00225
140	0.00223	0.00214	0.00232	0.00223	0.00240	0.00239
168	0.00227	0.00225	0.00234	0.00224	0.00235	0.00252
196	0.00233	0.00227	0.00237	0.00230	0.00245	0.00262
224	0.00240	0.00231	0.00238	0.00231	0.00241	0.00266
252	0.00244	0.00233	0.00239	0.00233	0.00244	0.00269
280	0.00248	0.00233	0.00242	0.00236	0.00249	0.00271

Table D-2: Shrinkage strains and specific creep

Days	T3	T3L3(15)	T3L3(25)	T3L25(15)	T3L25(25)	T1L
4	0.00008	0.00021	0.00019	0.00021	0.00015	0.00026
5	0.00015	0.00024	0.00021	0.00025	0.00019	0.00029
6	0.00021	0.00025	0.00025	0.00026	0.00021	0.00032
7	0.00027	0.00033	0.00026	0.00029	0.00024	0.00030
14	0.00032	0.00042	0.00035	0.00042	0.00026	0.00031
21	0.00037	0.00045	0.00043	0.00043	0.00034	0.00035
28	0.00038	0.00052	0.00048	0.00045	0.00041	0.00042
56	0.00049	0.00063	0.00053	0.00058	0.00050	0.00047
84	0.00057	0.00072	0.00067	0.00065	0.00052	0.00053
112	0.00066	0.00075	0.00072	0.00067	0.00055	0.00050
140	0.00070	0.00080	0.00074	0.00064	0.00054	0.00055
168	0.00070	0.00078	0.00070	0.00064	0.00050	0.00056
196	0.00070	0.00079	0.00070	0.00065	0.00053	0.00060
224	0.00072	0.00081	0.00072	0.00064	0.00049	0.00062
252	0.00070	0.00082	0.00071	0.00065	0.00047	0.00061
280	0.00073	0.00075	0.00070	0.00066	0.00050	0.00058

Specific creep						
Days	**T3**	**T3L3(15)**	**T3L3(25)**	**T3L25(15)**	**T3L25(25)**	**T1L**
4	0.000092	0.000069	0.000164	0.000135	0.000165	0.000159
5	0.000111	0.000076	0.000181	0.000108	0.000232	0.000205
6	0.000136	0.000111	0.000176	0.000133	0.000241	0.000205
7	0.000161	0.000098	0.000195	0.000154	0.000253	0.000230
14	0.000179	0.000113	0.000211	0.000205	0.000285	0.000266
21	0.000181	0.000160	0.000295	0.000232	0.000319	0.000278
28	0.000226	0.000162	0.000319	0.000268	0.000378	0.000285
56	0.000254	0.000229	0.000401	0.000311	0.000457	0.000342
84	0.000291	0.000246	0.000441	0.000390	0.000518	0.000415
112	0.000321	0.000284	0.000451	0.000448	0.000567	0.000455
140	0.000358	0.000313	0.000468	0.000486	0.000636	0.000498
168	0.000373	0.000368	0.000497	0.000490	0.000634	0.000547
196	0.000397	0.000375	0.000510	0.000520	0.000670	0.000575
224	0.000420	0.000383	0.000510	0.000529	0.000670	0.000582
252	0.000444	0.000390	0.000515	0.000536	0.000698	0.000598
280	0.000448	0.000421	0.000534	0.000544	0.000707	0.000618

Table D-3: Modulus of elasticity comparison

	Young's Modulus (psi)					
	T3	**T3L3(15)**	**T3L3(25)**	**T3L25(15)**	**T3L25(25)**	**T1L**
E (experimental)	3566757	3408364	3391827	3245208	2995858	3543135
E(ACI 209R)	4000337	3795831	3813937	3819095	3587899	4022418
E(Bazant B3)	3083695	2926049	2940007	2943982	2765763	3100716
E(CEB M90)	4282346	4135269	4148396	4152131	3982988	4298074
E(GL2000)	4551331	4377401	4267758	4235323	4195294	4567982
E(AASHTO)	4484001	4291497	4170144	4134245	4089941	4502431

APPENDIX E: CREEP PREDICTION MODEL COMPARISON

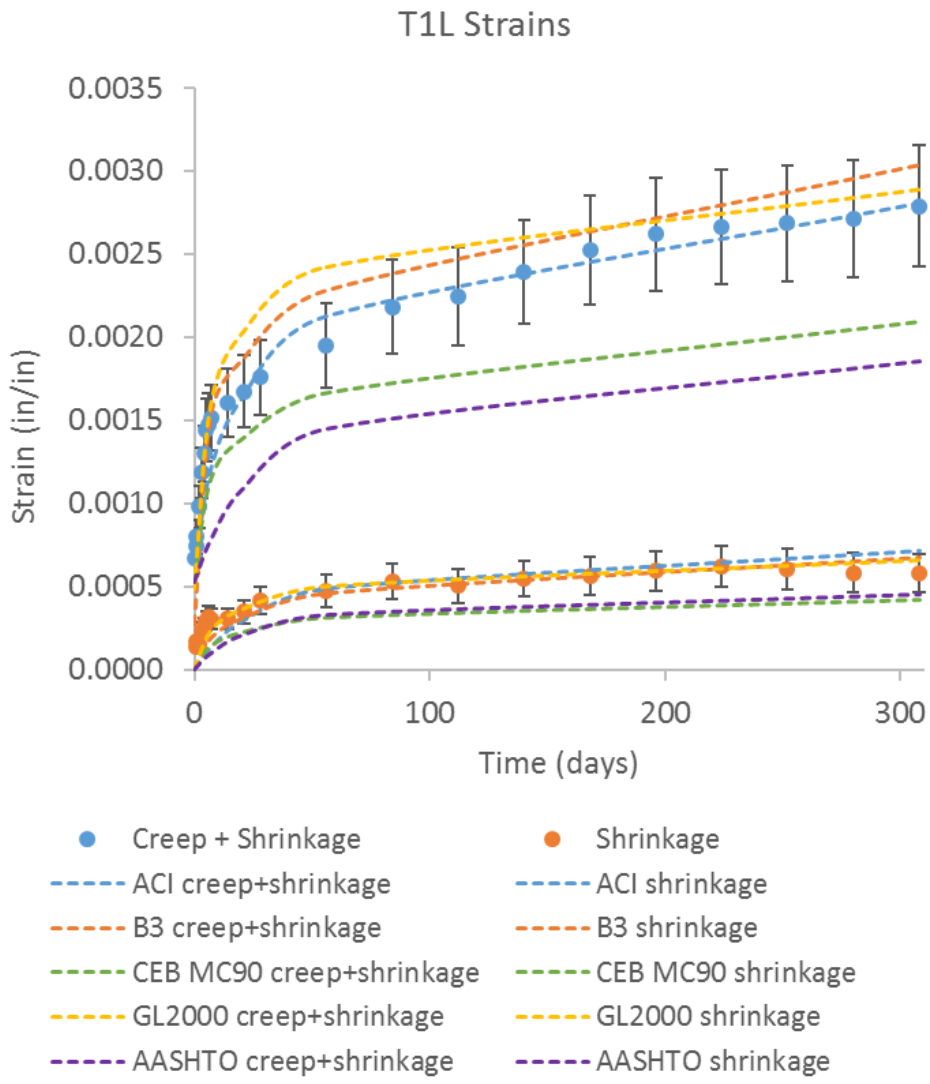

Figure E-1: T1L total creep and shrinkage strains

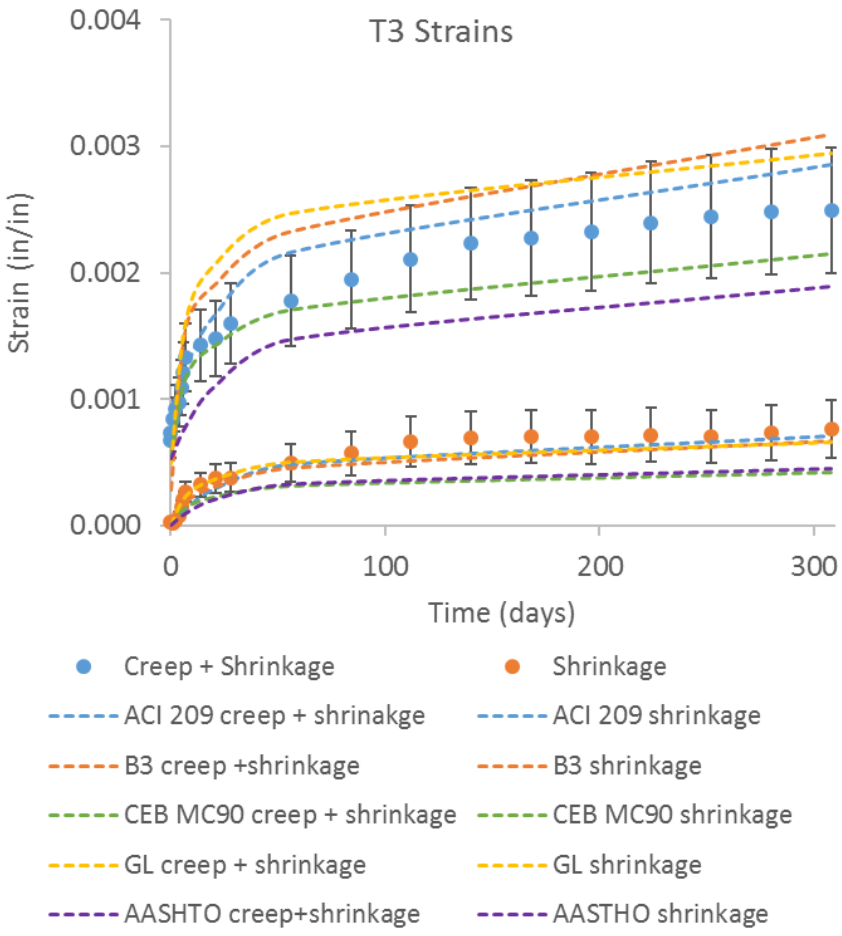

Figure E-2: T3 total creep and shrinkage strains

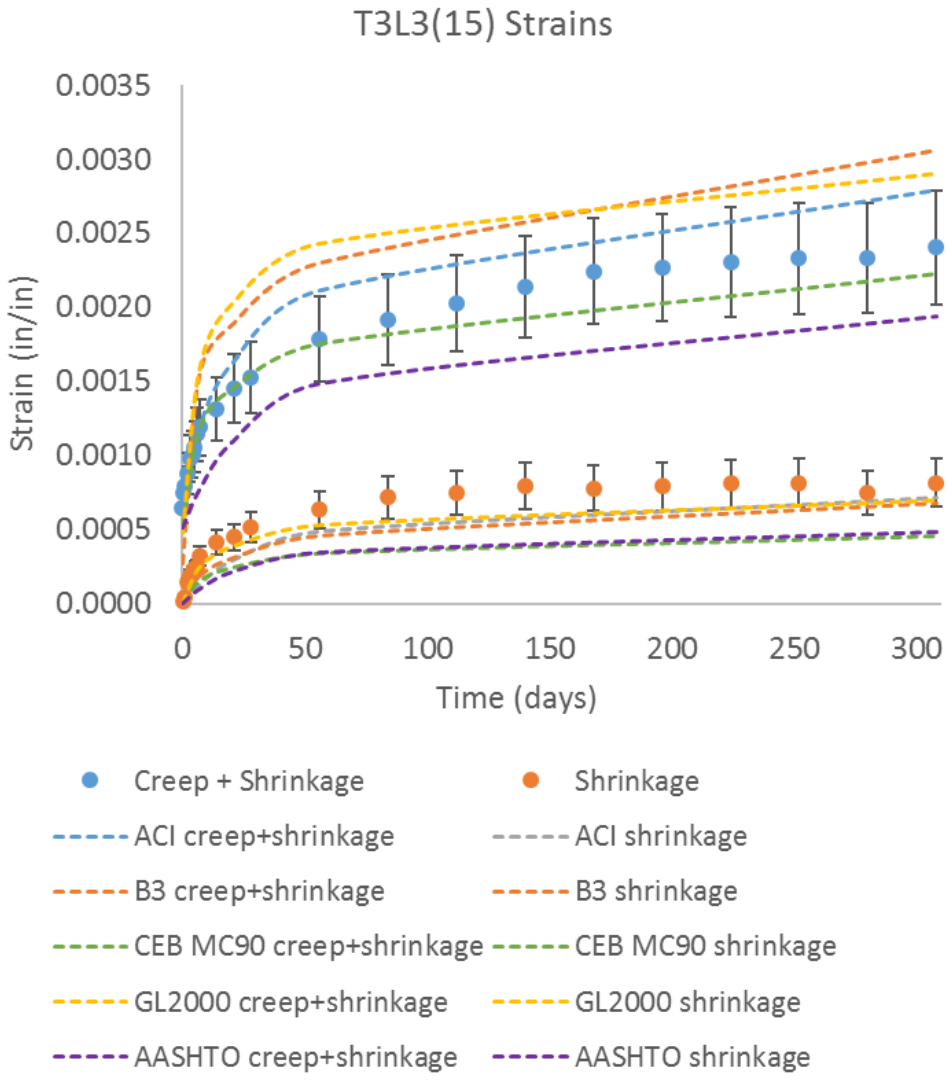

Figure E-3: T3L3(15) total creep and shrinkage strains

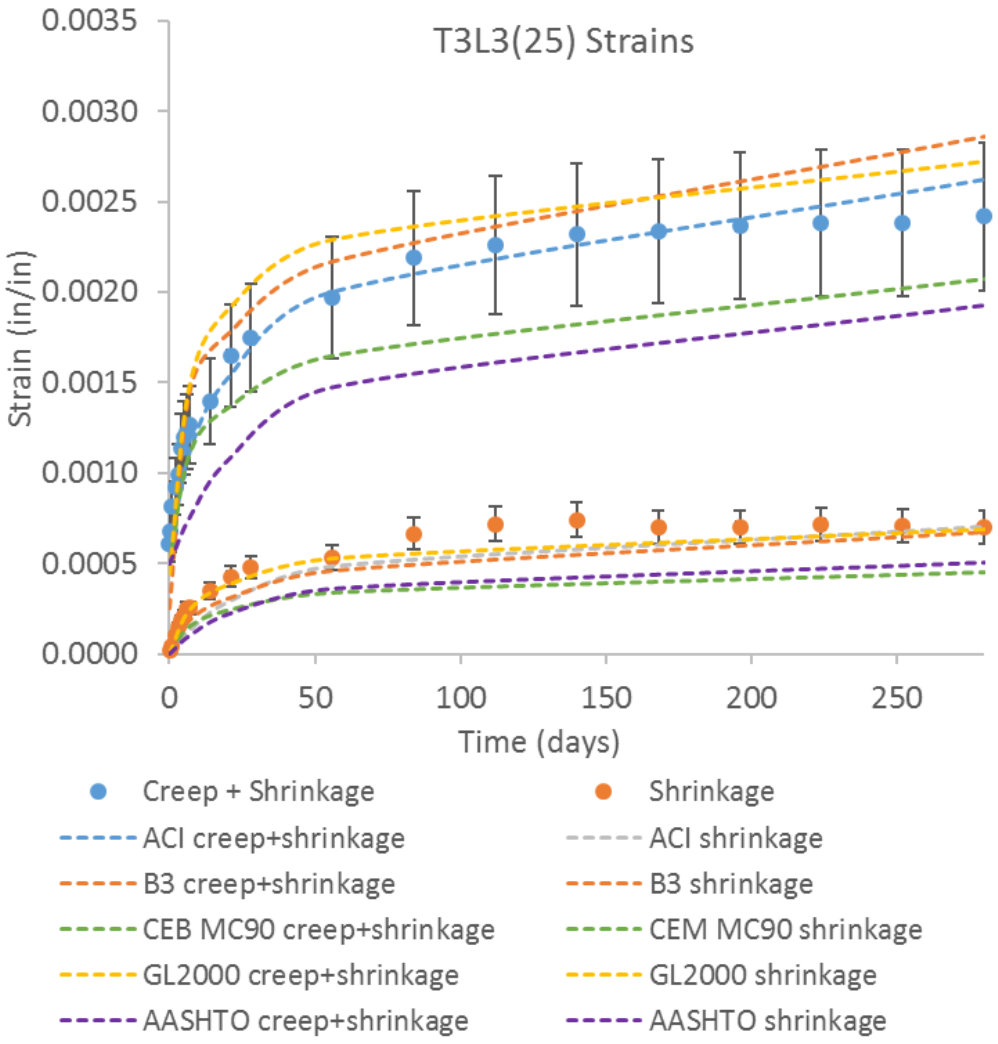

Figure E-4: T3L3(25) total creep and shrinkage strains

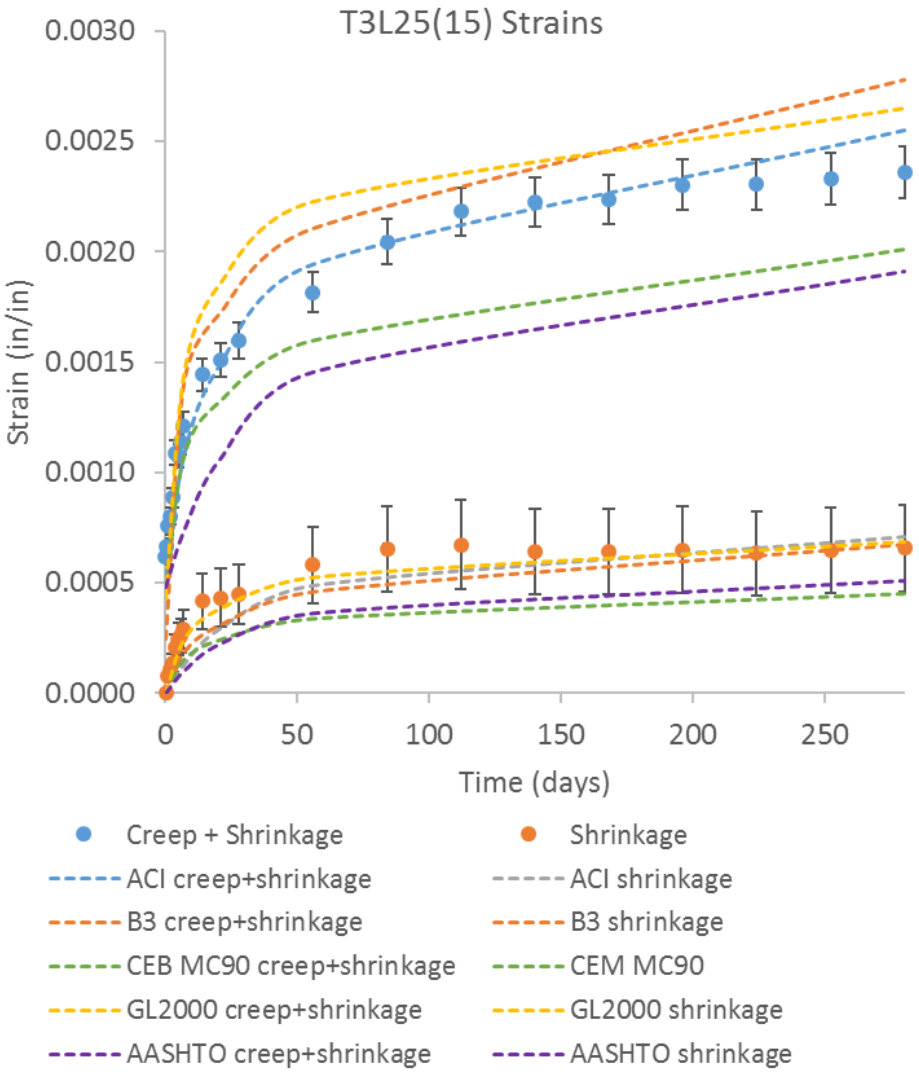

Figure E-5: T3L25(15) total creep and shrinkage strains

APPENDIX F: COMPARISON OF DRYING SHRINKAGE STUDIES

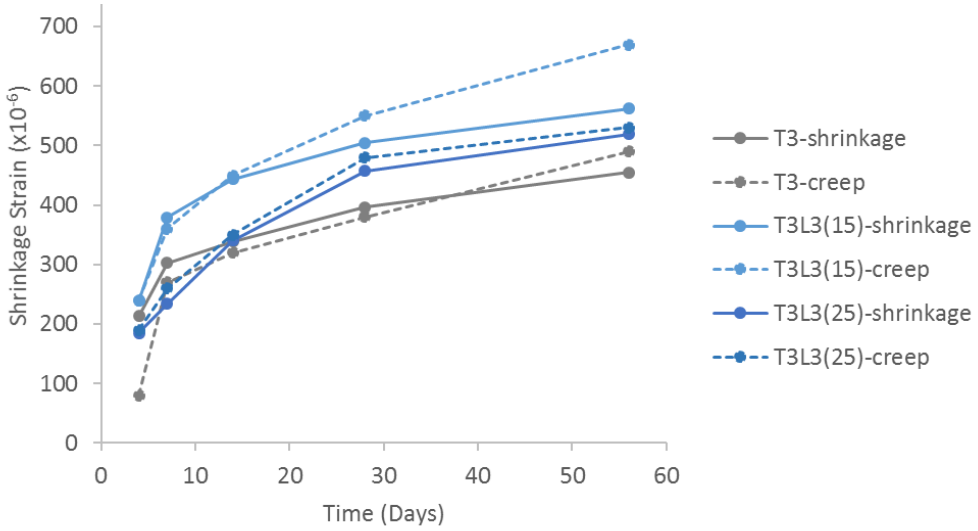

Figure F-1: Shrinkage comparison between ASTM C157 and C512

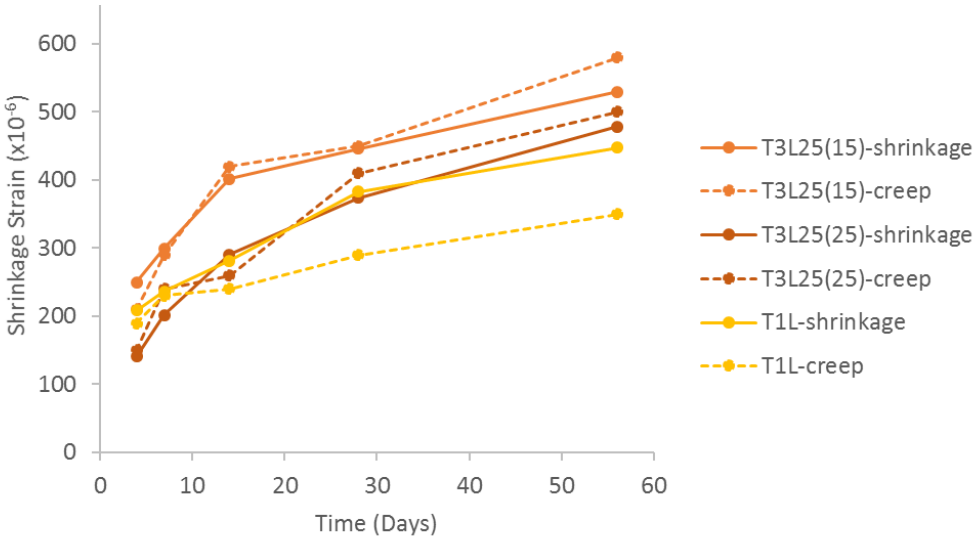

Figure F-2: Shrinkage comparison between ASTM C157 and C512

REFERENCES

1. Boden, T.A., G. Marland, and R.J. Andres, *Global, Regional, and National Fossil-Fuel CO2 Emissions. Carbon Dioxide Information Analysis Center*. 2010.

2. Scrivener, K., V. John, and E. Gartner, *Eco-efficient cements: Potential, economically viable solutions for a low CO2, cement based materials industry.* UNEP (United Nations Environment Program, 2016.

3. Müller, N. and J. Harnisch, *A blueprint for a climate friendly cement industry.* Gland: WWF lafarge conservation partnership, 2008.

4. Tennis, P., M. Thomas, and W. Weiss, *State-of-the-Art Report on Use of Limestone in Cements at Levels of up to 15%.* Illinois, accessed November, 2011. **9**: p. 2015.

5. Bonavetti, V., et al., *Limestone filler cement in low w/c concrete: a rational use of energy.* Cement and Concrete Research, 2003. **33**(6): p. 865-871.

6. Hooton, R., M. Nokken, and M. Thomas, *Portland-limestone cement: state-of-the-art report and gap analysis for CSA A 3000.* Cement Association of Canada. University of Toronto, 2007.

7. Team, P.S.-C.C.F., *Interim Guidelines for the Use of Self-Consolidating Concrete in PCI Member Plants.* PCI Journal, 2003. **48**(3): p. 14-18.

8. Snow, T., QC Manager at Metromont, *Personal Interview*. (2016, September 29).

9. Norten, T., Batch Plant Supervisor at Tindall, *Personal Interview*. (2016, October 20).

10. Voglis, N., et al., *Portland-limestone cements. Their properties and hydration compared to those of other composite cements.* Cement and Concrete Composites, 2005. **27**(2): p. 191-196.

11. Ye, G., et al., *Influence of limestone powder used as filler in SCC on hydration and microstructure of cement pastes.* Cement and Concrete Composites, 2007. **29**(2): p. 94-102.

12. Collepardi, M., S. Collepardi, and R. Troli. *Properties of SCC and flowing concrete*. in *Proceedings of the International Conference of Sustainable Construction Materials and Technologies, Coventry: Pub. UW Milwaukee CBU*. 2007.

13. ASTM Standard C595, *Standard Specification for Blended Hydraulic Cements*. ASTM International, West Conshohocken, PA, 2017.

14. Mehta, P.K. and P.J. Monteiro, *Concrete microstructure, properties and materials*. 2017.

15. Bentz, D.P., et al., *Limestone Fillers Conserve Cement; Part 1: An analysis based on Powers' model.* Concrete international, 2009. **31**(11): p. 41-46.

16. Bentz, D.P., et al., *Limestone fillers conserve cement; part 2: durability issues and the effects of limestone fineness on mixtures.* Concrete international, 2009. **31**(12): p. 35-39.

17. Jayapalan, A.R., B.Y. Lee, and K.E. Kurtis, *Can nanotechnology be 'green'? Comparing efficacy of nano and microparticles in cementitious materials.* Cement and concrete composites, 2013. **36**: p. 16-24.

18. Ramachandran, V.S. and C.-M. Zhang, *Influence of CaCO3 on hydration and microstructural characteristics of tricalcium silicate*. 1986: National Research Council Canada, Institute for Research in Construction.

19. Sato, T. and F. Diallo, *Seeding effect of nano-CaCO3 on the hydration of tricalcium silicate.* Transportation Research Record: Journal of the Transportation Research Board, 2010(2141): p. 61-67.

20. Oey, T., et al., *The filler effect: the influence of filler content and surface area on cementitious reaction rates.* Journal of the American Ceramic Society, 2013. **96**(6): p. 1978-1990.

21. Hooton, R., M. Nokken, and M. Thomas, *Portland-limestone cement: state-of-the-art report and gap analysis for CSA A 3000.* report prepared for St. Lawrence Cement, 2007.

22. Lothenbach, B., et al., *Influence of limestone on the hydration of Portland cements.* Cement and Concrete Research, 2008. **38**(6): p. 848-860.

23. De Weerdt, K., et al., *Synergy between fly ash and limestone powder in ternary cements.* Cement and concrete composites, 2011. **33**(1): p. 30-38.

24. Bentz, D.P., et al., *Multi-scale investigation of the performance of limestone in concrete.* Construction and Building Materials, 2015. **75**: p. 1-10.

25. Palm, S., et al., *Cements with a high limestone content–Mechanical properties, durability and ecological characteristics of the concrete.* Construction and building materials, 2016. **119**: p. 308-318.

26. Neto, C.S. and V.C. Campiteli, *The influence of limestone additions on the rheological properties and water retention value of Portland cement slurries*, in *Carbonate additions to cement*. 1990, ASTM International.

27. Bentz, D.P., *Blending different fineness cements to engineer the properties of cement-based materials.* Magazine of Concrete Research, 2010. **62**(5): p. 327-338.

28. Kumar, A., et al., *Simple methods to estimate the influence of limestone fillers on reaction and property evolution in cementitious materials.* Cement and Concrete Composites, 2013. **42**: p. 20-29.

29. Kumar, A., et al., *A comparison of intergrinding and blending limestone on reaction and strength evolution in cementitious materials.* Construction and Building Materials, 2013. **43**: p. 428-435.

30. Knop, Y. and A. Peled, *Setting behavior of blended cement with limestone: influence of particle size and content.* Materials and Structures, 2016. **49**(1-2): p. 439-452.

31. Yahia, A., M. Tanimura, and Y. Shimoyama, *Rheological properties of highly flowable mortar containing limestone filler-effect of powder content and W/C ratio.* Cement and concrete Research, 2005. **35**(3): p. 532-539.

32. Hu, C., F. De Larrard, and O.E. Gjørv, *Rheological testing and modelling of fresh high performance concrete.* Materials and Structures, 1995. **28**(1): p. 1.

33. Nadelman, E.I., *Hydration and microstructural development of portland limestone cement-based materials*. 2016, Georgia Institute of Technology.

34. Schmidt, M., et al., *Innovations in portland cement manufacturing.* Portland Cement Association: Skokie, Illinois, 2004.

35. ELDIDAMONY, H., et al., *Limestone as a retarder and filler in limestone blended cement.* INST CHEMICAL TECHNOLOGY, DEPT GLASS CERAMICS, 1995. **39**: p. 15-19.

36. Vuk, T., et al., *The effects of limestone addition, clinker type and fineness on properties of Portland cement.* Cement and concrete Research, 2001. **31**(1): p. 135-139.

37. Nehdi, M., S. Mindess, and P.-C. Aıtcin, *Rheology of high-performance concrete: effect of ultrafine particles.* Cement and Concrete Research, 1998. **28**(5): p. 687-697.

38. Tsivilis, S., et al., *A study on the parameters affecting the properties of Portland limestone cements.* Cement and Concrete Composites, 1999. **21**(2): p. 107-116.

39. Heikal, M., H. El-Didamony, and M. Morsy, *Limestone-filled pozzolanic cement.* Cement and Concrete Research, 2000. **30**(11): p. 1827-1834.

40. Ezziane, K., et al., *Effect of mineral additives on the setting of blended cement by the maturity method.* Materials and structures, 2010. **43**(3): p. 393-401.

41. Gajda, J., *Mass concrete for buildings and bridges*. 2007.

42. Alunno-Rosetti, V. and F. Curcio. *A contribution to the knowledge of the properties of portland-limestone cement concretes, with respect to the requirements of european and Italian*. in *Proceedings of the 10th International Congress on the Chemistry of Cement*. 1997.

43. Dhir, R., et al., *Evaluation of Portland limestone cements for use in concrete construction.* Materials and Structures, 2007. **40**(5): p. 459.

44. Bucher, B., A. Radlinska, and J. Weiss. *Preliminary comments on shrinkage and shrinkage cracking behavior of cement systems that contain limestone*. in *Concrete Technology Forum. Focus on Sustainable DevelopmentNational Ready Mixed Concrete Association*. 2008.

45. ACI Committee 237R, *Self-Consolidating Concrete,* ACI 237R-07, American Concrete Institute, Farmington Hills, MI, 2008.

46. Daczko, J., *Chapter 56: Self-Consolidating Concrete (SCC)*, in *STP37774S Significance of Tests and Properties of Concrete and concrete-Making Materials*, M. Vachon, Editor. 2006, West Conshohocken, PA. p. 637-645.

47. Daczko, J.A., *Self-consolidating concrete: applying what we know*. 2012: CRC Press.

48. Zhu, W. and J.C. Gibbs, *Use of different limestone and chalk powders in self-compacting concrete.* Cement and Concrete Research, 2005. **35**(8): p. 1457-1462.

49. Rear, K. and D. Chin, *Non-chloride accelerating admixtures for early compressive strength.* Concrete International, 1990. **12**(10): p. 55-58.

50. Petit, J.-Y., K.H. Khayat, and E. Wirquin, *Coupled effect of time and temperature on variations of yield value of highly flowable mortar*. Cement and Concrete Research, 2006. **36**(5): p. 832-841.

51. ACI Committee 209, *Guide for Modeling and Calculating Shrinkage and Creep in Hardened Concrete*, ACI 209.2R-08, American Concrete Institute, Farmington Hills, MI, 2008.

52. Branson, D.E. and M. Christiason, *Time Dependent Concrete Properties Related To Design-Strength and Elastic Properties, Creep, and Shrinkage.* Special Publication, 1971. **27**: p. 257-278.

53. Bazant, Z.P. and S. Baweja, *Creep and shrinkage prediction model for analysis and design of concrete structures: Model B3.* ACI Special Publications, 2000. **194**: p. 1-84.

54. Muller, H. and H. Hilsdorf, *Evaluation of the time-dependent behavior of concrete, summary report on the work of general task group 9.* CEB Bulletin d'Information, 1990(199): p. 290.

55. Gardner, N. and M. Lockman, *Design provisions for drying shrinkage and creep of normal-strength concrete.* Materials journal, 2001. **98**(2): p. 159-167.

56. ACI Committee 209, *Guide for Modeling and Calculating Shrinkage and Creep in Hardened Concrete*. ACI 209.2R-08, American Concrete Institute, Farmington Hills, MI, 2008.

57. Mehta, P.K., *Concrete. Structure, properties and materials.* 1986.

58. Neville, A.M., *Properties of concrete*. Vol. 4. 1995: Longman London.

59. Roussel, N., C. Stefani, and R. Leroy, *From mini-cone test to Abrams cone test: measurement of cement-based materials yield stress using slump tests.* Cement and Concrete Research, 2005. **35**(5): p. 817-822.

60. Zhang, Q., et al., *Long-term creep properties of cementitious materials: Comparing microindentation testing with macroscopic uniaxial compressive testing.* Cement and Concrete Research, 2014. **58**: p. 89-98.

61. Vandamme, M. and F.-J. Ulm, *Nanoindentation investigation of creep properties of calcium silicate hydrates.* Cement and Concrete Research, 2013. **52**: p. 38-52.

62. Vu, T.-S., G. Ovarlez, and X. Chateau, *Macroscopic behavior of bidisperse suspensions of noncolloidal particles in yield stress fluids.* Journal of Rheology, 2010. **54**(4): p. 815-833.

63. ASTM Standard C512, *Standard Test Method for Creep of Concrete in Compression*. ASTM International, West Conshohocken, PA, 2015.

64. ASTM Standard C150, *Standard Specification for Portland Cement*. ASTM International, West Conshohocken, PA, 2017.

65. Raymond Mill Limestone Grinder, available from: http://www.raymond-mill.com/products/Specific_Raymond_mill/70.html.

66. Li, X.-G., et al., *Decomposition kinetic characteristics of calcium carbonate containing organic acids by TGA.* Arabian Journal of Chemistry, 2017. **10**: p. S2534-S2538.

67. Michel, F. and L. Courard, *Particle size distribution of limestone fillers: granulometry and specific surface area investigations.* Particulate Science and Technology, 2014. **32**(4): p. 334-340.

68. Knop, Y. and A. Peled, *Packing density modeling of blended cement with limestone having different particle sizes.* Construction and Building Materials, 2016. **102**: p. 44-50.

69. ACI Committee 211, *Guide for Proportioning Concrete Mixtures with Ground Limestone and Other Mineral Fillers* ACI 211.7R-15, American Concrete Institute, Farmington Hills, MI, 2015.

70. ASTM Standard C1679, *Standard Practice for Measuring Hydration Kinetics of Hydraulic Cementitious Mixtures Using Isothermal Calorimetry*. ASTM International, West Conshohocken, PA, 2017.

71. ASTM Standard C191, *Standard Test Methods for Time of Setting of Hydraulic Cement by Vicat Needle*. ASTM International, West Conshohocken, PA, 2013.

72. ASTM Standard C187, *Standard Test Method for Amount of Water Required for Normal Consistency of Hydraulic Cement Paste.* ASTM International, West Conshohocken, PA, 2016.

73. ASTM Standarrd C305, *Standard Practice for Mechanical Mixing of Hydraulic Cement Paste and Mortars of Plastic Consistency*, ASTM International, West Conshohocken, PA, 2014.

74. ASTM Standrad C109, *Standard Test Method for Compressive Strength of Hydraulic Cement Mortars (Using 2-in. or [50-mm) Cube Specimens*, ASTM International, West Conshohocken, PA, 2016.

75. ASTM Standrad C511, *Standard Specification for Mixing Rooms, Moist Cabinets, Moist Rooms and Water Storage Tanks Used in the Tesitng of Hydraulic Cements and Concrete*, ASTM International, West Conshohocken, PA, 2013.

76. Okado, T., *Study on estimating method of yield value of fresh concrete using slump flow test.* Journal of the Japan Society of Civil Engineers, 1997. **578**: p. 19-29466.

77. Da Silva, W.R.L. and P. Štemberk, *Expert system applied for classifying self-compacting concrete surface finish.* Advances in Engineering Software, 2013. **64**: p. 47-61.

78. Esping, O., *Effect of limestone filler BET (H2O)-area on the fresh and hardened properties of self-compacting concrete.* Cement and Concrete Research, 2008. **38**(7): p. 938-944.

79. Ghezal, A. and K.H. Khayat, *Optimizing self-consolidating concrete with limestone filler by using statistical factorial design methods.* Materials Journal, 2002. **99**(3): p. 264-272.

80. Guemmadi, Z.h., et al., *Optimal criteria of Algerian blended cement using limestone fines.* Journal of Civil Engineering and Management, 2008. **14**(4): p. 269-275.

81. ASTM Standard C192, *Standard Practice for Making and Curing Concrete Test Specimens in the Laboratory*. ASTM International, West Conshohocken, PA, 2016.

82. ASTM Standard C1611, *Standard Test Method for Slump Flow of Self-Consoldating Concrete*. ASTM International, West Conshohocken, PA, 2014.

83. Horta, A., *Evaluation of Self-Consolidating Concrete for Bridge Structure Applications*. 2005, Georgia Institute of Technology.

84. Hawkins, P., P.D. Tennis, and R.J. Detwiler, *The use of limestone in Portland cement: a state-of-the-art review*. 2003: Portland Cement Association Skokie.

85. Heirman, G., et al., *Time-dependent deformations of limestone powder type self-compacting concrete.* Engineering Structures, 2008. **30**(10): p. 2945-2956.

86. Kenai, S., W. Soboyejo, and A. Soboyejo, *Some engineering properties of limestone concrete.* Materials and Manufacturing processes, 2004. **19**(5): p. 949-961.

87. Bažant, Z.P., M.H. Hubler, and Q. Yu, *Damage in prestressed concrete structures due to creep and shrinkage of concrete*, in *Handbook of Damage Mechanics*. 2015, Springer. p. 515-564.

88. Bazant, Z.P., *Mathematical modeling of creep and shrinkage of concrete*. 1988: Wiley.

89. Stanish, K., R.D. Hooton, and M. Thomas, *Testing the chloride penetration resistance of concrete: a literature review*. 2000: Department of Civil Engineering, University of Toronto Toronto, Ontario, Canada.

90. AASHTO Standard T358, *Standard method of test for surface resistivity indication of concrete's ability to resist chloride ion penetration*, American Association of State Highway and Transportation Officials, Washington, DC, 2015.

91. ASTM Standard C1202, *Standard Test Method for Electrical Indication of Concrete's Ability to Resist Chloride Ion Penetration*. ASTM International, West Conshohocken, PA, 2017.

92. AASHTO Standard T277, *Standard Method of Test for Rapid Determination of the Chloride Permeability of Concrete*. American Association of State Highway and Transportation Officials, Washington, DC, 2015.

93. Morris, W., E. Moreno, and A. Sagüés, *Practical evaluation of resistivity of concrete in test cylinders using a Wenner array probe.* Cement and concrete research, 1996. **26**(12): p. 1779-1787.

94. ASTM Standard C39, *Standard Test Method for Compressive Strength of Cylindrical Concrete Specimens*. ASTM International, West Conshohocken, PA, 2017.

95. ASTM Standard C157, *Standard Test Method for Length Change of Hardened Hydraulic-Cement Mortar and Concrete*. ASTM International, West Conshohocken, PA, 2017.

96. Kosmatka, S.H., B. Kerkhoff, and W.C. Panarese, *Design and control of concrete mixtures*. 2011: Portland Cement Assoc.

97. Chini, A.R., L.C. Muszynski, and J.K. Hicks, *Determination of acceptance permeability characteristics for performance-related specifications for Portland cement concrete*. 2003.

98. Nadelman, E.I. and K.E. Kurtis, *A resistivity-based approach to optimizing concrete performance.* Concrete international, 2014. **36**(5): p. 50-54.

99. Rupnow, T. and P. Icenogle, *Surface resistivity measurements evaluated as alternative to rapid chloride permeability test for quality assurance and acceptance.* Transportation Research Record: Journal of the Transportation Research Board, 2012(2290): p. 30-37.

100. Al-Amoudi, O.S.B., et al., *Correlation between compressive strength and certain durability indices of plain and blended cement concretes.* Cement and Concrete Composites, 2009. **31**(9): p. 672-676.

101. VOSOUGHI, P., et al., *An Investigation of the Possibility of Estimating the Compressive Strength of Concrete by Using its' Electrical Resistance.* Cumhuriyet Science Journal, 2015. **36**(4): p. 778-784.

102. Constantinides, G., F.-J. Ulm, and K. Van Vliet, *On the use of nanoindentation for cementitious materials.* Materials and structures, 2003. **36**(3): p. 191-196.

103. Nguyen, D.-T., et al., *Microindentation creep of secondary hydrated cement phases and C–S–H.* Materials and structures, 2013. **46**(9): p. 1519-1525.

104. Fisher-Cripps, A.C., *Nanoindentation.* Mechanical engineering series, 2002. **2**.

105. Jones, C.A. and Z.C. Grasley, *Short-term creep of cement paste during nanoindentation.* Cement and Concrete Composites, 2011. **33**(1): p. 12-18.

106. Zhang, Q., *Creep properties of cementitious materials: effect of water and microstructure: An approach by microindentation*. 2014, Université Paris-Est.

107. Oliver, W.C. and G.M. Pharr, *An improved technique for determining hardness and elastic modulus using load and displacement sensing indentation experiments.* Journal of materials research, 1992. **7**(6): p. 1564-1583.

108. Miller, M., et al., *Surface roughness criteria for cement paste nanoindentation.* Cement and Concrete Research, 2008. **38**(4): p. 467-476.

109. Han, J., et al., *Application of nanoindentation to investigate chemomechanical properties change of cement paste in the carbonation reaction.* Science China Technological Sciences, 2012. **55**(3): p. 616-622.

110. Němeček, J., *Creep effects in nanoindentation of hydrated phases of cement pastes.* Materials Characterization, 2009. **60**(9): p. 1028-1034.

111. Neville, A., M. Ward, and G.-S. Kwei, *Basic and drying creep of concrete.* Matériaux et Construction, 1969. **2**(2): p. 117.

112. l'Hermite, R., *Idées actuelles sur la technologie du béton*. 1955: La Documentation technique du batiment et des travaux publics.